Study of modified zeolites as heterogeneous catalysts for synthesis of petrochemicals and other organic compounds

A Thesis

Submitted in the partial fulfillment for the award of the degree of

DOCTOR OF PHILOSOPHY

SUBMITTED BY

PRIYANKA GAUTAM
(901709007)

Supervisors

Dr. Sanghamitra Barman
Professor
CHED

Dr. Amjad Ali
Professor
SCBC

SCHOOL OF CHEMISTRY AND BIOCHEMISTRY
Thapar Institute of Engineering & Technology
Patiala-147004, Punjab, India
3rd November, 2023

Dedicated to

my parents

and

family

Acknowledgments

This Ph.D. journey has been a very transformative for me. Everything about my time at T.I.E.T. has been incredible. New chances have been given to me, and they have been beneficial to me. Without the help and direction, I received from numerous people, I would not have been able to complete my Ph.D.

First and foremost, I want to express my sincere gratitude to ***GOD*** *for all of the blessings he has bestowed upon me during my efforts to finish this successful work of mine.*

It gives me great pleasure to express my gratitude to my supervisors, ***Dr. Sanghamitra Barman****, Associate Professor, Department of Chemical Engineering, TIET, Patiala, and* ***Dr. Amjad Ali****, Professor, School of Chemistry and Biochemistry, TIET, Patiala for their unwavering support & guidance regarding fundamental principles, helpful ideas that enabled me to successfully begin and complete my research work. They gave me the motivation I needed to keep going, keep learning new things, and fix my mistakes as I went.*

I want to express my gratitude to ***Dr. Satnam Singh, Head*** *of the School of Chemistry and Biochemistry, for giving me the chance to join this prestigious organization, giving me access to research facilities, and being so helpful and supportive. I would like to extend my sincere gratitude to* ***Dr. Bhaskar Chandra Mohanty,*** *Associate Professor,* ***Professor Ranjana Prakash****, Professor and* ***Dr. Soumen Basu,*** *Associate Professor, of my doctoral committee for their never-ending support, perceptive criticism, and strong interest in me during the course of my research. I'd want to thank SAI Labs, for NMR and SEM facilities. I'd also thank the School of Physics and Material Sciences (SPMS) for their facilities like XRD, and FE-SEM. I extend my thanks to* ***Mr. Chander Thakur*** *and office staff* ***Mr. Mayank Sharma****, and all the employees at the School of Chemistry and Biochemistry for their kind assistance and support.*

I'd like to express my deepest gratitude to ***Miss. Aastha Palta****, for her unwavering support and encouragement throughout this challenging journey. Her insightful discussions and critical feedback have helped shape the direction of my research. I'd also like to thank my soul sister,* ***Mrs. Nancy Rana****, for her tolerance and understanding when I needed to prioritize my studies.*

I gratefully acknowledge the help and support I got from my lab mates ***Dr. Abida****,* ***Dr. Avneet Kaur, Dr. Himmat Singh, Anshu Tyagi, Mallika Phull, Akanksha Ranade, Anuva Mondal, and Vidhi Tyagi****. My other research fellows* ***Pooja Soam, Parmjeet Kaur, Priya Kamboj, Kirti Singh, and Abinash Mohapatra*** *during my whole journey.*

Words are inefficient to express my gratitude towards ***Mrs. Phoolan Devi****, my grandmother,* ***Dr. Sunil Gautam*** *&* ***Mrs. Promila Gautam****, my parents,* ***Dr. Abhinav Gautam****, my elder brother, and* ***Dr. Drishti***

Rana, my sister-in-law who love me, support me and inspired me to follow my dreams. They have always supported me whether it is emotionally or financially and their belief in me has always kept my spirits and motivation high in tough times. Without them, my success and the completion of my Ph.D. degree would not have been possible.

I am also gratefully thankful to my other friends for their emotional support, encouragement, and patience during the difficult times of my Ph.D. journey.

Lastly, I would like to thank everyone in my life who encouraged me and helped me in whatever way possible.

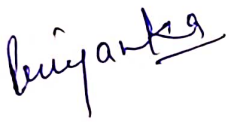

Priyanka Gautam

Certificate

This is to certify that the thesis entitled **"Study of modified zeolites as heterogeneous catalysts for synthesis of petrochemicals and other organic compounds"**, being submitted by **Priyanka Gautam,** School of Chemistry and Biochemistry, Thapar Institute of Engineering and Technology, Patiala for the award of degree Doctor of Philosophy, is a record bonafide of the research work carried out by her. Ms. Priyanka Gautam has worked under my guidance and supervision and has fulfilled the requirements for the submission of the thesis, which to my knowledge has reached the requisite standard. The results embodied in the thesis have not been submitted in part or full to any other University or Institute for the award of any degree or diploma.

Supervisors:

Dr. Sanghamitra Barman
Professor
CHED
TIET, Patiala

4/11/2023

Dr. Amjad Ali
Professor
SCBC
TIET, Patiala

Head:

4/11/23

Dr. Satnam Singh
Professor and Head
SCBC
TIET, Patiala.

Candidate's Declaration

I, hereby declare that the work presented in the thesis entitled **"Study of modified zeolites as heterogeneous catalysts for synthesis of petrochemicals and other organic compounds"** in the fulfillment of the requirement for the award of the degree of Philosophy, School of Chemistry and Biochemistry, Thapar Institute of Engineering and Technology, Patiala is an authentic record of my work carried out under the supervision of **Dr. Sanghamitra Barman**, Professor, and **Dr. Amjad Ali**, Professor, School of Chemistry and Biochemistry, Thapar Institute of Engineering and Technology, Patiala, India. The matter embodied in the thesis has not been submitted in part or full to any other University or Institute for the award of any degree in India or abroad.

Priyanka

Priyanka Gautam

Table of contents

List of Abbreviations

Abbreviation	Description
PBU	Primary Building Unit
SBU	Secondary Building Unit
IZA	International Zeolite Association
1-D	One Dimensional
2-D	Two Dimensional
3-D	Three Dimensional
IUPAC	International Union of Pure and Applied Chemistry
IZASC	International Zeolite Association Structure Commission
FAME	Fatty Acid Methyl Ester
BD	Biodiesel
GLY	Glycerol
AcA	Acetic acid
AcAn	Acetic anhydride
MAG	Monoacetylglycerol
DAG	Diacetylglycerol
TAG	Triacetylglycerol
LA	Levulinic acid
EtOH	Ethanol
GC	Glycerol carbonate
DMC	Dimethyl carbonate
CARG	Compound Annual Rate of Growth
XRD	X-Ray Diffraction
SEM	Scanning Electron Microscopy
EDS	Energy Dispersive X-ray Spectroscopy
FESEM	Field Emission Scanning Electron Microscopy
FTIR	Fourier Transform Infra-Red
XPS	X-ray Photoelectron Spectroscopy
HR-TEM	High-Resolution Transmission Electron Microscopy
BET	Brunauer-Emmett-Teller

BJH	Barret-Joyner-Halenda
NH_3-TPD	Ammonia Temperature Programmed Desorption
MPAES	Microwave Plasma-Atomic Emission Spectroscopy
DLS	Dynamic Light Scattering
HPLC	High-Performance Liquid Chromatography
RI	Refractive Index
FT-NMR	Fourier Transform-Nuclear Magnetic Resonance
^{1}H-NMR	Proton- Nuclear Magnetic Resonance
^{13}C-NMR	Carbon- Nuclear Magnetic Resonance
TMS	Trimethyl Silane
HRMS	High-Resolution Mass Spectroscopy
JCPDS	Joint Committee for Powder Diffraction Standards
D_2O	Deuterium oxide
$CDCl_3$	Deuterated chloroform
TLC	Thin Layer Chromatography
IPA	Isopropyl Alcohol
ACN	Acetonitrile
$\%C_{GC}$	Percentage of GC
UV	Ultraviolet
TCD	Thermal Conductivity Detector
RBF	Round Bottom Flask

List of Symbols

Symbols	Description
θ	Theta
R	Gas Constant
K	Rate Constant
T	Temperature
A	Pre-exponential factor
E_a	Activation energy
%	Percentage
°	Degree
K	Kelvin
℃	Degree celcius
wt%	Weight percent
v/v	Volume by volume
h	hour
min	minutes
M	Molar
mL	Millilitre
mm	millimeter
µm	Micrometer
µL	Microlitre
Å	Angstrom
nm	Nanometer
cm^{-1}	Centimeter inverse
eV	Electron volt
mmol/g	Millimole per gram
m^2/g	Metre square per gram
cc/g	Gram per cubic centimetre

List of Figures

List of Tables

List of Schemes

Abstract

The thesis thoroughly covers the esterification of glycerol and levulinic acid, transesterification of glycerol, and alkylation of indole. Esterification, transesterification, and alkylation of low-valued chemicals were done so as to convert these to industrially important products like monoacetin, diacetin, glycerol carbonate, levulinate ester, and indole derivatives etc. Various homogeneous and heterogeneous catalysts such as HZSM-5, USY, Beta, and ammonium form of mordenite zeolites were used in the esterification, transesterification, and alkylation reactions. A detailed description of the catalyst such as its composition, structure, and properties has been discussed. In order to enhance the catalyst activity and reactivity towards the desired reaction, zeolites were further altered with various metals and functional groups. In order to understand, the influences of loading on the catalytic performance of the zeolites, yield, and selectivity of the product in specific reactions, characterization of catalysts was done by EDS, XRD, FE-sSEM, HRTEM, XPS, DLS, BET, and TPD.

The reactant conversion depends on the activity of the catalyst, catalyst loading, reactant mole ratio, and reaction temperature. The outlined mechanisms of different reactions showed that the catalyst pore size and the type of pore as well as the feed composition of binary mixtures play important roles in the formation of the desired product. The activity of the zeolite also depends on the type of ions exchanged with the Na^+ and H^+ ions present in the framework of the zeolite.

Besides evaluating the catalytic performance, the kinetic parameters of the reactions were also evaluated. The activation energy for the transesterification reaction was found to be 34.60 kJ/mol. The activation energy for the esterification reaction of glycerol with acetic was found to be 63.72 kJ/mol and for levulinic acid and ethanol esterification, it came out to be 19.57 kJ/mol.

In the esterification of glycerol, 98.32% conversion of glycerol was obtained at optimized reaction conditions with a mixture of monoacetin and diacetin which are used as precursors in the food, cosmetic industries etc. The catalyst was reused for 4 reaction cycles. The reaction follows pseudo-first-order reaction kinetics. The esterification reaction of levulinic acid with ethanol was performed using sulfuric acid-modified zeolite Y catalyst which produced 96% ethyl levulinate which is directly used as Diesel Miscible Biofuel in car engines. To check the

stability of the catalyst, it was reused for up to 4 cycles. The esterification of levulinic acid with ethanol followed pseudo-first-order reaction kinetics.

Glycerol and dimethyl carbonate were transesterified using a Li-modified zeolite beta catalyst which produced 81.48% glycerol carbonate at optimized reaction conditions and it is used in pharmaceuticals, paints industries etc. The catalyst was reused for up to 5 reaction cycles with 100% selectivity of glycerol carbonate. The experimental data followed second-order reaction kinetics.

The sulfuric acid-treated mordenite (SO_3H@Mor) zeolite was used as a catalyst for the synthesis of 3-alkylated indole from indole and methyl vinyl ketone which is a good precursor for anti-cancer treatment. A maximum of 92% β-alkylated indole was obtained with no side product. The catalyst was reused for up to 3 reaction cycles. The system followed a pseudo-first-order reaction.

Keywords:

Cerium-modified ZSM-5 zeolite, sulfuric acid-treated zeolite Y and mordenite, Li-modified zeolite beta, esterification reaction, transesterification reaction, alkylation reaction, mono and diacetyl glycerol, ethyl levulinate, glycerol carbonate, 3-alkylated indole, kinetic study.

CHAPTER 1

INTRODUCTION & LITERATURE REVIEW

This chapter comprehensively overviews the esterification, transesterification, and alkylation processes. Various homogeneous and heterogeneous catalysts used in the esterification, transesterification, and alkylation processes are also briefly discussed. A thorough description of these zeolites' such as composition, structure, and characteristics, has been reported. The literature on esterification, transesterification, and alkylation processes is also thoroughly reviewed in this chapter. There has been extensive discussion of various types of catalysts, including homogeneous and heterogeneous catalysts. The zeolites and modified zeolites used in this investigation have also been discussed.

1.1. Introduction

1.1.1. Esterification reaction

Due to environmental concerns about pollution in the air and emissions of greenhouse gases, as well as worries about the reliability of energy and the eventual extinction of fossil resources, governments worldwide have recently established laws encouraging renewable energy sources. The regulations in the transportation sector call for biofuels like ethanol and biodiesel (BD) to eventually replace conventional fuels. It burns more cleanly than diesel fuel derived from petroleum and emits fewer harmful pollutants like sulfur dioxide, carbon monoxide, and particulate matter.

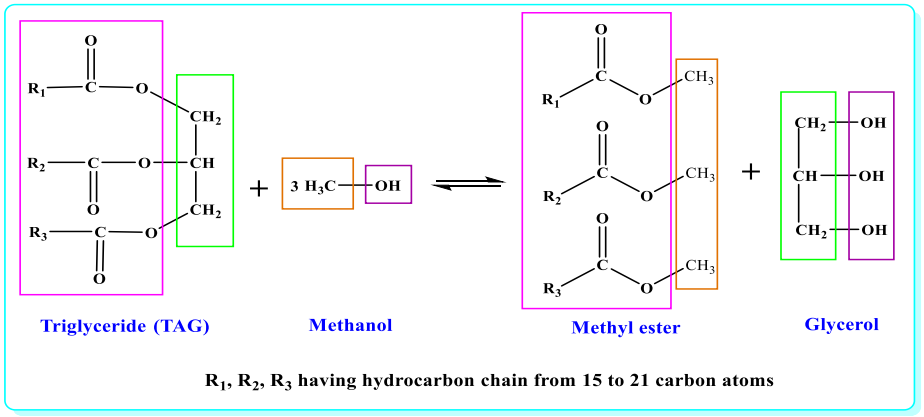

Scheme 1.1. The overall reaction for biodiesel production via methanolysis of vegetable oils.

BD is a long-chain fatty acid mono-alkyl ester. Transesterification is the process by which triglycerides, present in animal and plant fats, are transformed into fatty acid methyl esters (FAMEs), which are the key component of BD. In this method, methanol is often used as the alcohol, and a catalyst such as sodium hydroxide or potassium hydroxide is frequently utilized to accelerate the reaction. According to the stoichiometry of the transesterification

reaction, three moles of alcohol are required for every mole of triglycerides to form three moles of FAMEs and one mole of glycerol (GLY), as illustrated in **Scheme 1.1**. This means about 10 of the BD produced is GLY, which can be further processed for other applications.

The production of BD in different countries on the basis of data taken from the year 2021 is shown in **Figure 1.1**. Due to the BD industry's rapid growth, there is now an avoidable oversupply of GLY on the market. Due to this, the demand for GLY for its conventional uses, such as in foods, cosmetics, and pharmaceuticals, is anticipated to rise more slowly than the supply. Also, the excess is continuously being added to a generally stable demand. As a result, to avoid saturation of the marketplace and ensure the long-term viability of the BD industry, it has become extremely important to discover alternative methods of using GLY from BD manufacturing and transforming it into valuable products.

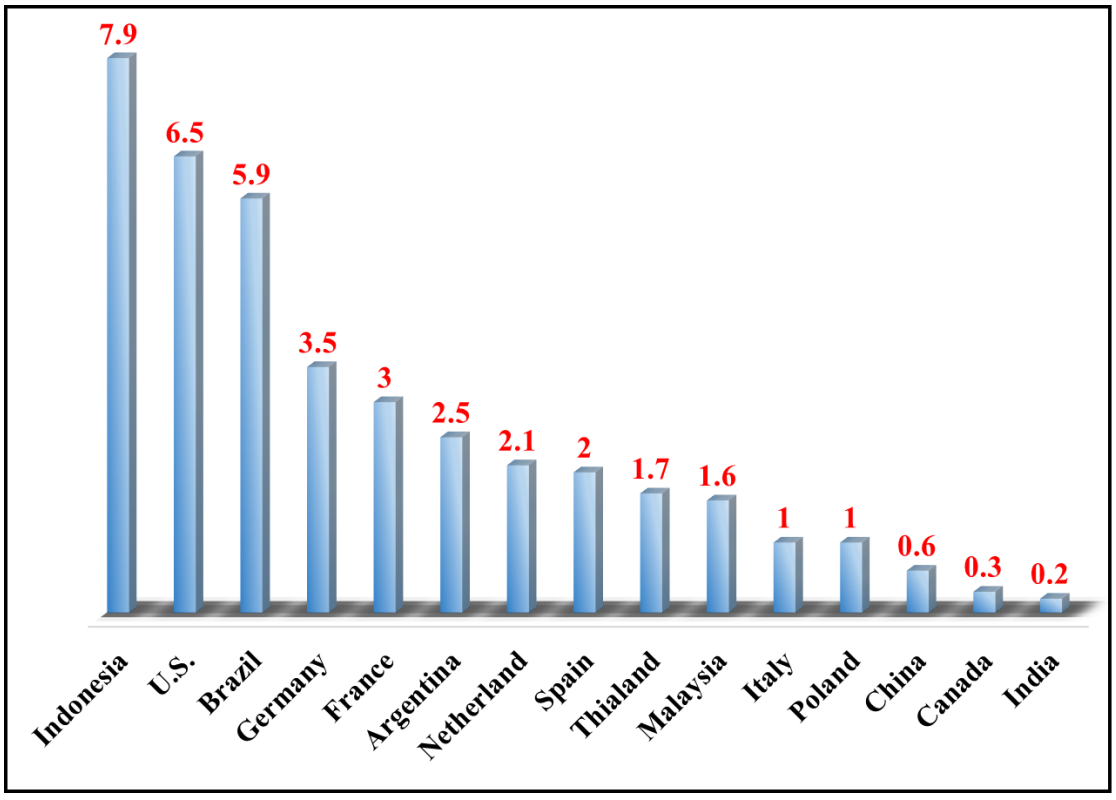

Figure 1.1. Biodiesel production in billion liters in various countries.

1.1.1.1. Esterification of glycerol to produce esters

GLY (1,2,3-propanetriol), known as glycerine in the commercial world, is a sweet, viscous, colorless liquid having the chemical formula $C_3H_8O_3$. GLY is a tri-alcohol with three carbon atoms linked to three hydrophilic hydroxyl groups.[1] It is commonly used as a humectant in the food and cosmetic industries due to its ability to attract and retain moisture. It is also used as a

solvent in pharmaceuticals, as a plasticizer in the production of plastics, and as a component in antifreeze formulations.[2] GLY can make additives by reacting with carboxylic acids to produce esters. The esterification of GLY with acetic acid (AcA) or acetic anhydride (AcAn) to form acetins, esters of glycerol as shown in **Scheme 1.2**, is a popular item for fuel additive applications.[3] The three compounds that are synthesized depending on how significant the response are monoacetin, diacetin, and triacetin, also known as monoacetylglycerol (MAG), diacetylglycerol (DAG), and triacetylglycerol (TAG). (**Figure 1.2**).

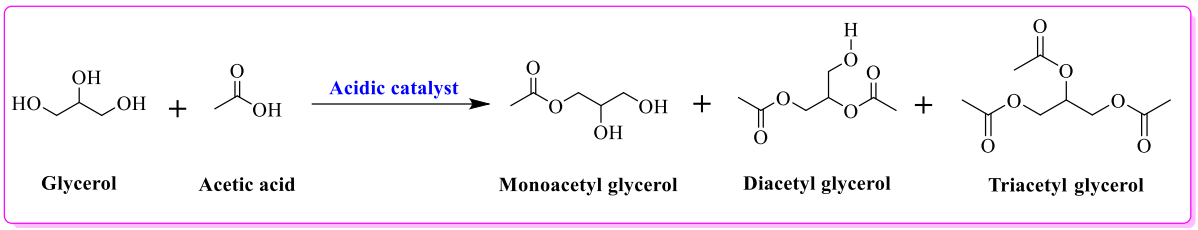

Scheme 1.2. Esterification of glycerol and acetic acid.

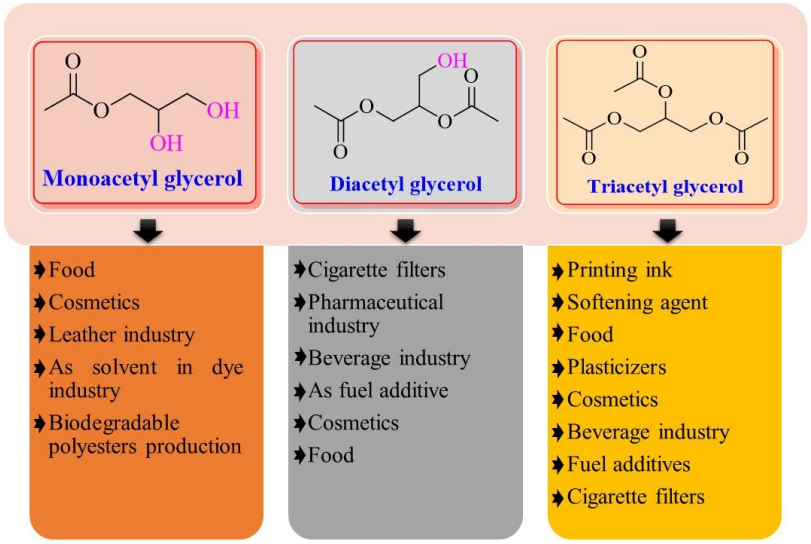

Figure 1.2. Applications of derivatives of glycerol.

1.1.1.2. Esterification of levulinic acid to produce levulinate ester

Levulinic acid (LA) is a biomass-derived chemical compound useful in synthesizing various value-added products. A large amount of biomass (~70 billion tons) is produced naturally by photosynthesis, and merely 3-4% is utilized by humans. Many valuable materials can be obtained from biomass, but the present work focuses only on synthesizing levulinate ester from LA.[4] Esters of levulinic acid produced by esterification reaction can be used as fuel additives for diesel fuel, biodiesel, and gasoline as it has non-toxicity, high flash point, and good

lubrication (Scheme 1.3). Aside from these applications, it is also employed as a monomer for various polymers, plasticizers, and solvents in the flavouring industry, as well as resin precursors in the refining of mineral oils, pharmaceutical industries, and so on, as shown in Figure 1.3.[5] When all the esters derived from levulinic acid using different alcohols are compared, ethyl levulinate distinguishes apart due to its physiochemical features such as thermal stability, high viscosity, low toxicity, and fluid dynamic stability at moderate temperatures. Additionally, ethyl levulinate can be utilised directly as a Diesel Miscible Biofuel (DMB) in automobile engines up to 5 weight percent.[6]

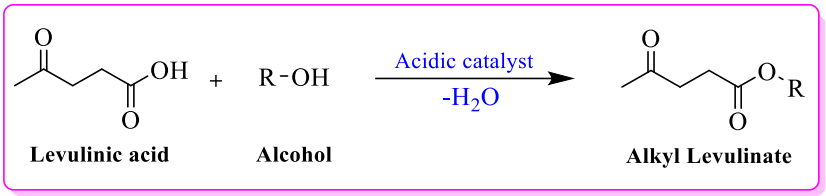

Scheme 1.3. Esterification of levulinic acid and alcohol.

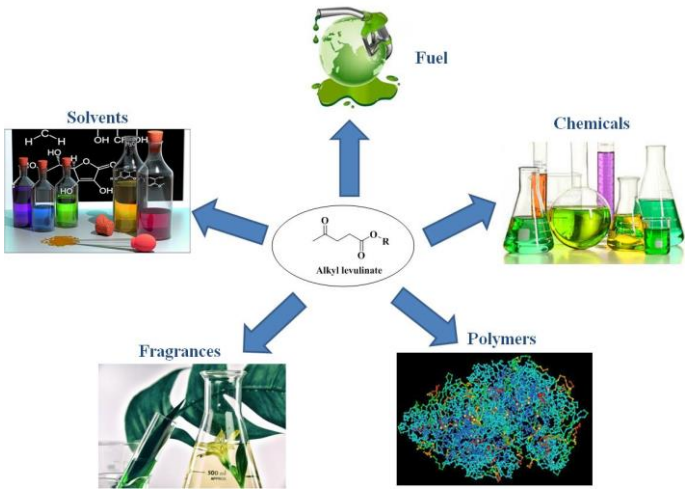

Figure 1.3. Applications of alkyl levulinate esters.

1.1.2. Transesterification of glycerol to produce glycerol carbonate

GC is an organic compound with the chemical formula $C_4H_6O_4$. It is also known as glycerin carbonate or cyclic glycerol carbonate. This compound is a cyclic ester of GLY and carbonic acid. Its IUPAC name is 4-hydroxymethyl-1,3-dioxolane-2-one. GC is a clear, colorless liquid with a slightly sweet odor. It is readily soluble in a variety of organic solvents and water.[7] It is commonly used as a building block in synthesizing various organic compounds, such as polyesters, polyurethanes, and polycarbonates. It has good properties like a high boiling point and low flammability, which got attention towards GC. GC has many potential applications,

such as solvent for coating, adhesives, and pharmaceuticals, as well as an electrolyte component for lithium-ion batteries shown in **Figure 1.4**.[8] Due to its low toxicity and environmental impact, it is also considered as a bio-based and biodegradable solvent. It is widely used in producing fibers, plastics, paints, and biological lubricants, as a solvent in cosmetic industries.[9] The projected growth of the GC market is also noteworthy, with a predicted hike of around 7% per year and an estimated value of US$ 2.4 billion by 2030. This growth could be attributed to the increasing demand for eco-friendly products and the trend toward sustainable manufacturing practices.[10]

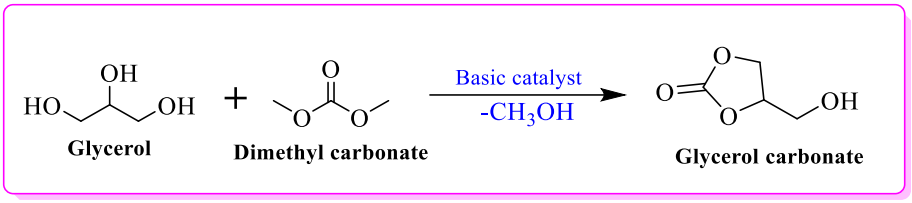

Scheme 1.4. Transesterification of glycerol and dimethyl carbonate.

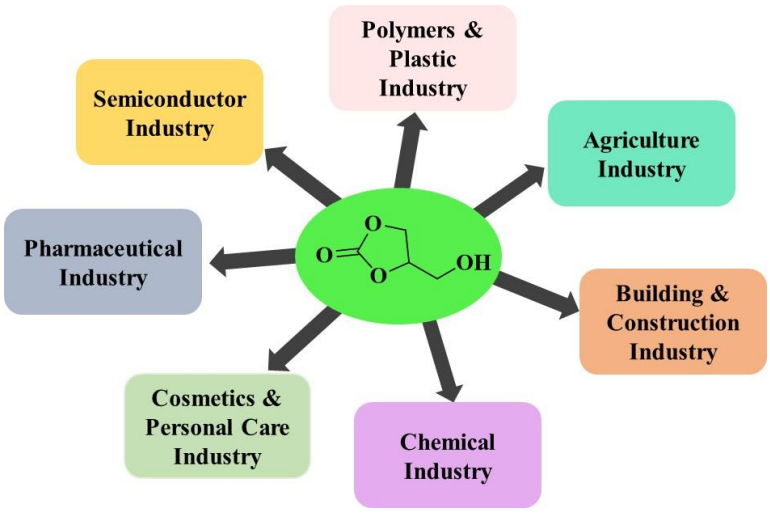

Figure 1.4. Applications of glycerol carbonate.

1.1.3. Alkylation of indole to produce 3-alkylated indole

Recently, a lot of attention has been paid to the production of efficient and approachable methods for establishing carbon-carbon and carbon-heteroatom bonds in order to produce useful molecules. In medical chemistry, heterocyclic molecules are of primary significant interest. A heterocyclic nitrogen, according to the Food and Drug Administration database, a heterocyclic nitrogen is found in nearly 60% of unique small-molecule medicines. The Friedel-Crafts alkylation process, which involves catalytic enantioselective additions of indoles to

unsaturated carbonyl compounds, has recently gained a lot of interest. The indole core is the most widely used nitrogen-based heterocyclic fragment in synthesizing pharmaceuticals and agrochemicals **(Figure 1.5)**.[11] The Indole moiety is found in a variety of natural compounds. Both synthetic and biological chemists recognize the importance of indoles. The indole moiety is the basis for the most common bioactive alkaloids. Medical chemists frequently use indole-based compounds as target pharmacophores in developing therapeutic medicines. The presence of this motif in natural and bioactive products continues to be a driving force in the development of novel approaches for discovering valuable molecules. Alkylation of indole with methyl vinyl ketone (MVK) produces β-indolylketones, which have gained much attention as crucial building blocks in synthesizing many natural products and physiologically active chemicals. Additionally, the antibacterial action of β-indolylketones has been explored.[12]

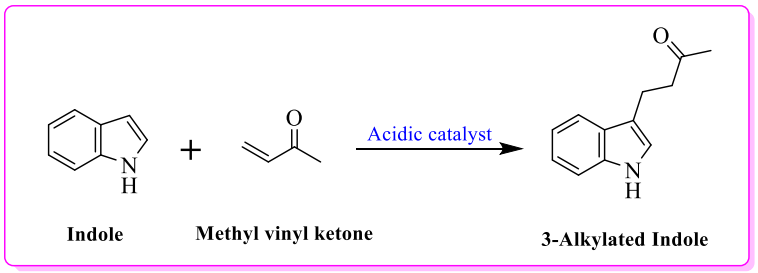

Scheme 1.5. Alkylation of Indole and methyl vinyl ketone.

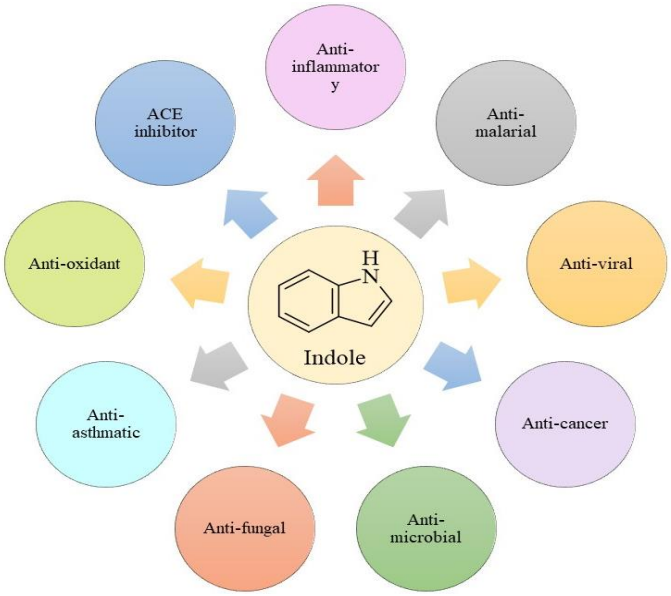

Figure 1.5. Indole application in medical sciences.

1.1.4. Catalysts used for esterification, transesterification, and alkylation reactions

Earlier, the esterification reaction was performed in the presence of a homogeneous catalyst such as hydrofluoric, sulphuric acid, nitric acid, hydrochloric acid, and p- toluene sulfonic acid. However, these strong liquid acids are unfavorable because they are hazardous, corrosive, and challenging to remove from liquid products. Besides these, a liquid catalyst is not environment-friendly and is unsuitable for reactors due to its corrosive nature. To overcome these drawbacks, various solid acid catalysts in the esterification reaction of GLY and acetic acid have been reported in the literature, like molecular sieves, ion-exchanged resins, transition metals oxides, Amberlyst-36, Amberlyst-15, zeolites, zirconia-based acid catalysts, cesium phosphotungstate catalyst, sulfonic acid functionalized SBA-15 catalysts, etc. But none of these heterogeneous catalysts exhibit promising results.[13]

Esterification of LA can be performed in the liquid- phase using sulfuric acid, phosphoric acid or hydrochloric acid, polyphosphoric acid, or p-toluenesulfonic acid. The usage of homogeneous catalysts causes serious problems related to the environment, such as handling and transportation, toxicity, equipment corrosion, disposal, and regeneration. These shortcomings of homogeneous catalysts led to the development of environmentally friendly heterogeneous catalysts with significant catalytic activity, renewability, and stability in the reaction media. These heterogeneous catalysts are like resins, silica-based, heteropoly acids, zirconia-based, zeolites, bio-catalysts, etc., used for different reactions.[14]

Fundamental catalysts are used for the transesterification reaction of GLY for the synthesis of GC. Many homogeneous catalytic systems are reported in the literature, *viz.*, K_2CO_3, trimethylamine, ionic liquids, alkali, and alkali earth metals hydroxides. Although excellent results are obtained from these catalysts, they also have disadvantages like difficulty separating from the reaction mixture, and their reusability is impossible. To conquer these drawbacks, heterogeneous catalysts were adopted in the transesterification reaction. Researchers have used a range of fundamental heterogeneous catalysts in recent years *viz.*, metal oxides and mixed metal oxides show high GC yield and leaching problems that decrease their reusability properties. Literature shows some catalysts with lithium metal such as alkali metal silicates (Li, Na, K), Li/CaO-La_2O_3, Li/Mg composite, $LiNO_3/Mg_4AlO_{5.5}$, Li/ZnO, Li/CFA, Li_4SiO_4, Li-oil palm ash zeolite, Li/ZrO_2, and K-zeolite, anion exchange resins, Na- based zeolites, different metal composites of MCM41, etc. used for the transesterification reaction of GLY and DMC.[9]

Synthesis of β-indolylketone from indole is generally carried out in the presence of various catalysts possessing acidic properties. Because of their unusual reactivities and selectivity, some of the acidic catalysts like p-toluene sulfonic acid (PTSA), $NO^+ BF_4^-$, $Bi(OTf)_3$, $HfCl_4$, and $ScCl_3$, CAN, $InBr_3$, PDA, GaI_3, FAP, PVSA, $GaCl_3$, $Cu(OTF)_2$, $Zr(O^tBu)_4$, $CeCl_3.7H_2O$-NaI, SmI_3, I_2, $InCl_3$, $FeCl_3$, copper salts, and acidic clays have received a lot of research.[12]

Zeolites have received more interest because of their pore size, tuneable acidity, and insertion of other metals or any functional groups into the framework. As a heterogeneous catalyst, zeolite's shape and size selectivity properties have gained considerable significance in the chemical industry.

1.1.5. Zeolite as a Heterogeneous Catalyst

A heterogeneous catalyst is a substance that participates in a chemical reaction but remains in a different phase than reactants and products. Zeolites are frequently employed as heterogeneous catalysts in various chemical reactions. Zeolites are inorganic crystalline materials that come under the family of the framework aluminosilicate materials of tectosilicate type having evenly distributed micropores in the molecular dimensions. Zeolite comes from the Greek words "Geo" and "Lithos-" which means boil and stone, respectively. The framework of zeolites is constructed by the interconnection of tetrahedra comprising oxygen (O), silicon (Si), and aluminum (Al) atoms. AlO_2 and SiO_2 constitute the fundamental units having oxygen as sharing ion which further forms the alumina (AlO_4^{5-}) and silica (SiO_4^{4-}) tetrahedral. The elementary unit of zeolite contains Al and Si ions having +3 and +4 charge, respectively, connected with O ions having a -2 charge, which creates an overall negative charge on the framework. The negative charge generated by trivalent charged Al in the zeolite framework is further balanced by the group I or II metal ions or the water molecule.[15] The general formula for the zeolite unit cell is expressed as:

$$M_{x/n}\,[(AlO_2)_y\,(SiO_2)_z].mH_2O$$

Where, M represents exchangeable metal ion (generally from group I or II), n represents cation valency, y, and z are the total tetrahedra attached per unit cell, and m is the water molecules present per unit cell.

1.1.5.1. Structural Analysis of Zeolites

The zeolite framework is quite complex to study. So, it is subdivided into smaller units to study its properties. The zeolite unit's building block is usually named as the primary building unit (PBU). These PBU further combine by sharing an O atom with the adjacent tetrahedral of PBU, which results in the formation of secondary building units (SBU) shown in **Figure 1.6**. The polymerization of alumina and silica tetrahedral forms sheets like polyhedral, which further combines in the form of cubes, hexagonal prisms, and truncated octahedral. This leads to its 3D structure with open voids, responsible for their unique character towards the reaction.[16]

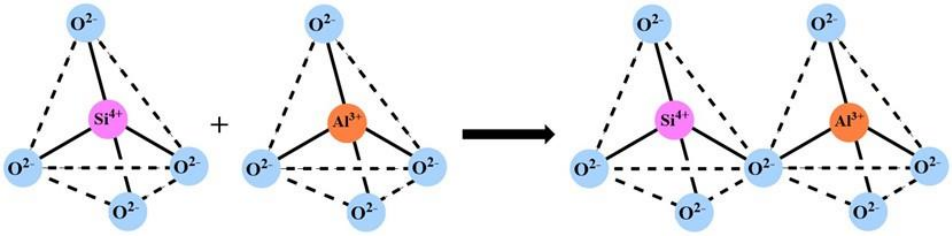

Figure 1.6. Formation of SBU from PBU.

The International Zeolite Association (IZA) has classified 235 different zeolite structures depending upon the size of the opening, i.e. the pores and how many ways a molecule can diffuse within a crystal shown in **Figure 1.7**. The pores present in the zeolites are responsible for their One-dimensional (1-D), two-dimensional (2-D), and three-dimensional (3-D) structures as these pores are aligned in one, two, and three directions, respectively. Hence, the smaller the pore size or dimension of the zeolite, the more would hinder the diffusion paths, which ultimately restricted the entrance of bulkier molecules within the zeolite in the catalysis process.[17]

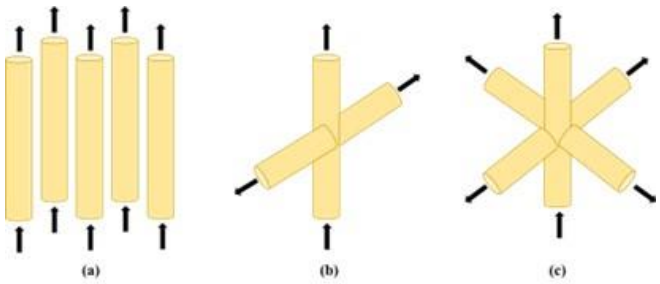

Figure 1.7. Different ways of diffusion of a molecule within the zeolite.

The active sites of zeolite structures are categorized using Bronsted and Lewis acidity. The zeolite develops Bronsted acidity whenever a proton is a charge-balancing cation for the anionic framework. Lewis's acid is a trigonally coordinated aluminum atom that acts as an

electron acceptor. At higher temperatures (>773 K), dehydroxylation can convert Bronsted acid sites to Lewis acid sites. Lewis' acid sites are also produced during the hydrothermal treatment of zeolites, which prompts nearly Bronsted acid sites to become active (**Figure 1.8)**.

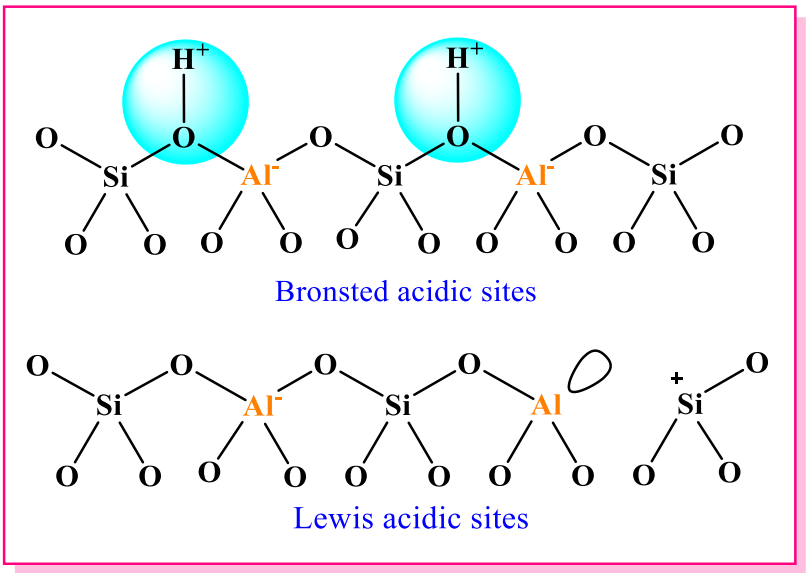

Figure 1.8. Acidic sites of the zeolite.

1.1.5.2. Properties of Zeolite as heterogeneous catalyst

Some of the important properties of zeolites as heterogeneous catalyst has been discussed below.[18]

i. **Shape selectivity:** Zeolites have high selectivity for specific molecules based on their shape and size. This property makes them useful in purifying and separating various chemicals and gases.

ii. **Thermal stability:** Zeolites are very stable under high temperatures and pressure. This makes zeolites useful in catalytic reactions that require very high temperatures.

iii. **Crystalline structure:** Zeolites can have a variety of crystal structures and chemical compositions, making them useful in a wide range of applications.

iv. **Regenerability:** Zeolites can be regenerated and reused multiple times without significantly losing their properties. S-

v. **Ion exchange property:** Zeolites exchange cations or anions with other ions in the solution they are present. This property makes them useful for the purification and softening of water.

vi. **Porosity:** Zeolites have a highly porous structure with a large surface area, which makes them useful as catalysts and adsorbents.

vii. **Acid resistance:** Zeolites are highly resistant to acidic conditions, making them useful in various applications in industries.

1.1.5.3. Modification of zeolite

Ion exchange is the most common method for modifying zeolites. Metal ions from groups such as alkali and alkaline earth, transition, and rare earth elements are frequently regarded as promoters for zeolite catalysts. Metal ion modification has been shown to improve zeolites' activity, selectivity, and stability (**Figure 1.9)**.[19]

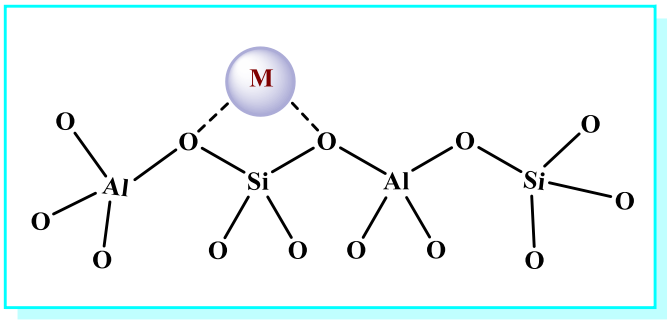

Figure 1.9. An ion-exchange method in the zeolite.

1.1.5.4. Applications of Zeolites

Zeolites have vast applications in industrial and agricultural—technical, medical, and commercial industries. Due to the wide range of applications of zeolite, it is also known as a magical stone. Zeolites can be used as catalysts in the petrochemical industry, adsorbents for water, soil, and air purification processes, and as detergents for laundry purposes. In the synthetic industry, zeolites are extensively employed due to their very high thermal stability, shape selectivity, and recyclability. Examples are Friedel-Craft alkylation and acylation reactions. Zeolites are suitable adsorbents used for water purification and softening. Zeolites can also separate specific gas, e.g., carbon dioxide, sulfur dioxide, and water removal from low-grade natural gas streams. In agriculture, a natural zeolite named “clinoptilolite” is used as a soil treatment by providing the slow release of potassium. Synthetic zeolites, when added to asphalt concrete, reduce the consumption of fossil fuels by releasing less carbon dioxide. Synthetic zeolites are widely used as a catalyst in petrochemical industries, generally in cracking reactions. Zeolites possess acidic properties and are also used in many acid-catalyzed reactions like esterification, alkylation, isomerization, etc. (**Figure 1.10)**[15]

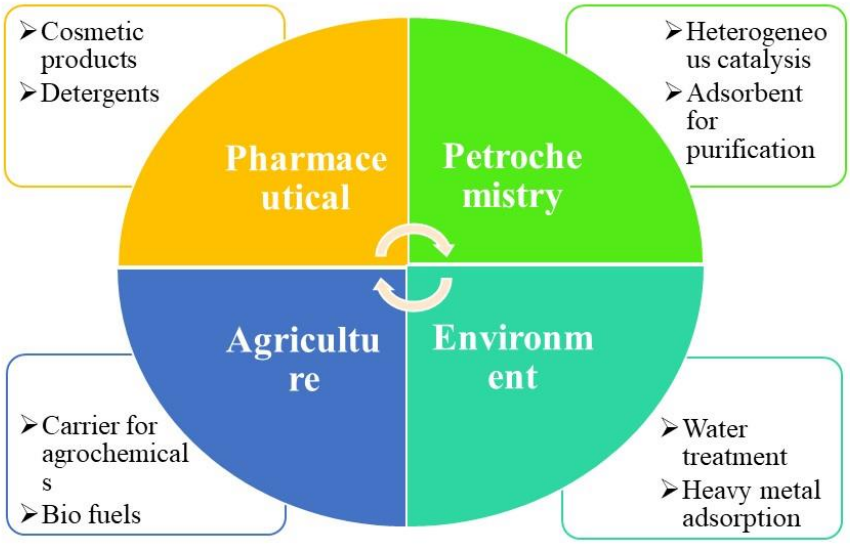

Figure 1.10. Overview of broad applications of zeolites.

1.2. Literature review

1.2.1. Esterification reactions

The esterification reaction is carried out only in the presence of a catalyst. Catalysts can either be homogeneous or heterogeneous catalysts, but the esterification reaction favors acid catalysts. Various catalysts used for the esterification reactions are discussed below.

Homogeneous catalysts

For the esterification reaction, a various homogeneous catalysts have been used, including H_2SO_4, HCl, H_3PO_4, p-toluene sulphonic acid, etc. These catalysts are utilized in synthesizing of acetins because they initiate higher glycerol (GLY) conversion, good product selectivity, and cost-effectiveness. These acids protonate the carbonyl group of the carboxylic acid, making it more reactive to the alcohol's nucleophilic attack.

Heterogenous catalysts

Heterogenous catalysts were used in place of homogeneous catalysts, as they provide recyclability, simpler separation from the reaction mixture, reusability, high activity, and thermal stability, heterogeneous due to which these are frequently utilized in esterification reactions.

1.2.1.1. Esterification of glycerol to produce esters

Earlier, the **esterification reaction of glycerol** was performed in the presence of a homogeneous catalyst such as HF, H_2SO_4, HNO_3, HCl, and PTSA.[3,20] However, these strong liquid acids are unfavorable because they are hazardous, corrosive, and challenging to remove from liquid products. To overcome these drawbacks, various solid acid catalysts used for the esterification reaction of GLY and AcA have been reported in the literature, like heteropolyacid-based ionic liquids,[21] transition metals oxides,[22] Amberlyst-36,[23,24] Amberlyst-15,[25,26] zeolites,[1,25,27–31] zirconia-based acid catalysts,[32] Cs-containing ZrO_2 catalyst,[33] propyl sulfonic acid functionalized SBA-15,[1] ion-exchange resins,[34] SnO_2-based solid acids,[35] lewatit catalyst,[36] molybdophosphoric heteropolyacid impregnated on HNTs,[37] sulphuric acid-functionalized siliceous zirconia,[38] $Fe_3O_4@SiO_2@SO_4^{2-}$,[39] $Fe_3O_4@SiO_2@PO_4^{3-}$,[40] alumina-based,[41] Polymer based-solid acid,[42] EPS Foam-Based PSSA Catalyst,[43] LFuS,[44] $[BS_2TMEDA]HPW_{12}O_{40}$,[45] TRGO,[46] Sn-DTP-K10 clay,[47] Zr-ZA,[31] Y_2O_3,[48] Steapsin lipase,[49] etc.

Zeolite as catalyst

Kirumakki et al., studied the liquid phase esterification of C3 and C4 alcohols on acetic acid using zeolites Hβ, HY, and HZSM5. Different alcohols were esterified with acetic acid under optimized reaction conditions: acetic acid: alcohol = 1:1 (mol/mol), catalyst amount 0.5 g, temperature 383 K, and time 1 hour. Alcohols are active in the following order: n-propyl > n-butyl > iso-propyl > iso-butyl alcohol, and zeolites in the following order: Hβ > HZSM5 > HY. The Eley-Rideal pathway was discovered to be used in the esterification reaction.[50]

Ferreira et al., neutralized the commercial HUSY zeolite (Si/Al = 30) by coating it with dodecamolybdophosphoric acid. To get NaUSY, the HUSY zeolite protons were interchanged with sodium ions by treating it with 2 M NaCl at 80 ℃ followed by washing with distilled water and drying at 120 ℃. Furthermore, the PMo-NaUSY catalyst was prepared by incorporation of dodecamolybdophosphoric acid on NaUSY by treating phosphoric acid and molybdenum (VI) oxide. The above-prepared catalyst (PMo-NaUSY) was utilized in 1.9 wt% amount for GLY acetylation with AcA to achieve 68% GLY conversion in acetins at optimized reaction conditions, 0.2 g of catalyst amount, AcA:GLY mole ratio 10:1, reaction temperature 120 ℃, and reaction time of 3 h.[27]

Zhou et al. used various solid catalysts like ion-exchange resins, Amberlyst15 (A-15-1, A-15-2), zeolites (HZSM-5, HUSY) to study the acetylation of glycerol and acetic acid. Reactions were onducted at 9:1 AcA:GLY mole ratio, at 110 ℃ and 3 h reaction time. Out of all the solid catalysts, A-15-1 showed maximum GLY conversion of 97.1%, followed by A-15-2 with 93.5% GLY conversion. HZSM-5 exhibit GLY conversion of 85.6% with 22.7%, and 7.7% of DAG and TAG. Also, HUSY showed 78.4% GLY conversion, 20.6% DAG, and 5.6% TAG.[25]

In addition, Marwan et al., performed GLY acetylation by employing heterogeneous chemically activated natural zeolites (CAN-zeolites), to acquire complete GLY conversion with 8.3% TGA selectivity at 90 ℃.[30]

Costa et al., investigated the glycerol acetylation utilizing various solid acid catalysts, including two microporous zeolites (H-ZSM-5 and H-Beta) and a mesoporous material (SBA-15 functionalized with propylsulfonic groups). The reaction was carried out with a 6:1 molar ratio of AcA:GLY, a catalyst dosage of 4 wt%, a reaction temperature of 120 ℃, and 4.5 hours of reaction time. The Pr-SO_3H-SBA-15 catalyst was shown to be effective. In 2.5 hours, the Pr-

SO_3H-SBA-15 catalyst proved to best, having higher conversion (96%) and selectivity to DAG and TAG (87%). Among the zeolites, HZSM-5 demonstrated the highest activity, with 40% MAG and 40% DAG, connected with the high acidic strength of HZSM-5's active sites.[1]

Cahyono et al., tested the Zr-Zeolite catalyst on glycerol acetylation with acetic acids to produce triacetin. This was accomplished by impregnating natural zeolite with $ZrOCl_2.8H_2O$ at 80 ℃ after activating it with a strong acid (H_2SO_4). At various temperatures, the catalyst's performance in the glycerol acetylation was assessed, and their results were evaluated in comparison to different commercial catalysts. For a catalyst concentration of 10%, reaction temperatures of 110 ℃, and a reaction time of 30 minutes, the findings for glycerol conversion and triacetin selectivity were 94.56% and 26%, respectively.[28]

Liu et al., synthesized the HZSM-5/MCM-41 catalyst by reacting ZSM-5 zeolite powder with NaOH and Na_2SiO_3 using CTAB as surfactant followed by autoclaving the reaction mixture for 48 hours at 120 ℃. Further, the mixture was subjected to H_2SO_4, crystallized, and washed numerous times with deionized water and ethanol. The obtained solid material was named ZSM-5/MCM-41 which was dried at 100 ℃ and calcined at 550 ℃ for 5 h. The synthesized catalyst was used for GLY acetylation, 1.5 g of catalyst efficiently utilized AcA to GLY having molar ratio 9:1, at 125 ℃, achieving 100% of GLY conversion and 81.9% of TGA selectivity in 24 h. The same catalyst was reused four times without any notable loss in its activity up to four cycles.[51]

Krisdiyanto et al., studied the diffractogram of X-ray diffraction analysis which revealed that zirconium-impregnated natural zeolite (ZA-Zr) catalysts were successfully synthesized. The treatment of zeolite with Zr metal impregnation increased the acidity of the zeolite to 6.79 mmol/gram for the ZA/Zr-10 catalyst. The existence of triacetin products was discovered after analyzing the esterification product base using infrared spectra and a mass spectrometry chromatogram.[31]

The majority of zeolite-based acidic heterogeneous catalysts used for GLY acetylation reaction were able to acquire high GLY conversion up to 100% having good thermal stability of up to 120 ℃ and longer reaction period of up to 24 h. One of the concerning things observed with this catalyst was low TGA selectivity and low reusability as mentioned in **Table 1.1**.

Table 1.1. Synthesis of glycerol esters using zeolites as heterogeneous catalysts.

Sr. No.	Mole ratio (GLY :AcA)	Catalyst/ amount (wt%)	Temp (°C)	Time (h)	GLY conversion (%)	Product (%)			Catalyst reusability	Ref
						MAG	DAG	TAG		
1.	10:1	PMo3_NaUSY/2	120	3.0	68.0	37.0	59.0	2.0	4	27
2.	-	NaUSY/1.9	-	3.0	14.0	64.0	25.0	1.0	-	27
3.	9:1	HUSY/2.65	110	4.5	78.4	-	20.6	5.6	-	25
4.	9:1	HZSM-5/2.65	110	4.5	85.6	-	25.7	7.7	-	25
5.	NR	Zr zeolite	110	0.5	94.56	7.0	68.0	26.0	-	28
6.	6:1	H-Beta/5	100	4.5	91.3	21.0	61.0	18.0	-	1
7.	6:1	H-ZSM-5/5	100	4.5	93.5	40.0	40.0	-	-	1
8.	9:1	HZSM-5/MCM-41/1.5	125	24	100	0.20	17.9	91.3	4	51
9.	9:1	ZM/1.5	125	24	92.6	55.9	23.4	20.7	-	51
10.	9:1	CAN-Zeolite^{M}/3	90	1.5	100	43.0	48.6	8.3	-	30
11.	9:1	CAN-Zeolite^{M}/3	90	1.0	95.0	80.1	15.4	4.5	-	30
12.	-	ZA-Zr	115	4	-	-	-	-	-	31

1.2.1.2. Esterification of levulinic acid to produce levulinate esters

Esterification of Levulinic acid can be performed in the liquid- phase using H_2SO_4, H_3PO_4 or HCl, PTSA.[52,53] The usage of homogeneous catalysts causes serious problems related to the environment, such as handling and transportation, toxicity, equipment corrosion, disposal, and regeneration. Due to the disadvantages of homogeneous catalysts, environment-friendly heterogeneous catalysts with significant catalytic activity, renewability, and stability in the reaction media have been developed. These heterogeneous catalysts are like PDVTA-SO_3H,[54] zirconia-based,[55–60] heteropoly acids,[61–68] silica-based,[69–73] zeolites,[74–82] bio-catalysts,[83–87] WO_3-SBA-16[88], wheat straw,[89] resins,[90–93] SAFBPIL,[94] carbon-based,[95–99] ammonium and silver co-doped phosphotungstic acid,[100] etc., used for different reactions.

Zeolite as catalyst

Fernandes et al., performed the esterification of levulinic acid and ethanol using various zeolites and it was found that H-MCM-22 gave the maximum conversion of 12% of levulinic acid at optimized conditions, levulinic acid: ethanol 1:5, catalyst amount 2.5 wt% at 70 ℃ for 5 h reaction time.[92]

Maheria et al., investigated all parameters for the esterification of levulinic acid with n-butyl alcohol using an H-BEA catalyst, covering the effect of acid-to-alcohol mole ratio, catalyst dosage, and reaction time. Experiments were conducted at acid-to-alcohol mole ratios of 1:6, 1:7, and 1:8 for 4 hours at a reaction temperature of 120 °C, resulting yield of 82.2%.[57]

Patil et al., used H-BEA0.10 as a catalyst to esterify levulinic acid with ethanol. The mole ratio of EtOH/LA was adjusted from 4 to 10 in order to determine the best reactant mole ratio, and maximum conversion was obtained at 6:1. After that, no significant change was observed. All the reactions were performed at 20 wt% catalyst loading for 5 h of reaction time at 78 ℃ reaction temperature.[79]

Nandiwale et al., synthesized H-ZSM-5 and Meso-HZ-5 to synthesize of octyl levulinate. Reactions were performed at 25.4 wt% of catalyst, reaction temperature 373 K, and the mole ratio of levulinic acid to octanol of 1:6 for 4 h of reaction time. The maximum yield obtained for Meso-HZ-5 was found to be 99% at optimized reaction conditions.[82]

Nandiwale et al., used a DH-ZSM-5 catalyst for esterifying levulinic acid with ethanol. Maximum levulinic acid conversion was obtained at optimum conditions: a catalyst to levulinic

acid ratio of 0.20, ethanol to levulinic acid mole ratio of 8:1, reaction temperature 393 K, and reaction time of 5 h.[77]

Nandiwale et al., investigated levulinic acid esterification using n-butanol. Micro/Meso-HZ-5 catalyst was used to select the optimum reaction parameters. The catalytic performance of the catalyst was studied by varying the reaction parameters like reaction time from 30 to 360 min and temperature from 373 to 403 K for a 6:1 reactant mole ratio at 20 wt% of catalyst loading. The best results were obtained at a temperature of 393 K with time of 300 min.[75]

Nandiwale et al., performed the synthesis of n-hexyl levulinate using a Hierarichal-HZ-5 catalyst. The reaction was carried out at temperature 401 K for 5 h. The mole ratio of 9 and catalyst to levulinic acid ratio of 0.24 are the optimum parameters for the maximum yield of ester. At optimized reaction conditions, the maximum yield of 97.4% for product i.e. n-hexyl levulinate was obtained.[81]

Dugkhuntod et al., Hierarchical ZSM-12 nanolayers were successfully synthesised using a one-pot hydrothermal technique for the catalytic esterification of levulinic acid with ethanol to ethyl levulinate. At optimized reaction conditions of Levulinic acid to ethanol mole ratio 1:1, catalyst loading of 10 wt% at 100 ℃ for 24 hours, 78.5% of levulinic acid conversion.[101]

Imeyn et al., carried out esterification of levulinic acid with ethanol over ZSM-12-120h catalyst for 24 h of reaction time at a temperature of 100 ℃, ethanol to levulinic acid mole ratio 1:1 with 0.1 g of catalyst dosage and 56.3% levulinic acid conversion and 87.2% of ethyl levulinate was achieved.[102]

Morawala et al., modified H-BEA zeolite using the TTAB to synthesize n-butyl levulinate at temperature 120 ℃, levulinic acid: n-butanol mole ratio, 1:10, catalyst, 13 wt%, the reaction time, 6 h, which exhibited maximum ester yield of 91.51% and 99% levulinic acid conversion.[103]

Morawala et al., synthesized n-butyl levulinate using mesoporous BETA zeolite. At a temperature of 120 °C, a mole ratio of levulinic acid:n-butanol of 1:7, a catalyst of 10% by weight, and a reaction period of 4 hours, a yield of 60.2% of n-butyl levulinate was achieved.[104]

Krishnamurthy et al., prepared various CornBEA zeolites to synthesize heptanol levulinate using heptanol and levulinic acid. Out of all the prepared catalysts, CornBEA (500) showed

the best result with 90% levulinic acid conversion at optimized reaction conditions, levulinic acid:heptanol 1:5, catalyst amount 100 mg, temperature 100 ℃ at a reaction time of 5 h.[105]

Table 1.2 displays a literature review for the esterification of levulinic acid with various alcohols utilizing zeolite as a catalyst. The excess reactants restrict the catalyst's active site, which results in a drop in conversion, and an increase in the mole ratio above a specific concentration inhibits the reactions, levulinic acid conversion depends significantly on the catalyst concentration in the reaction fluid. Ester yield rises as catalyst weight increases, while reaction yield declines after a certain weight. The existence of too many active sites may be the cause of increased ester yield.

Table 1.2. Synthesis of levulinate esters using zeolites.

Sr. No.	Reactants	Product	Catalyst/ amount	Mole ratio (LA:Alcohol)	Temp (°C)	Time (h)	Catalyst reusability	% Yield	Ref
1.	LA + Ethanol	Ethyl levulinate	H-MCM-22/2.5	1:5	70	5	-	-	92
2.	LA + n-Butanol	n-Butyl levulinate	H-BEA/ 10wt%	1:7	120	4	5	82.2	57
3.	LA + n-Butanol	n-Butyl levulinate	H-MOR/ 10wt%	1:7	120	4	-	29.5	57
4.	LA + n-Butanol	n-Butyl levulinate	H-Y/ 10wt%	1:7	120	4	-	32.2	57
5.	LA + n-Butanol	n-Butyl levulinate	H-ZSM-5/ 10wt%	1:7	120	6	-	30.6	57
6.	LA + Ethanol	Ethyl levulinate	H-$BEA_{0.10}$/ 20wt%	1:6	78	5	4	40	79
7.	LA + Octanol	Octyl levulinate	Meso-HZ-5/ 25.4wt%	1:7.56	120	4	7	99	82
8.	LA + Ethanol	Ethyl levulinate	DH-ZSM-5/ 20wt%	1:8	120	5	6	95	77
9.	LA + n-Butanol	n-Butyl levulinate	Micro/meso-HZ-5/ 20wt%	1:6	120	5	7	98	75
10.	LA + n-Hexanol	n-Hexyl levulinate	Hierarichal-HZ-5/ 24wt%	1:9	128	5	5	97.2	81
11.	LA + Ethanol	Ethyl levulinate	Hierarichal-ZSM-12/ 10	1:1	100	24	-	-	101
12.	LA + Ethanol	Ethyl levulinate	ZSM-12/ 0.1g	1:1	100	24	-	87.2	102
13.	LA + n-Butanol	n-Butyl levulinate	MTCK/ 13wt%	1:10	120	6	4	91.51	103
14.	LA + n-Butanol	n-Butyl levulinate	Mesoporous BEA/ 10wt%	1:7	120	4	4	90.7	104
15.	LA + Heptanol	Heptyl levulinate	CornBEA/ 100 mg	1:5	100	5	-	90	105

1.2.2. Transesterification of glycerol to produce glycerol carbonate

Homogeneous catalysts

Homogeneous catalysts like H_2SO_4 and p-tolenesulfonic acid have shown poor catalytic activity for transesterification reactions. In addition, these catalysts also have certain drawbacks, such as corrosion of reactors and pipelines and difficulty in separating them from the reaction mixture. Numerous homogeneous catalytic systems, such as K_2CO_3, trimethylamine, ionic liquids, and alkali and alkali earth metal hydroxides, are documented in the literature.[85] used for the synthesis of GC due to their high conversion rate under milder reaction conditions. Other basic catalysts like triethylamine and N-heterocyclic carbenes also show excellent conversion of GLY. However, one of the major challenges associated with these catalysts is the separation and neutralization of the catalyst after the reaction is completed.

Heterogeneous catalysts

Heterogeneous catalysts are typically more stable and easily separable from the reaction mixtures, making them more practical for industrial use. These catalysts often have higher surface areas and can be more easily optimized for specific reactions, allowing for greater control and efficiency in chemical processes. Heterogeneous catalysts are used in chemical reactions to increase the reaction rate without being consumed. In transesterification reactions, catalysts possessing basic properties are used to synthesize GC. However, acidic catalysts are not commonly used in the production of GC due to their lesser activity. Basic catalysts are utilized for the transesterification process of glycerol in the manufacture of GC. A variety of basic heterogeneous catalysts have been used by researchers in the past few decades *viz.*, MgO,[106,107] CaO,[108] CaO-ZrO_2,[109] Mg/ZnO,[110] Ca-Al hydrocalumite,[111] mixed oxides,[112–116] $NaAlO_2$ doped CaO,[117] Na_2SiO_3,[118] oil palm empty fruit bunch ash,[119] Ti-SBA-15,[120] Ni/FA,[121] K-TUD-1,[122] Co/MCM-41,[123] Mo/MCM-41,[124] K-zeolite,[125] anion exchange resins,[126] Na-based zeolites,[127] etc. Catalysts like metal oxides and mixed metal oxides show high GC yield and leaching problems that decrease their reusability property. Lithium nitrate shows a strong ion size effect of all alkali metals, which is responsible for creating strong basic sites. Literature shows some catalysts with lithium metal such as alkali metal silicates (Li, Na, K),[128] Li/CaO-La_2O_3,[129] Li/Mg composite,[130] $LiNO_3/Mg_4AlO_{5.5}$,[131] Li/ZnO,[132] Li/MCM-41,[133] Li/CFA,[134] Li_4SiO_4,[135] Li-oil palm ash zeolite,[136] Li/ZrO_2,[137] used for the transesterification reaction of GLY and DMC.

Zeolite as catalyst

Saiyong et al., used mild reaction conditions for the esterification of GLY with DMC over several basic zeolites. It was discovered that compared to homogeneous catalysts like NaOH and K_2CO_3, the NaY zeolite has a greater selectivity for GC (100%) than heterogeneous bases like CaO and SrO. Experiments with several base zeolites revealed that the transesterification reaction was highly dependent on catalyst structure. Base zeolites with tiny pore diameters, such as 3A, 4A, and NaZSM-5, were inactive under mild circumstances, but NaY and Na with larger pores displayed outstanding GC yields. A maximum yield of 80% was obtained at 10 wt% catalyst amount with GLY:DMC mole ratio 1:3, reaction time of 4 h at 70 ℃. Na-Y catalyst showed recyclability up to 5 reaction cycles.[128]

Algoufi et al., discovered that the synthesized K-zeolite was functional in the transesterification of GLY with DMC. GLY was completely converted into 96% GC at DMC:GLY mole ratio of 3:1, a catalyst loading of 4%, and a reaction temperature of 75 ℃, the procedure yielded 100% and 96% GC, respectively. The catalyst showed good stability during the recycling studies and was maintained for four consecutive runs.[126]

Table 1.3 displays the comparison of previously studied zeolites for the transesterification of glycerol. According to the literature, detection of product was performed using GC but, in our study, GC was calculated using NMR formula.

Table 1.3. Comparison with previously reported zeolites.

Sr. No.	Catalyst/ amount	Mole ratio (GLY: DMC)	Temp (℃)	Method for detection	% Yield	Time (h)	Selectivity of GC (%)	Catalyst reusability	Reaction kinetics	Ref
1.	Na-Y/ 10 wt%	1:3	70	GC	80	4	99	5	-	128
2.	K-Zeolite/ 4wt%	1:3	75	GC	96	1.5	100	4	-	126

1.2.3. Alkylation of indole with methyl vinyl ketone

Homogeneous catalysts

The synthesis of -indolylketone derivatives from indoles and -unsaturated carbonyl ketones at room temperature was carried out by Ji et al. using PTSA, which they found to be a reasonably priced, inventive, useful, and efficient catalyst. To produce maximum isolated yield (92%), 1 mmol of indole and 1 mmol of α,β-unsaturated with 0.1 mmol of PTSA were utilized in the presence of ethanol as the solvent. Different derivatives were also synthesized, and they exhibit good yield.[138]

Ekbote et al., used Polyvinylsulfonic acid as a homogeneous Brønsted acid catalyst. They studied the alkylation of indole reaction using indole and chalcone in 1:1 ratio dissolved in absolute ethanol; then the catalyst is dissolved, stirred, and heated to 80 °C for 6 hours. After that the reaction mixture is neutralized with a saturated sodium bicarbonate solution. The solid appeared, washed with cold water, then hot water and finally with cold ethanol, purified with column chromatography petroleum ether: ethyl acetate as solvent system. Isolated yield obtained up to 80%.[11]

Heterogeneous catalysts

Yadav et al., did alkylation of indole and 2-methylindole with electron-deficient olefins using indium trichloride as a catalyst. The reaction proceeded in dichloromethane at room temperature giving 3-alkylated indoles. The yield obtained was 90% and the catalyst was recovered and recycled.[139]

Reddy et al., did the alkylation of indole with various α,β-unsaturated ketones with bismuth triflate as a catalyst. The reaction has been studied at ambient temperature with acetonitrile as solvent for 1 to 2 h and produces the corresponding 3-alkylated indoles with excellent yields.[140]

Yadav et al. investigated the conjugate addition of indoles to α,β–unsaturated ketones using the innovative recyclable catalyst $Cu(OTf)_2$-[bmim]BF_4. The enones exhibit improved reactivity in ionic liquids, which speeds up the reaction process and dramatically raises yield. The reaction was carried out with 10% of the new catalyst, and 90% yield was attained. The catalyst was reused four to five times. To investigate the broadness of the substrate, 15 derivatives with yield of products ranging from 85 to 95% were synthesized.[141]

Huang et al., performed Michael addition reaction using 10 mol% GaI_3 as a catalyst. The reaction was between indoles and α, β-unsaturated ketones in CH_2Cl_2 at room temperature to

give 3-substituted indoles. The reaction was studied for various time periods which showed various yields. The yield obtained was as high as 90%. He also concluded that α,β-unsaturated aldehydes and esters do not give Michael addition products, under the same circumstances.[142]

Tahir et al. performed the alkylation of indole with fluorapatite-doped zinc bromide (Zn-FAP) as a heterogeneous solid acid catalyst. They used indole and their derivatives and olefin taken in a 1:1 mmol ratio and catalyst taken in acetonitrile and refluxed it. The crude product was washed with ethyl acetate and purified through column chromatography on silica gel (eluant: hexane/EtOAc 8:2). Yield obtained was up to 98%.[143]

Kawatsura et al., demonstrated the conjugate additions of heterocyclic compounds, including indoles, pyrrole, pyrazole, and imidazole, that are catalyzed by scandium chloride ($ScCl_3$) and hafnium chloride ($HfCl_4$). The conjugate addition of indoles to α,β-unsaturated carbonyl compounds was successfully catalyzed by $HfCl_4$, and the product was produced with excellent yield (99%). $HfCl_4$ or $ScCl_3$ may also be used to catalyze the pyrrole reaction, which resulted in up to 99% yields of 2,6-dialkylated pyrroles. Additionally, the 1-position of the pyrazoles and imidazoles underwent conjugate addition, which resulted in the production of several substituted heterocyclic compounds (17) in good yields.[144]

Yadav et al., used several catalysts to carry out the 100% atom-efficient Michael addition of indole to methyl vinyl ketone, facetted silica tube functionalized with sulfated zirconia was synthesized and then employed for this process. The influence of a mesoporous tubular structure on silica in forming mild acidic sites is explored. Tetraethylorthosilicate and (dl)-tartaric acid were used to manufacture these silica tubes in a basic solution. The effects of several parameters including agitation speed, catalyst loading, concentration, and temperature were examined on conversion and reaction rate. A kinetic model for the reaction was developed, and it was discovered that it follows the LHHW model with overall second-order kinetics due to poor species adsorption. The catalyst is reusable to a good extent.[145]

Zhang et al., investigated the effect of solvent on the alumina-promoted C3-alkylation of indoles with α,β-unsaturated ketones. Lipophilic solvents were typically preferable to hydrophilic solvents, with hexanes providing excellent yields of 3-alkyl indole derivatives. Thus, a new low-cost and straight forward procedure was performed for achieving this Michael alkylation using acidic alumina and hexanes. The scope has twenty-four substrate examples, with reaction yields ranging from 61% to 96%. This new technique comes out to be competitive because of the cost savings and ease of removing alumina through filtration.[146]

Table 1.4 displays the results obtained from the literature of past few years. According to the literature, reactions were performed in the presence of organic solvents which are not good for environment. The reusability of catalyst was not studied in the literature.

Table 1.4. Comparison with previously reported catalysts.

Sr. No.	Mole ratio (Indole: MVK)	Catalyst, amount	Temperature (°C)	Time	Solvent	Yield (%)	Catalyst reusability	Ref
1.	1:1	PTSA, 10 mol%	r.t.	2 h	Anhydrous ethanol	92	-	138
2.	1:1	PVSA, 10 mol%	80 °C	6 h	Ethanol	75	-	11
3.	1:1	$InCl_3$, 10 mol%	r.t.	3 h	Dichloromethane	90	-	139
4.	1:1	$Bi(OTf)_3$, 3 mol%	r.t.	1 h	Acetonitrile	90	-	140
5.	1:1	$Cu(OTf)_2$, 10 mol%	r.t.	3.5 h	[bmim]BF_4	90	-	141
6.	1:1	GaI_3, 10 mol%	r.t.	1 h	Dichloromethane	90	-	142
7.	1:1	Zn-FAP, 0.2 g	-	4 h	Acetonitrile	94	-	143
8.	1:1.5	$HfCl_4$, 0.1 mmol	r.t.	15 min	Acetonitrile	93	-	144
9.	1:1.5	$ScCl_3$, 0.1 mmol	r.t.	6 h	Acetonitrile	92	-	144
10.	1:1.3	SZ/ST. 0.02g/cm^3	60 °C	3 h	Toluene	-	-	145
11.	1:1.3	Al_2O_3	68 °C	2 h	Hexane	94	-	146

1.3. Justification of the present work

Based on the literature discussed in the above section, the following gaps have been observed.

i. These esterification/transesterification processes have reportedly been carried out using homogeneous catalysts. These liquid catalysts exhibit greater catalytic activity and selectivity for the desired products, but they also have some major drawbacks, such as reactor corrosion, difficulty in separating from the product/unreacted reactant, and difficulties of reuse in the reaction mixture. As a result, these issues have been dealt with heterogeneous catalysts that have been properly modified.
ii. In addition, when utilizing solid catalysts, deactivation of the catalyst and leaching of active sites are serious issues that limit the yield of the product, causing a gradual decline in the catalytic activity. To solve this issue, zeolites must be modified with the appropriate ingredient to the reaction systems.
iii. Zeolites have never been employed in the alkylation reaction of indole with methyl vinyl ketone.

1.4. Objectives

The following objectives have been set for the proposed work:

- To modify zeolites (e.g. mordenite, ZSM-5) with suitable metal (e.g. Ce, La, etc).
- Characterization of modified zeolites by EDS, XRD, SEM, BET, FTIR, TPD.
- To use the prepared catalysts in optimizing the reaction parameter in transalkylation and esterification reaction for better selectivity of the products.
- To study the kinetics of the alkylation/transalkylation and esterification reactions.

References

1 B. O. Dalla Costa, H. P. Decolatti, M. S. Legnoverde and C. A. Querini, *Catal. Today*, 2017, **289**, 222–230.

2 M. Pagliaro, R. Ciriminna, H. Kimura, M. Rossi and C. Della Pina, *Angew. Chemie - Int. Ed.*, 2007, **46**, 4434–4440.

3 K. Abida and A. Ali, *J. Indian Chem. Soc.*, 2022, **99**, 100459.

4 K. Yan, C. Jarvis, J. Gu and Y. Yan, *Renew. Sustain. Energy Rev.*, 2015, **51**, 986–997.

5 K. C. Badgujar, V. C. Badgujar and B. M. Bhanage, *Fuel Process. Technol.*, 2020, **197**, 106213.

6 P. Gautam, S. Barman and A. Ali, *Biofuels, Bioprod. Biorefining*, 2022, 1–21.

7 Z. I. Ishak, N. A. Sairi, Y. Alias, M. K. T. Aroua and R. Yusoff, *Catal. Rev. - Sci. Eng.*, 2017, **59**, 44–93.

8 A. O. Esan, A. D. Adeyemi and S. Ganesan, *J. Clean. Prod.*, 2020, **257**, 120561.

9 D. Procopio and M. L. Di Gioia, *Catalysts*, 2022, **12**, 50.

10 N. Rozulan, S. A. Halim, N. Razali and S. S. Lam, *Biomass Convers. Biorefinery*, 2022, **12**, 4665-4682.

11 S. S. Ekbote, A. G. Panda, M. D. Bhor and B. M. Bhanage, *Catal. Commun.*, 2009, **10**, 1569–1573.

12 M. J. Naim, O. Alam, J. Alam, F. Bano and P. Alam, *Int. J. Pharma Sci. Res.*, 2016, **7**, 51–62.

13 P. Gautam, S. Barman and A. Ali, *Int. J. Chem. React. Eng.*, 2020, **18,** 20200081.

14 P. Gautam, S. Barman and A. Ali, *ChemistrySelect*, 2022, **7**, 1–9.

15 Y. Li, L. Li and J. Yu, *Chem*, 2017, **3**, 928–949.

16 M. K. Gebru, *Miaphysite Christol.*, 2019, 1–18.

17 T. Derbe, S. Temesgen and M. Bitew, *Adv. Mater. Sci. Eng.*, 2021, 1-17.

18 M. Moliner, C. Martínez and A. Corma, *Angew. Chemie - Int. Ed.*, 2015, **54**, 3560–3579.

19 R. Saharan, G. Halder and S. Barman, *Int. J. Chem. React. Eng.*, 2019, **17**, 1–12.

20 Y. Liu, E. Lotero and J. G. Goodwin, *J. Mol. Catal. A Chem.*, 2006, **245**, 132–140.

21 M. Y. Huang, X. X. Han, C. Te Hung, J. C. Lin, P. H. Wu, J. C. Wu and S. Bin Liu, *J. Catal.*, 2014, **320**, 42–51.

22 W. Hu, Y. Zhang, Y. Huang, J. Wang, J. Gao and J. Xu, *J. Energy Chem.*, 2015, **24**, 632–636.

23 M. Aghbashlo, M. Tabatabaei, H. Rastegari and H. S. Ghaziaskar, *J. Clean. Prod.*, 2018, **183**, 1265–1275.

24 H. Rastegari, H. S. Ghaziaskar and M. Yalpani, *Ind. Eng. Chem. Res.*, 2015, **54**, 3279–3284.

25 L. Zhou, E. Al-Zaini and A. A. Adesina, *Fuel*, 2013, **103**, 617–625.

26 L. Zhou, T. H. Nguyen and A. A. Adesina, *Fuel Process. Technol.*, 2012, **104**, 310–318.

27 P. Ferreira, I. M. Fonseca, A. M. Ramos, J. Vital and J. E. Castanheiro, *Catal. Commun.*, 2009, **10**, 481–484.

28 R. B. Cahyono, Z. Mufrodi, A. Hidayat and A. Budiman, *ARPN J. Eng. Appl. Sci.*, 2016, **11**, 5194–5197.

29 J. Liu, Z. Wang, Y. Sun, R. Jian, P. Jian and D. Wang, *Chinese J. Chem. Eng.*, 2019, 1073–1078.

30 M. Marwan, E. Indarti, D. Darmadi, W. Rinaldi, D. Hamzah and T. Rinaldi, *Bull. Chem. React. Eng. & Catal.*, 2019, **14**, 672–677.

31 D. Krisdiyanto, T. Farihah and H. Supriyati, 2023, **12**, 61–67.

32 P. S. Reddy, P. Sudarsanam, G. Raju and B. M. Reddy, *Catal. Commun.*, 2010, **11**, 1224–1228.

33 K. Jagadeeswaraiah, M. Balaraju, P. S. S. Prasad and N. Lingaiah, *Appl. Catal. A Gen.*, 2010, **386**, 166–170.

34 S. Kale, S. B. Umbarkar, M. K. Dongare, R. Eckelt, U. Armbruster and A. Martin, *Appl. Catal. A Gen.*, 2015, **490**, 10–16.

35 B. Mallesham, P. Sudarsanam and B. M. Reddy, *Ind. Eng. Chem. Res.*, 2014, **53**, 18775–18785.

36 L. Setyaningsih, F. Siddiq and A. Pramezy, *MATEC Web Conf.*, 2018, **154**, 2–5.

37 A. B. S. Neto, A. C. Oliveira, E. Rodriguez-Castellón, A. F. Campos, P. T. C. Freire, F. F. F. Sousa, J. M. Filho, J. C. S. Araujo and R. Lang, *Catal. Today*, 2020, *349*,57-67.

38 K. Abida and A. Ali, *Chem. Pap.*, 2020, **74,** 3627-3639.

39 K. Abida, B. Chudasama and A. Ali, *J. Chem.*, 2020, **44,** 9365-9376.

40 K. Abida, A. Ali and R. Jindal, 2021.

41 S. A. Rane, S. M. Pudi and P. Biswas, *Chem. Biochem. Eng. Q.*, 2016, **30**, 33–45.

42 R. Mou, X. Wang, Z. Wang, D. Zhang, Z. Yin, Y. Lv and Z. Wei, *Fuel*, 2021, **302**, 121175.

43 R. Manurung, A. Saputra, H. Inarto and A. G. A. Siregar, *Rasayan J. Chem.*, 2022, **15**, 2053–2058.

44 R. Li, Z. Wei, H. Li, Z. Yin and Z. Wang, *Renew. Energy*, 2022, **201**, 125–134.

45 B. Guang, W. Zhang, Y. Wu, Y. Xiao, M. Su and Y. Liu, *Catal. Letters*, 2023, **153,** 1625-1634.

46 A. Malaika, K. Ptaszyńska, J. Gaidukevič and M. Kozłowski, *Fuel*, 2022, **313,** 122987.

47 J. Keogh, C. Jeffrey, M. S. Tiwari and H. Manyar, *Ind. Eng. Chem. Res.*, 2022.

48 A. Fidelis Uchenna, R. Irmawati, Y. H. Taufiq-Yap, S. Mohd Izham and U. I. Nda-Umar, *Arab. J. Chem.*, 2023, **16**, 104865.

49 P. J. Britto, R. M. Kulkarni, S. Veluturla and A. Narula, *Biocatal. Agric. Biotechnol.*,

2023, **48**, 102641.

50 S. R. Kirumakki, N. Nagaraju and K. V. R. Chary, *Appl. Catal. A Gen.*, 2006, **299**, 185–192.

51 J. Liu, Z. Wang, Y. Sun, R. Jian, P. Jian and D. Wang, *Chinese J. Chem. Eng.*, 2019, **27**, 1073–1078.

52 M. P. Negus, A. C. Mansfield and N. E. Leadbeater, *J. Flow Chem.*, 2015, **5**, 148–150.

53 B. C. Windom, T. M. Lovestead, M. Mascal, E. B. Nikitin and T. J. Bruno, *Energy and Fuels*, 2011, **25**, 1878–1890.

54 Y. Tian, R. Zhang, W. Zhao, S. Wen, Y. Xiang and X. Liu, *Catal. Letters*, 2020, **150**, 3553–3560.

55 Y. Kuwahara, W. Kaburagi, K. Nemoto and T. Fujitani, *Appl. Catal. A Gen.*, 2014, **476**, 186–196.

56 D. Unlu, O. Ilgen and N. Durmaz Hilmioglu, *Chem. Eng. Res. Des.*, 2017, **118**, 248–258.

57 K. C. Maheria, J. Kozinski and A. Dalai, *Catal. Letters*, 2013, **143**, 1220–1225.

58 F. Su, Q. Wu, D. Song, X. Zhang, M. Wang and Y. Guo, *J. Mater. Chem. A*, 2013, **1**, 13209–13221.

59 N. A. S. Ramli, D. Sivasubramaniam and N. A. S. Amin, *Bioenergy Res.*, 2017, **10**, 1105–1116.

60 G. D. Yadav and A. R. Yadav, *Chem. Eng. J.*, 2014, **243**, 556–563.

61 Q. jie Luan, L. jun Liu, S. wen Gong, J. Lu, X. Wang and D. mei Lv, *Process Saf. Environ. Prot.*, 2018, **117**, 341–349.

62 M. Wu, Q. Q. Zhao, J. Li, H. Y. Wu, X. C. Zheng, X. X. Guan and P. Liu, *J. Exp. Nanosci.*, 2016, **11**, 1331–1347.

63 S. Dharne and V. V. Bokade, *J. Nat. Gas Chem.*, 2011, **20**, 18–24.

64 N. Lucas, L. Gurrala and A. Athawale, *J. Porous Mater.*, 2019, **26**, 1335–1343.

65 K. Manikandan and K. K. Cheralathan, *Appl. Catal. A Gen.*, 2017, **547**, 237–247.

66 G. Pasquale, P. Vázquez, G. Romanelli and G. Baronetti, *Catal. Commun.*, 2012, **18**, 115–120.

67 M. Wu, X. Zhang, X. Su, X. Li, X. Zheng, X. Guan and P. Liu, *Catal. Commun.*, 2016, **85**, 66–69.

68 C. B. Vilanculo, L. C. de Andrade Leles and M. J. da Silva, *Waste and Biomass Valorization*, 2020, **11**, 1895–1904.

69 J. A. Melero, G. Morales, J. Iglesias, M. Paniagua, B. Hernández and S. Penedo, *Appl. Catal. A Gen.*, 2013, **466**, 116–122.

70 K. Yan, G. Wu, J. Wen and A. Chen, *Catal. Commun.*, 2013, **34**, 58–63.

71 R. Maggi, N. R. Shiju, V. Santacroce, G. Maestri, F. Bigi and G. Rothenberg, *Beilstein J. Org. Chem.*, 2016, **12**, 2173–2180.

72 N. A. S. Ramli, N. I. Hisham and N. A. S. Amin, *Sains Malaysiana*, 2018, **47**, 1131–1138.

73 F. Yang and J. Tang, *ChemistrySelect*, 2019, **4**, 1403–1409.

74 A. Najafi Chermahini and M. Nazeri, *Fuel Process. Technol.*, 2017, **167**, 442–450.

75 K. Y. Nandiwale and V. V. Bokade, *Chem. Eng. Technol.*, 2015, **38**, 246–252.

76 P. Parthasarathy and S. K. Narayanan, *Environ. Prog. Sustain. Energy*, 2014, **33**, 676–680.

77 K. Y. Nandiwale, P. S. Niphadkar, S. S. Deshpande and V. V. Bokade, *J. Chem. Technol. Biotechnol.*, 2014, **89**, 1507–1515.

78 K. Y. Nandiwale, S. K. Sonar, P. S. Niphadkar, P. N. Joshi, S. S. Deshpande, V. S. Patil and V. V. Bokade, *Appl Catal A-Gen*, 2013, **460**, 90-98.

79 C. R. Patil, P. S. Niphadkar, V. V. Bokade and P. N. Joshi, *Catal. Commun.*, 2014, **43**, 188–191.

80 M. Wu, Q. Q. Zhao, J. Li, X. L. Su, H. Y. Wu, X. X. Guan and X. C. Zheng, *J. Porous*

Mater., 2016, **23**, 1329–1338.

81 K. Y. Nandiwale and V. V. Bokade, *Process Saf. Environ. Prot.*, 2016, **99**, 159–166.

82 K. Y. Nandiwale, S. K. Yadava and V. V. Bokade, *J. Energy Chem.*, 2014, **23**, 535–541.

83 G. D. Yadav and I. V. Borkar, *Ind. Eng. Chem. Res.*, 2008, **47**, 3358–3363.

84 K. C. Badgujar and B. M. Bhanage, *Fuel Process. Technol.*, 2015, **138**, 139–146.

85 A. Lee, N. Chaibakhsh, M. B. A. Rahman, M. Basri and B. A. Tejo, *Ind. Crops Prod.*, 2010, **32**, 246–251.

86 L. Zhou, Y. He, L. Ma, Y. Jiang, Z. Huang, L. Yin and J. Gao, *Bioresour. Technol.*, 2018, **247**, 568–575.

87 H. M. Salvi and G. D. Yadav, *Biocatal. Agric. Biotechnol.*, 2019, **18**, 101038.

88 S. S. Enumula, V. R. B. Gurram, R. R. Chada, D. R. Burri and S. R. R. Kamaraju, *J. Mol. Catal. A Chem.*, 2017, **426**, 30–38.

89 C. Chang, G. Xu and X. Jiang, *Bioresour. Technol.*, 2012, **121**, 93–99.

90 M. B. Kokare, V. Ranjani and C. S. Mathpati, *Chem. Eng. Res. Des.*, 2018, **137**, 577–588.

91 M. A. Tejero, E. Ramírez, C. Fité, J. Tejero and F. Cunill, *Appl. Catal. A Gen.*, 2016, **517**, 56–66.

92 D. R. Fernandes, A. S. Rocha, E. F. Mai, C. J. A. Mota and V. Teixeira Da Silva, *Appl. Catal. A Gen.*, 2012, **425**–**426**, 199–204.

93 V. Trombettoni, L. Bianchi, A. Zupanic, A. Porciello, M. Cuomo, O. Piermatti, A. Marrocchi and L. Vaccaro, *Catalysts*, , DOI:10.3390/catal7080235.

94 A. G. Khiratkar, K. R. Balinge, M. Krishnamurthy, K. K. Cheralathan, D. S. Patle, V. Singh, S. Arora and P. R. Bhagat, *Catal. Letters*, 2018, **148**, 680–690.

95 M. M. Zainol, M. Asmadi and N. A. S. Amin, *Chem. Eng. Sci.*, 2022, **247**, 117079.

96 M. M. Zainol, N. Aishah, S. Amin and M. Asmadi, *Renew. Energy*, 2019, **130**, 547–

557.

97 X. C. Zheng, N. Li, M. Wu, X. X. Guan and X. L. Zhang, *Res. Chem. Intermed.*, 2017, **43**, 6651–6664.

98 M. M. Zainol, N. A. S. Amin and M. Asmadi, *Fuel Process. Technol.*, 2017, **167**, 431–441.

99 C. Liu, K. Zhang, Y. Liu and S. Wu, 2019, **14**, 2186–2196.

100 X. Zhou, Z. X. Li, C. Zhang, X. P. Gao, Y. Z. Dai and G. Y. Wang, *J. Mol. Catal. A Chem.*, 2016, **417**, 71–75.

101 P. Dugkhuntod, T. Imyen, W. Wannapakdee, T. Yutthalekha, S. Salakhum and C. Wattanakit, *RSC Adv.*, 2019, **9**, 18087–18097.

102 T. Imyen, K. Saenluang, P. Dugkhuntod and C. Wattanakit, *Microporous Mesoporous Mater.*, 2020, 110768.

103 D. H. Morawala, D. R. Lathiya, A. K. Dalai and K. C. Maheria, *Catal. Today*, 2020, **348**, 177–186.

104 D. H. Morawala, A. K. Dalai and K. C. Maheria, *Catal. Letters*, 2020, **150**, 1049–1060.

105 M. Swaminathan and M. Krishnamurthy, 2022, Available at SSRN 4290471.

106 M. Manikandan and P. Sangeetha, *ChemistrySelect*, 2019, **4**, 6672–6678.

107 F. Paquin, J. Rivnay, A. Salleo, N. Stingelin and C. Silva, *J. Mater. Chem. C*, 2015, **3**, 10715–10722.

108 W. Roschat, S. Phewphong, T. Kaewpuang and V. Promarak, *Mater. Today Proc.*, 2018, **5**, 13909–13915.

109 X. Zhang, S. Wei, X. Zhao, Z. Chen, H. Wu, P. Rong, Y. Sun, Y. Li, H. Yu and D. Wang, *Appl. Catal. A Gen.*, , DOI:10.1016/j.apcata.2019.117313.

110 G. Pradhan and Y. C. Sharma, *Fuel*, 2021, **284**, 118966.

111 L. Zheng, S. Xia, X. Lu and Z. Hou, *Cuihua Xuebao/Chinese J. Catal.*, 2015, **36**,

1759–1765.

112 M. Malyaadri, K. Jagadeeswaraiah, P. S. Sai Prasad and N. Lingaiah, *Appl. Catal. A Gen.*, 2011, **401**, 153–157.

113 G. Parameswaram, P. S. N. Rao, A. Srivani, G. N. Rao and N. Lingaiah, *Mol. Catal.*, 2018, **451**, 135–142.

114 Y. Li, H. Zhao, W. Xue, F. Li and Z. Wang, *Nanomaterials*, 2022, **12**, 1972.

115 S. E. Kondawar, C. R. Patil and C. V. Rode, *ACS Sustain. Chem. Eng.*, 2017, **5**, 1763–1774.

116 P. Zhang, Y. Chen, M. Zhu, C. Yue, Y. Dong, Y. Leng, M. Fan and P. Jiang, *Catal. Letters*, 2020, **150**, 2863–2872.

117 A. Chotchuang, P. Kunsuk, A. Phanpitakkul, S. Chanklang, M. Chareonpanich and A. Seubsai, *Catal. Today*, 2022, **388**–**389**, 351–359.

118 S. Wang, P. Hao, S. Li, A. Zhang, Y. Guan and L. Zhang, *Appl. Catal. A Gen.*, 2017, **542**, 174–181.

119 P. U. Okoye, S. Wang, L. Xu, S. Li, J. Wang and L. Zhang, *Energy Convers. Manag.*, 2019, **179**, 192–200.

120 P. Devi, U. Das and A. K. Dalai, *Chem. Eng. J.*, 2018, **346**, 477–488.

121 S. Bepari, N. C. Pradhan and A. K. Dalai, *Catal. Today*, 2017, **291**, 36–46.

122 S. Arora, V. Gosu and V. Subbaramaiah, *Mol. Catal.*, 2020, **496**, 111188.

123 S. Arora, V. Gosu, V. Subbaramaiah and T. C. Zhang, *Can. J. Chem. Eng.*, 2021, 1868–1883.

124 P. Sikarwar, U. K. A. Kumar, V. Gosu and V. Subbaramaiah, *J. Environ. Chem. Eng.*, 2018, **6**, 1736–1744.

125 Y. T. Algoufi and B. H. Hameed, *Fuel Process. Technol.*, 2014, **126**, 5–11.

126 A. V. Shvydko, S. A. Prihod'ko and M. N. Timofeeva, *Catal. Ind.*, 2022, **14**, 181–188.

127 S. Pan, L. Zheng, R. Nie, S. Xia, P. Chen and Z. Hou, *Cuihua Xuebao/Chinese J.*

Catal., 2012, **33**, 1772–1777.

128 N. Hindryawati, G. P. Maniam, M. R. Karim and K. F. Chong, *Eng. Sci. Technol. an Int. J.*, 2014, **17**, 95–103.

129 H. Maleki, M. Kazemeini, A. S. Larimi and F. Khorasheh, *J. Ind. Eng. Chem.*, 2017, **47**, 399–404.

130 Z. Liu, B. Li, F. Qiao, Y. Zhang, X. Wang, Z. Niu, J. Wang, H. Lu, S. Su, R. Pan, Y. Wang and Y. Xue, *ACS Omega*, 2022, **7,** 5032-5038.

131 Z. Liu, J. Wang, M. Kang, N. Yin, X. Wang, Y. Tan and Y. Zhu, *J. Ind. Eng. Chem.*, 2015, **21**, 394–399.

132 X. Song, Y. Wu, F. Cai, D. Pan and G. Xiao, *Appl. Catal. A Gen.*, 2017, **532**, 77–85.

133 S. Arora, V. Gosu, U. K. A. Kumar and V. Subbaramaiah, *J. Clean. Prod.*, 2021, **295**, 126437.

134 S. Arora, V. Gosu, V. Subbaramaiah and B. H. Hameed, *J. Environ. Chem. Eng.*, 2021, **9**, 105999.

135 J. X. Wang, K. T. Chen, J. S. Wu, P. H. Wang, S. T. Huang and C. C. Chen, *Fuel Process. Technol.*, 2012, **104**, 167–173.

136 W. A. Khanday, P. U. Okoye and B. H. Hameed, *Energy Convers. Manag.*, 2017, **151**, 472–480.

137 A. Kaur and A. Ali, *Ind. Eng. Chem. Res.*, 2020, **59**, 2667–2679.

138 S. Ji and S. Wang, 2005, *Ultrason. Sonochem.*, **12**, 339–343.

139 S. Abraham, B. V. S. Reddy and G. Sabitha, *Synth.*, 2001, 2165–2169.

140 A. V. Reddy, K. Ravinder, T.V. Goud, P. Krishnaiah, T.V. Raju and Y. Venkateswarlu, *Tetrahedron Lett.*, 2003, **44**, 6257–6260.

141 J. S. Yadav, B. V. S. Reddy, G. Baishya, K. V Reddy and A. V Narsaiah, *Tetrahedron*, 2005, **61**, 9541–9544.

142 Z. Huang, J. Zou and W. Jiang, *Tetrahedron Lett.*, 2006, **47**, 7965–7968.

143 R. Tahir and K. Banert, *Appl Catal A-Gen.,* 2006, **315**, 147–149.

144 M. Kawatsura, S. Aburatani and J. Uenishi, *Tetrahedron*, 2007, **63**, 4172–4177.

145 G. D. Yadav and A. R. Yadav, *Microporous Mesoporous Mater.*, 2014, **195**, 180–190.

146 X. Zhang, E. J. Mensah, J. Deobald and J. Magolan, *Adv. Synth. Catal.*,2019, **361,** 5548-5551.

CHAPTER 2

MATERIALS, SYNTHESIS AND CHARACTERIZATION OF CATALYSTS

Chapter 2 covers the topics of materials, synthesis, and characterization of catalysts, providing a comprehensive description of the materials utilized in this study, modification of the catalysts, experimental procedure, product analysis, and catalyst characterization techniques for esterification, transesterification, and alkylation reactions. Since different modified catalysts are used in the current work, it is essential to characterize them to understand how loading affects the modification of the zeolites. Commercially available HZSM-5, USY, Beta, and ammonium forms of mordenite zeolites were modified with different metals and functional groups and used as catalysts for esterification, transesterification, and alkylation processes. The characterization of the zeolites involved a range of techniques including EDS, XRD, SEM, TEM, XPS, DLS, BET, and TPD. These techniques were employed to quantify the loading into the zeolite and to analyze its impact on crucial parameters of the parent zeolite, such as crystallinity, morphology, particle size, acidity, and surface area.

2.1. Chemicals

The following chemicals were procured from Alfa Aesar Company:

- HZSM-5 zeolite
- Y zeolite
- Beta zeolite
- Mordenite zeolite

The following chemicals were procured from Loba Chemie Pvt. Ltd.:

- Extra pure glycerol
- Sulphuric acid (98% extra pure)
- Solvents like ethanol, ethyl acetate, hexane, and methanol
- Potassium nitrate ($KMnO_4$)
- Lithium nitrate ($LiNO_3$), magnesium nitrate ($Mg(NO_3)_2$), and potassium nitrate (KNO_3)

The following chemicals were procured from Spectrochem:

- Glacial acetic acid
- Dimethyl carbonate
- Ethanol (>99%), propanol (>99%), and butanol (>99%)
- Indole
- Methyl vinyl ketone

The following chemical was procured from CDH Chemicals India Ltd.:

- Ammonium ceric nitrate

The following chemical was procured from Sigma Aldrich (USA):

- D_2O and $CDCl_3$ were used for NMR

2.2. Catalyst modification

2.2.1. Modification of HZSM-5 zeolite

The HZSM-5 zeolite obtained was already in the H form. Prior to the ion exchange procedure, the sample was heated for three hours at 623 K to remove contaminants, moisture, or gas from the zeolite surface and pores. The process of modification is shown in **Figure 2.1**. Zeolite was modified by the ion exchange procedure, which involved putting a precise amount of zeolite into a solution of ceric ammonium nitrate in a flat bottom flask. The HZSM-5 zeolite was refluxed with 1 %, 3 %, 5 %, and 7 % of ceric ammonium nitrate solutions. The modified zeolites were designated Ce_1ZSM-5, Ce_3ZSM-5, Ce_5ZSM-5, and Ce_7ZSM-5, respectively.,. The round-bottom flask was fitted with a refluxing setup and subjected to continuous heating and swirling at 373 K for 24 hours. Following this, the modified zeolite was filtered and thoroughly washed using deionized water to eliminate any excess ions. Lastly, the CeZSM-5 was dried at 333 K for 14 hours and subsequently calcined at 823 K for 4 hours under atmospheric environment.[1]

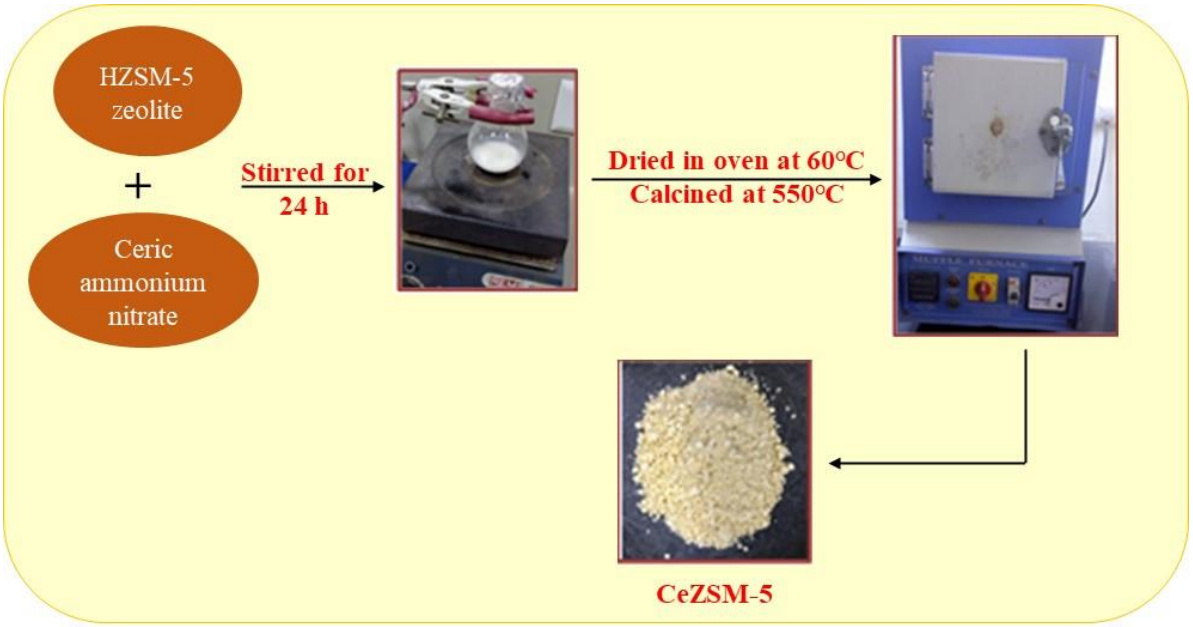

Figure 2.1. Steps for the synthesis of the CeZSM-5 composite.

2.2.2. Modification of Y zeolite

Zeolite is dried out by being calcined at 623 K for three hours before usage. Then it is refluxed with a 0.5 M sulfuric acid solution, which is to be taken in the 1:4 mole ratios of zeolite and

sulfuric acid solution. After 6 hours of refluxing, the catalyst is filtered, and it was washed with distilled water to maintain a neutral pH. Subsequently, the catalyst was dried in an air-dry oven at 100 ℃ overnight and later calcined at 500 ℃ for 2 hours under atmospheric environment. Thus, zeolite Y is modified with sulfuric acid and named SY shown in **Figure 2.2.**[2]

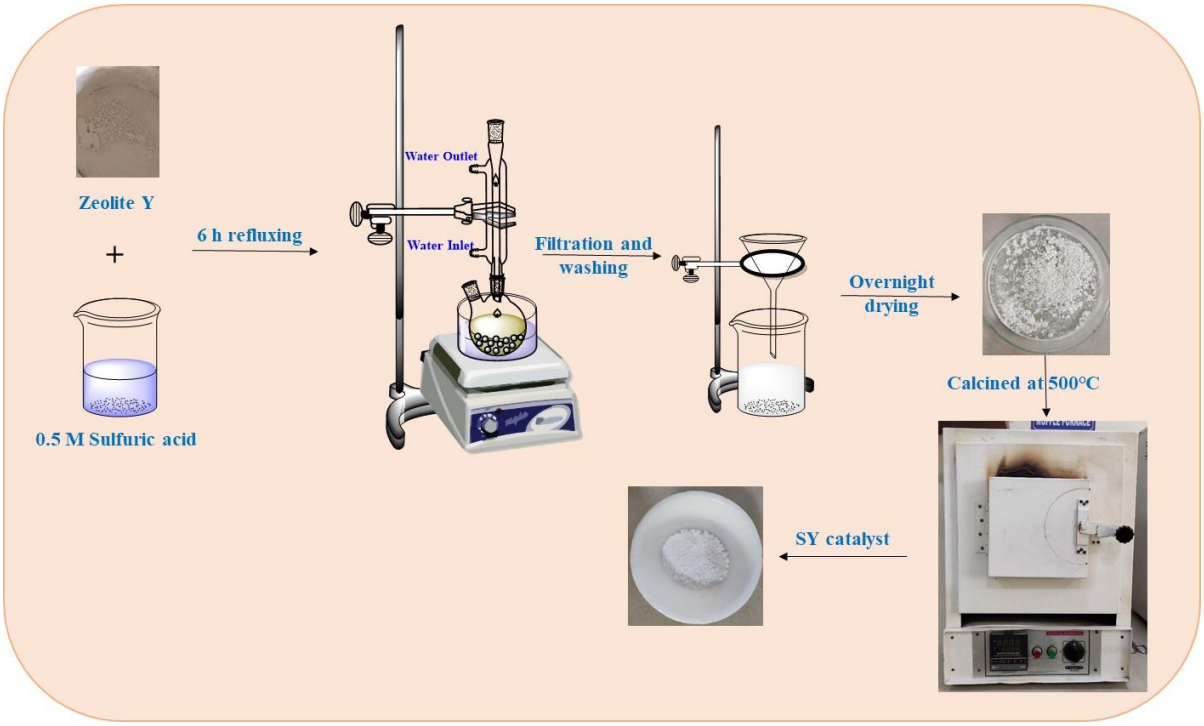

Figure 2.2. Diagrammatic representation of the steps of the Modification of zeolite Y using sulfuric acid.

2.2.3. Modification of beta zeolite

Zeolite was calcined at 350 °C for 3 hours to change it from its ammonium form to its hydrogen form. By this step, the H-form of zeolite beta was prepared and was ready to be used in the reaction. 30 ml solution of lithium nitrate salt was prepared at a particular concentration and was mixed with 1g of zeolite beta. The solution mentioned above was continuously mixed at 35 °C for 4 h. It was then oven-dried at 120 °C for 12 h. At last, the calcination process of the obtained white powder was done at 700 ℃ for 4 h under atmospheric environment. Thus, the incorporation of lithium in the zeolite was done by this procedure. Similarly, the same procedure impregnated metals like Mg and K on the zeolite. Different concentrations of metal-modified zeolite were designated as $Li_x\beta$ where x represents metal content in wt%, M represents loaded metal, and β represents zeolite beta. The flowchart of the modification process of zeolite beta is shown in **Figure 2.3**.

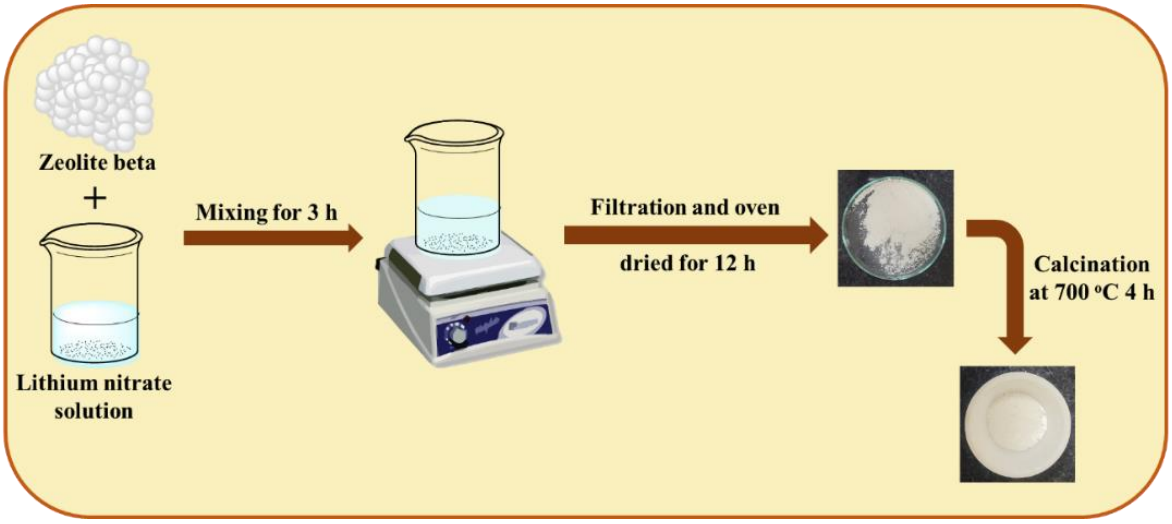

Figure 2.3. Diagrammatic representation of Li-modified zeolite beta.

2.2.4. Modification of mordenite zeolite

The first step was completely drying out the moisture in the mordenite zeolite by calcining it at 200 °C for two hours. Then, a beaker containing a solution of sulfuric acid with a 3 M concentration was filled with 500 mg of zeolite. The above-prepared solution was stirred at 35 °C for around 12 hours. Overnight, the solution was dried in the oven after filtering. The sample obtained was calcined at 500 °C for 2 hours under atmospheric environment, and white-colored powder was obtained, which is sulfuric acid-modified mordenite zeolite (Figure 2.4).

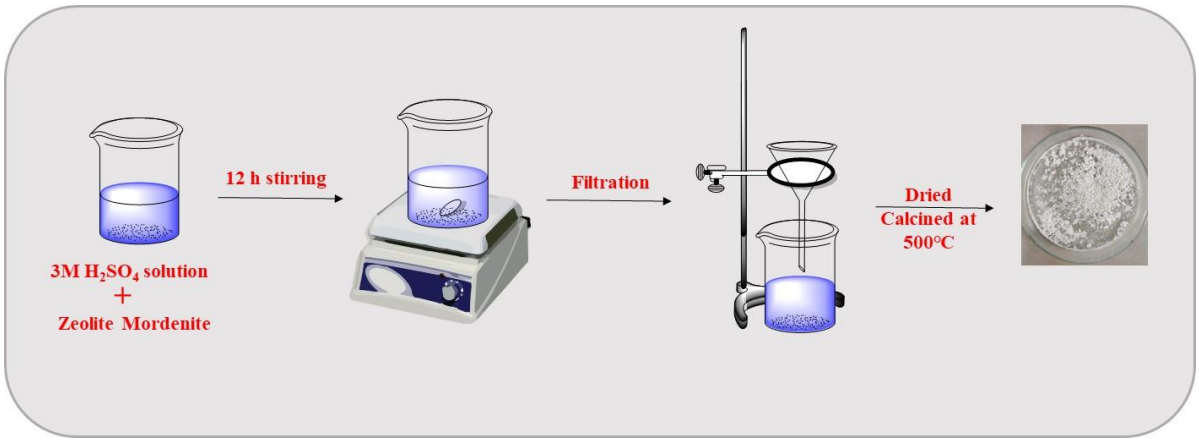

Figure 2.4. Diagrammatic representation of sulfuric acid-treated mordenite zeolite.

2.3. Experimental procedure

2.3.1. Synthesis of esters of glycerol

The experiment was conducted in a 100 mL two-necked round bottom flask outfitted with a water-cooled condenser, magnetic stirrer, oil bath, and thermometer. For the synthesis of mono and diacetin, experiments were conducted with a variety of parameters, including the acetic acid to glycerol mole ratio (1 to 11), reaction temperature (30-120 °C), and catalyst loading (2-10 wt%). At a particular time interval, the aliquots were withdrawn and analyzed in an HPLC.

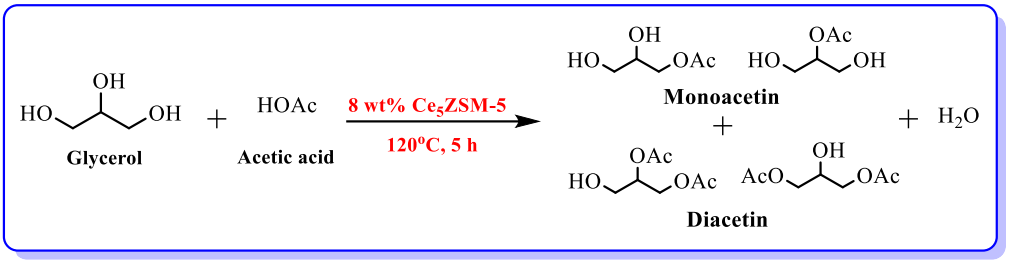

Scheme 2.1. Synthesis of glycerol esters.

2.3.2. Synthesis of levulinate esters

The esterification of levulinic acid with alcohol was conducted in a 100 mL two-necked round bottom flask equipped with a thermocouple, water-cooled condenser, and magnetic stirrer to control the reaction temperature. The study investigated the impact of various parameters, including reactant mole ratio, reaction time, reaction temperature, and catalyst weight percentage. The experiments encompassed a levulinic acid to alcohol mole ratio ranging from 1:1-1:13, reaction times of 1 to 5 hours, reaction temperatures from 40 ℃ to 100 ℃, and catalyst weight percentages of 2 to 12 wt %, aiming to optimize product yield. After completion of the reaction, the catalyst was separated using the centrifugation method. Subsequently, the remaining ester and water in the reaction mixture were separated using the rotary evaporator. Each experimental run was performed in triplicates, and average values were calculated for data analysis. The collected samples were analyzed using High-Performance Liquid Chromatography (HPLC) technique.

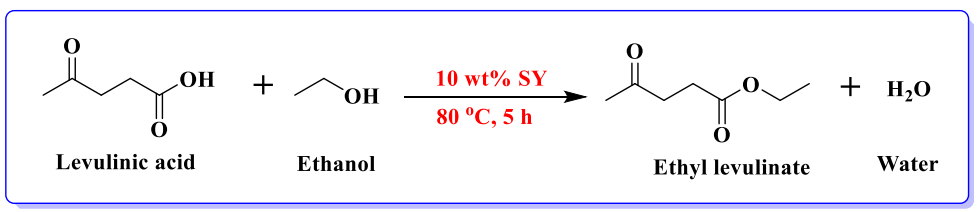

Scheme 2.2. Synthesis of levulinate esters.

2.3.3. Synthesis of glycerol carbonate

A metal-modified zeolite beta catalyst was used to transesterify GLY and DMC to produce GC. In this experiment, the catalyst and reactants were mixed in a 50 mL two-necked round bottom flask (RBF) and positioned inside the oil bath. The oil bath was equipped with a water-cooling condenser, and was placed on a magnetic stirrer, to which a thermocouple was attached. The magnetic stirrer and thermocouple were inserted into the oil bath to monitor the reaction temperature. In a typical reaction, 0.054, and 0.107 moles of GLY and DMC were added in RBF before the precise quantity of the appropriate catalyst was added. The reaction was carried out at 95 °C for 4 h. Aliquots were taken out after every hour to check the performance of the catalyst and its feasibility for the scale-up reaction, where its reusability was checked. Thin Layer Chromatography (TLC) was adopted to observe the reaction's progress having ethyl acetate as the mobile phase and aluminum silica plates as the stationary phase. Firstly, TLC was run in the ethyl acetate solvent, and after that, it was air-dried and dipped in the $KMnO_4$ solution. The brown color of the present components was developed on the TLC plate against the purple color of $KMnO_4$ by gently heating it with a hot air gun. The reaction was stopped when it reached the desired point, and the catalyst was isolated from the reaction via filtration or centrifugation method and washed with methanol. It was dried in an oven at 120 °C overnight and recalcined at 700 °C. The left-out reaction mixture containing DMC and methanol was evaporated using a rotary evaporator at 65 °C. A blank reaction was also performed to check the role of Li present in the catalyst. The GC obtained was then characterized by ^{1}H-NMR, ^{13}C NMR, and FTIR spectroscopy.

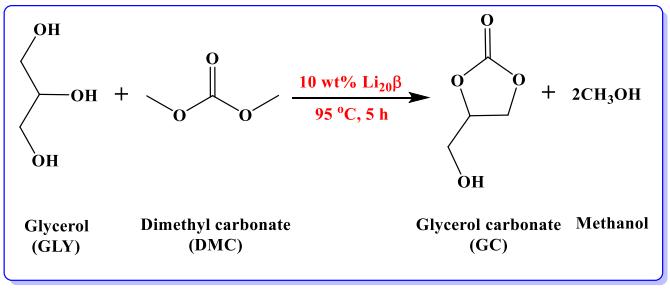

Scheme 2.3. Synthesis of glycerol carbonate.

2.3.4. Synthesis of 3-alkylated indole

The alkylation of indole with methyl vinyl ketone using sulfuric acid-modified mordenite zeolite was performed in a 10 mL reaction tube which was sealed from the top. The reaction was performed at 35 ℃ and the thermocouple dipped in the oil bath maintained the temperature of the reaction placed on the magnetic stirrer. In the glass tube, indole and methyl vinyl ketone were added followed by the addition of sulfuric acid-modified mordenite zeolite and 2 mL of ethanol as solvent. Several reaction conditions were investigated for the catalyzed reaction. The catalyst concentration ranged from 2.5 to 10 wt%, and ethanol was utilized as the solvent. The reaction time varied between 5 to 20 minutes, and the ratio of indole to methyl vinyl ketone equiv. was adjusted from 1:1 to 1:3 equiv. Once the reaction was complete, the catalyst was recovered through filtration, and the excess solvent was removed using a rotary evaporator. The obtained product underwent purification via column chromatography, and its structure was confirmed by ^{1}H-NMR and ^{13}C NMR.

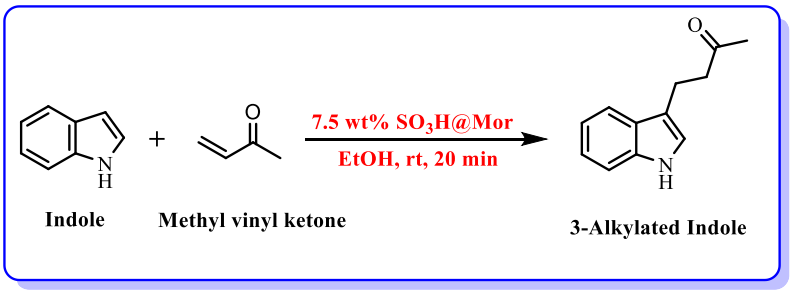

Scheme 2.4. Synthesis of 3-alkylated indole.

2.4. Product analysis

2.4.1. Analysis of esters of glycerol

High-Pressure Liquid Chromatography (HPLC) was used to analyze and quantify the product. The instrument used was an Agilent 1260 infinity series HPLC with a refractive index (RI) detector. A column with 5 mm particles and an inner diameter of 4.6 mm makes up the stationary phase. The RX-SIL column was used for the esterification of GLY with AcA, and the ratio of IPA to hexane of 60/40: v/v was used as the mobile phase with a flow rate of 0.6 mL/min.

The selectivity of each product and conversion of glycerol were calculated as follows:

$$Glycerol\ conversion\ (\%) = \frac{amount\ of\ glycerol\ converted}{total\ amount\ of\ glycerol} \times 100$$

$$Selectivity\ (\%) = \frac{amount\ of\ glycerol\ converted\ to\ product}{total\ amount\ of\ converted\ glycerol} \times 100$$

2.4.2. Analysis of levulinate esters

The instrument Agilent 1260 infinite series HPLC with a refractive index (RI) detector was used for the analysis and quantification. The C18 column (250 × 4.6 mm, 5µm) was used to esterify LA with different alcohols. Also, the 30:70 (v/v) ratio of acetonitrile (ACN) to water was taken with a flow rate of 0.3 mL/min. 20 µL sample was injected into the system to analyze every sample using a RI (refractive index) detector. The product was quantified by calculating the percentage of the peak area related to the reactant (GLY) and product of the specified reaction with respect to the total area of the chromatogram.

2.4.3. Analysis of glycerol carbonate

2.4.3.1. Thin Layer Chromatography

Thin Layer Chromatography (TLC) was used to analyze the reaction mixture of the transesterification of GLY and DMC. Silica-packed aluminum TLC plates were used as the stationary phase and ethyl acetate as the mobile phase to elute the components. A glass capillary removed a small amount of the reaction mixture from the flask and diluted with ethyl acetate. Based on the affinity of the stationary and mobile phases on the TLC plate, the various components present in the mixture were separated. Spots are invisible to the naked eye; thus the plate was submerged in the $KMnO_4$ solution to reveal components with purple color. Following this, the purple TLC plate was heated with a hot air gun, and specks of yellow color appeared on its surface. The visible spots represent the desired product or other reaction components.

2.4.3.2. Fourier Transform-Nuclear Magnetic Resonance

The JEOL ECS-400 (400 MHz) instrument was used to record the Fourier Transform-Nuclear Magnetic Resonance (FT-NMR) of the GLY and GC having tetramethyl silane (TMS) as an internal reference. The NMR spectra's chemical shifts (δ) were expressed in parts per million (ppm). Deuterated water (D_2O) was used for the FT-NMR analysis. ^{1}H-NMR of all the samples

were analyzed using a software called MestReNova. ^{1}H NMR (400 MHz, D_2O): δ (ppm) 4.80-4.75 (m, 1H), 4.47-4.42 (t, *J* = 12 Hz, 1H), 4.23-4.19 (q, 1H), 3.73-3.69 (dd, *J* = 16,4 Hz, 1H), 3.58-3.55 (m, 1H), 3.54-3.50 (dd, *J* = 12,4 Hz, 1H), 3.44-3.40 (dd, *J*= 8,4 Hz, 3H), 3.35-3.31 (dd, *J*= 12,4 Hz, 3H) (**Figure A1**). ^{13}C NMR (100 MHz, D_2O): δ (ppm) 157.90, 78.04, 72.05, 66.83, 62.48, 60.91 (**Figure A2**).

The obtained reaction mixture containing GC and GLY was then quantified using ^{1}H-NMR spectroscopy shown in **Figure A3** using the following equation (1):[3]

$$\%C_{GC} = 100 \times \left(\frac{I_{c_1}}{I_d + I_{c_2}}\right)$$

Where,

$\%C_{GC}$ = percentage of GC

I_{c_1} = one of the methylene proton's (c_1) integral of non-superimposed doublets of GC

$I_d + I_{c_2}$ = complete integral of the methylene proton (c_2) doublet of the superimposed protons of GC and the methine proton (d) of GLY

2.4.4. Analysis of 3-alkylated indole

2.4.4.1. Thin Layer Chromatography

The reaction's progress was monitored using TLC (Thin Layer Chromatography), and G254 silica gel was used to prepare the TLC plate. Ethyl acetate and hexane were employed to elute the components, while TLC plates served as the stationary phase. A capillary tube deposits a small amount of the diluted product and indole (the reactant) solution close to the bottom edge of a TLC plate. For TLC, the solvent (1:9 EtOH:hexane) was utilized. The sample is eluted when the solvent meets the sample mixture and is carried up the plate by capillary action. Next, a UV light is used to see the TLC plate.

2.4.4.2. Column chromatography

Column chromatography was performed for the purification of the product. Silica gel mesh size 60-120 μ was used here for the purification method. It involves a stationary solid phase that adsorbs and separates the compounds moving through it with a liquid mobile phase. This method involves separation of compounds based on their varying adsorption to the adsorbent,

enabling them to pass through the column at different rates. Depending on the polarity of the chemical, column chromatography is a preparative method used to purify the component.

2.4.4.3. Fourier Transform-Nuclear Magnetic Resonance

Tetramethyl silane (TMS) was employed as an internal reference in the Fourier Transform-Nuclear Magnetic Resonance (FT-NMR) measurements of the product using the JEOL ECS-400 (400 MHz) instrument. Chemical shifts (δ) in the NMR spectra were quantified as parts per million (ppm). The samples for the FT-NMR analysis were prepared using $CDCl_3$ as solvent. All the products' ^1H and ^{13}C-NMR data were analyzed using MestReNova software. ^1H NMR (400 MHz, $CDCl_3$): δ 7.95 (brs, 1H), 7.59 (d, *J* = 7.8Hz, 1H), 7.35 (d, *J* = 9.7Hz, 1H), 7.21- 7.16 (m, 1H), 7.12 (t, *J* = 7.5Hz, 1H), 6.98 (s, 1H), 3.04 (t, *J* = 7.4 Hz, 2H), 2.84 (t, *J* = 7.5 Hz, 2H), 2.14 (s, 3H) ppm (**Figure B1**); ^{13}C NMR (100 MHz, $CDCl_3$): δ 19.45, 30.24, 44.21, 111.16, 115.29, 118.67, 119.35, 121.58, 122.21, 127.30, 136.37, 208.76 ppm shown in **Figure B2.**

2.5. Catalyst characterization techniques

2.5.1. X-ray diffraction

X-ray diffraction (XRD) analysis was performed on the prepared catalysts to examine their crystal structure. X-ray diffraction is a technique that measures the diffraction patterns of X-rays scattered by the atoms in the material, enabling the analysis of crystal structures. The XRD patterns were recorded using PANalytical's X'Pert Pro and Rigaku SmartLab SE instruments, utilizing monochromatic Cu-Kα radiation with a wavelength of 1.54060 Å as the X-ray source. The scanning range covered an angle from 5 to 90 degrees. The obtained diffraction patterns were compared to the database files provided by the Joint Committee on Powder Diffraction Standards (JCPDS) to identify the crystal structures present in the prepared catalysts. The JCPDS database is widely recognized for its collection of diffraction patterns for numerous crystal structures, facilitating the identification of unknown samples.

2.5.2. SEM, FESEM & EDS

SEM (Scanning Electron Microscope) and FESEM (Field Emission Scanning Electron Microscopy) are techniques used to image high-resolution samples using an electron beam generated from X-rays. EDS (Energy Dispersive X-ray Spectroscopy) is a technique often used in conjugation with Sem and FESEM to analyze the chemical composition of a sample. The JEOL JSM 6510LV and the Zeiss instrument were employed in this SEM and FESEM,

respectively. With FESEM EDS, detecting and analyzing smaller features and elements within a sample is possible. Samples were prepared using the drop-cast technique.

2.5.3. High-Resolution Transmission Electron Microscopy

High-Resolution Transmission Electron Microscopy (HRTEM) is a powerful imaging technique to investigate a material's structural and morphological properties at the atomic scale. HRTEM passes an electron beam through a thin sample and records the resulting transmission pattern with a detector. The JEOL JEM 2100 PLUS was used for the HRTEM analysis. The sample was mixed with ethanol and ultrasonicated for 1 hour to get a well-dispersed suspension for this analysis. This ensures that the sample is evenly distributed and that no large aggregates or clumps could interfere with the imaging results.

2.5.4. Fourier Transform Infrared

FTIR (Fourier Transform Infrared) spectroscopy is a popular analytical technique for determining the surface functional groups on a solid sample. The Agilent Cray-660 FTIR spectroscopy was used in the 450 to 4000 cm^{-1} range. The FTIR of the pyridine-saturated sample was performed to study the sample's Bronsted and Lewis acidic sites. For this study, the samples were saturated with pyridine initially dried at room temperature, then in an oven for 2 h, and lastly calcined at 200 ℃ for 10 min. Before analysis, a homogenous mixture of sample and KBr was prepared, and then the prepared mixture was placed onto a pellet die. Once the pellet was formed, the sample was ready for analysis and placed onto the sample holder.

2.5.5. X-ray Photoelectron Spectroscopy

X-ray Photoelectron Spectroscopy (XPS) was performed using Thermo Fisher ESCALAB Xi+ instrument to identify the elements in the samples. An ESCA X-ray Photoelectron Spectrometry equipment connected with a monochromatized alumina source was used to determine the elements' surface elemental electronic state and binding energy. Air contamination of the sample is minimized by placing the powdered samples in the XPS chamber for two hours before the examination. The instrument was in operation at 15 kV and 20 mA.

2.5.6. Ammonia- Temperature Programmed Desorption

NH_3-TPD (Temperature Programmed Desorption) was used to calculate the acidic strength of the catalysts, and the instrument used for this technique was BELCAT II from the

MicrotracBEL Corporation. For this technique, 0.05 g of catalyst was introduced into a glass tube placed inside the instrument. The catalyst sample underwent a Helium gas flush at 300 ℃ for 1 hour to eliminate adsorbed gases and any moisture. Following this step, the catalyst surface was exposed to pure ammonia gas at 100 ℃ for 30 minutes to adsorb ammonia gas. Subsequently, the sample was heated to the target temperature under a Helium atmosphere, and the quantification of desorbed ammonia was performed using a thermal conductivity detector (TCD).

2.5.7. Dynamic Light Scattering

Dynamic Light Scattering (DLS) or Photon Correlation Spectroscopy (PCS) is a highly effective technique used to investigate macromolecule diffusion in solution. Through the measurement of the diffusion coefficient, and subsequently the calculation of hydrodynamic radii, valuable information about the size and shape of macromolecules can be obtained. Zeta Potential Analyzer having model name ZEN 3600, Malvern (U.K.) instrument was used to perform the DLS analysis.

2.5.8. Brunauer-Emmett-Teller

The Brunauer, Emmett, and Teller (BET) tests were performed to measure the surface area and porosity of the sample using the instrument Quantachrome NOVA touch. Before analysis, moisture or any physically adsorbed species was removed to get accurate results. The sample was typically pretreated under a nitrogen atmosphere at high temperatures. The pretreatment was conducted at 200 ℃ for 2 h in this case. In the BET technique, the amount of gas (nitrogen) adsorbed onto the sample at different pressures is used to calculate the sample's surface area and other properties.

2.6. Catalyst characterization

2.6.1. X-ray Diffraction

Detailed XRD spectra of all the modified and unmodified zeolites have been discussed in this section.

X-ray diffraction (XRD) patterns of HZSM-5 and Cerium-modified HZSM-5 zeolite are shown in **Figure 2.5**. It is clear from the XRD pattern that modification of zeolite with cerium has been successfully done. The characteristic peaks of CeO_2 are obtained at $2\theta = 28.5°$, 46.3°, 56.28° having planes (111), (220), (311) respectively, which corresponds to face-centered cubic (fcc) phase of CeO_2 with JCPDS/PDF 34-0394.[4] In Ce-HZSM-5, the intensities of the distinctive peaks are lower than in unmodified zeolite, but the overall XRD pattern

demonstrates that the zeolite's structural integrity has not changed. The XRD pattern also shows peaks at 2θ = 14.7°, and 20-25°, which are the characteristic peaks of parent ZSM-5 zeolite observed in the modified form.[5,6]

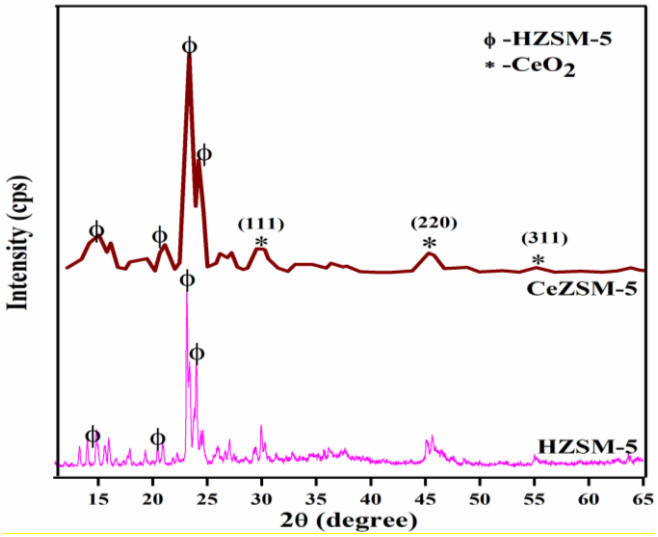

Figure 2.5. Powder X-ray diffraction pattern of HZSM-5 and Cerium-modified HZSM-5.

XRD patterns of HY and sulfuric acid-treated zeolite Y (SY) zeolites are shown in **Figure 2.6**. It is clear from the XRD patterns that the characteristic peaks of HY zeolite are retained even after modification with sulfuric acid. The diffraction peaks obtained at 2θ values 6.15°, 15.7°, 18.8°, 20.5°, 23.8°, 27.3° and 31.7° correspond to the characteristic peaks of Faujasite zeolite Y (HY) topology has reflection plans (111), (331), (333), (440), (533), (642) and (555) respectively. All these peaks are present even after modification with sulphuric acid. However, the intensities of peaks of zeolite Y decrease after modification with sulphuric acid. This is due to the transformation of the crystalline phase to non-crystalline silica.[7,8]

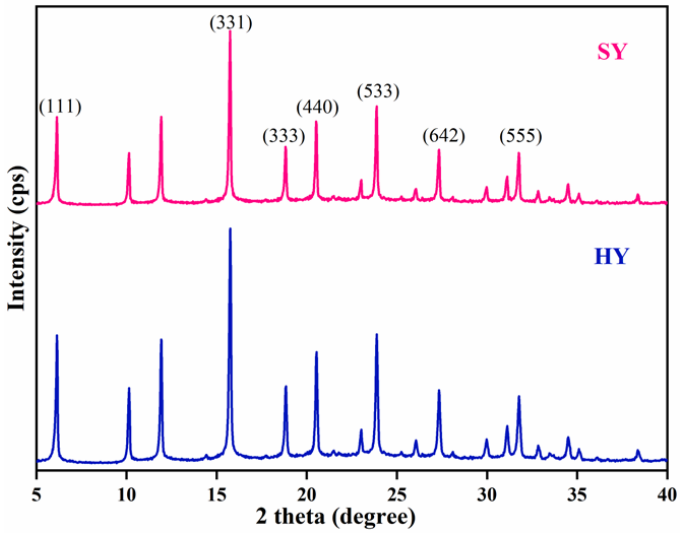

Figure 2.6. XRD patterns of HY and SY zeolites.

Figure 2.7(a) shows the XRD plots for the comparison of alkali and alkaline metal such as Li, Mg and K respectively. The XRD plot of zeolite beta and $Li_{20}\beta$ zeolite with different phases that are formed, shown in the **Figure 2.7(b)**. The characteristic peaks of $LiAlO_2$ (JCPDS card no. 38-1464), Li_2SiO_3 and Li_4SiO_4 have been shown in the graph.[9] It is visible from the XRD pattern that there is no change in the structure of the zeolite framework even after the modification with active metal.

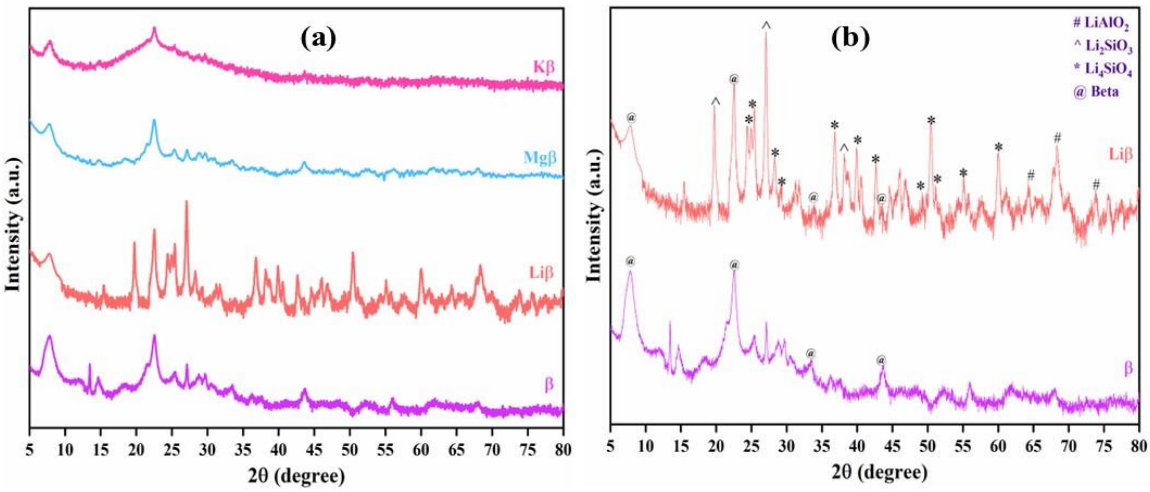

Figure 2.7. XRD patterns of (a) Comparison of beta, Li, Mg, and K-modified beta zeolite (b) different phases of Li with alumina and silica.

Figure 2.8 depicts the XRD patterns of mordenite and SO_3H@Mor zeolites. The XRD patterns show that the characteristic peaks of mordenite zeolite are retained even after the treatment with sulfuric acid. The diffraction peaks obtained at 2θ values of 6.54°, 8.72°, 9.74°, 13.54°, 15.32°, 19.72°, 22.49°, 25.82°, 26.50°, 31.14°, 35.96°, 44.68°, 46.86°, and 48.83° correspond to the typical peaks of the pure mordenite with reflection plans (111), (020), (200), (111), (310), (330), (150), (202), (350), (402), (352), (732), (841), and (104), respectively. All of these peaks are present even after sulfuric acid treatment. However, the intensities of zeolite Y peaks drop after sulfuric acid alteration. This is related to the conversion of crystalline silica to non-crystalline silica.

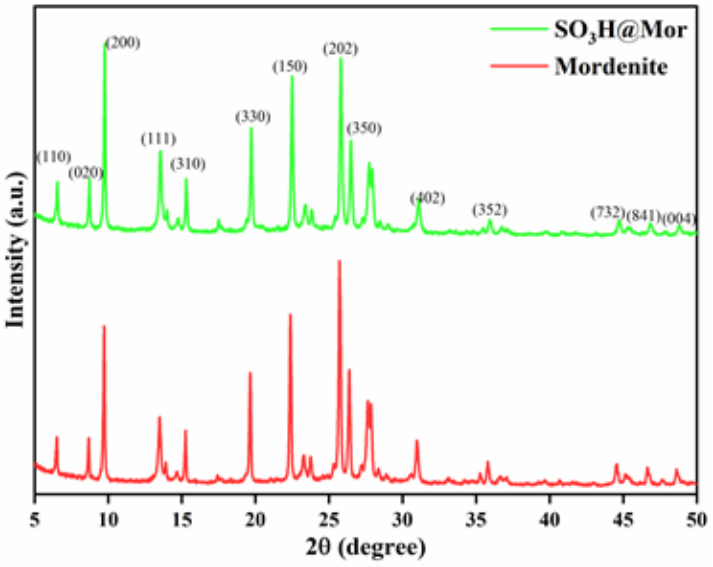

Figure 2.8. XRD spectrum of mordenite and SO_3H@Mor zeolites.

2.6.2. SEM, FE-SEM & EDS

SEM, FESEM and EDS explained the elemental composition and surface morphology of the catalyst. The elemental composition of zeolite is estimated by the area under the peak for individual elements. This section gives the detailed study of these techniques and comparing with the parent zeolites.

EDS spectra as shown in **Figure 2.9(a)** clarify the presence of cerium in the zeolite. The structure of the modified catalyst indicates almost the same morphology as that of the parent zeolite. The O, Al, and Si peaks in the EDS spectrum depict the presence of alumina and silica in the zeolite and confirm that the zeolite structure is unaltered even after modification. The uniform distribution O, Al, and Ce are confirmed by colour mapping as shown in **Figures 2.9(c), 3(d), and 3(e)**. The morphology of the crystal shows the particles are cuboidal and regular in shape and white particles confirm the presence of CeO_2 on the surface of the catalyst shown in **Figure 2.9(b)**.[4]

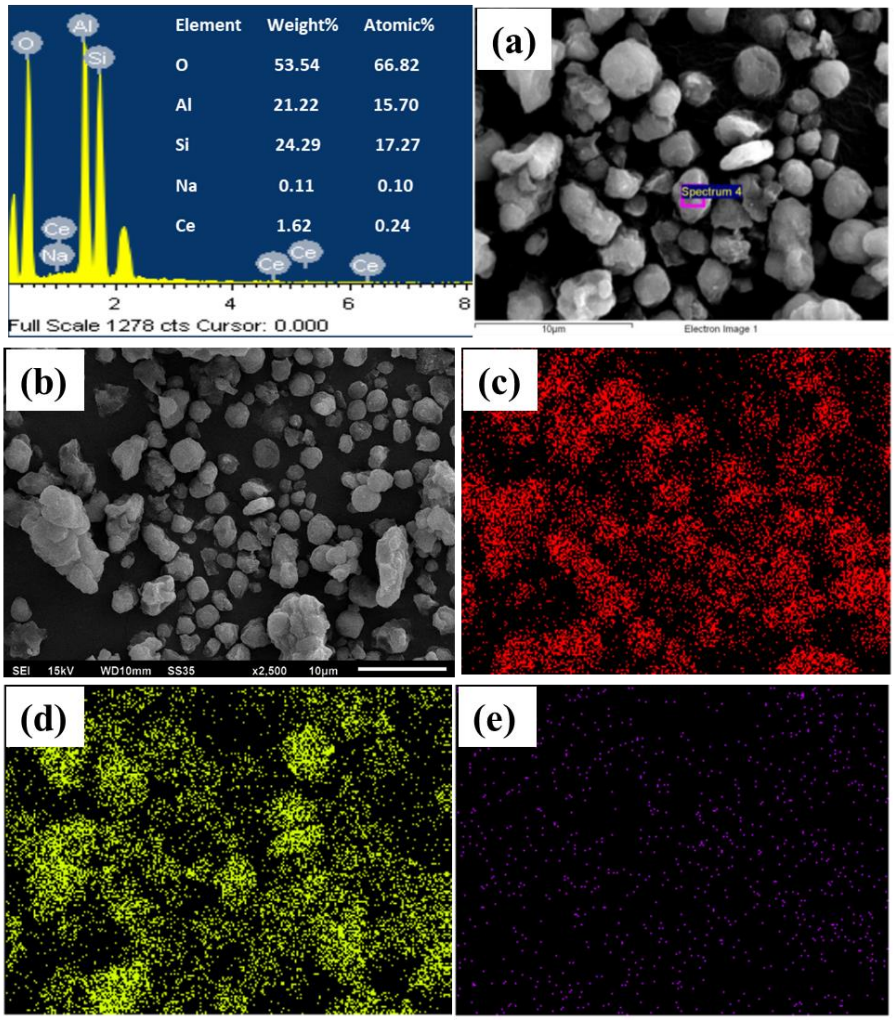

Figure 2.9. (a) EDS spectra, (b) SEM images, and (c, d, e) images showing the elemental mapping of the distribution of oxygen, aluminum, and cerium in the Ce_5ZSM-5.

Figure 2.10(a) depicts the EDS spectra. The SEM image in **Figure 2.10(b)** displays the identical morphology as the parent zeolite in **Figure 2.10(c)**. The presence of silica and alumina is confirmed by peaks of elements oxygen, aluminium, and silicon, which means that the zeolite structure remains unaltered even after modification. The pyramidal geometry are seen in the SEM images of the HY and SY zeolites, which exhibit irregular morphologies and sizes.[10] The samples' typical particle size ranges from 600 to 800 nm.[11] Color mapping of each element revealed that all elements were distributed uniformly on the zeolite surface. All of the elements were distributed uniformly on the zeolite surface, according to colour mapping of all the components. The elemental color mapping is shown in **Figure 2.10(d)**.

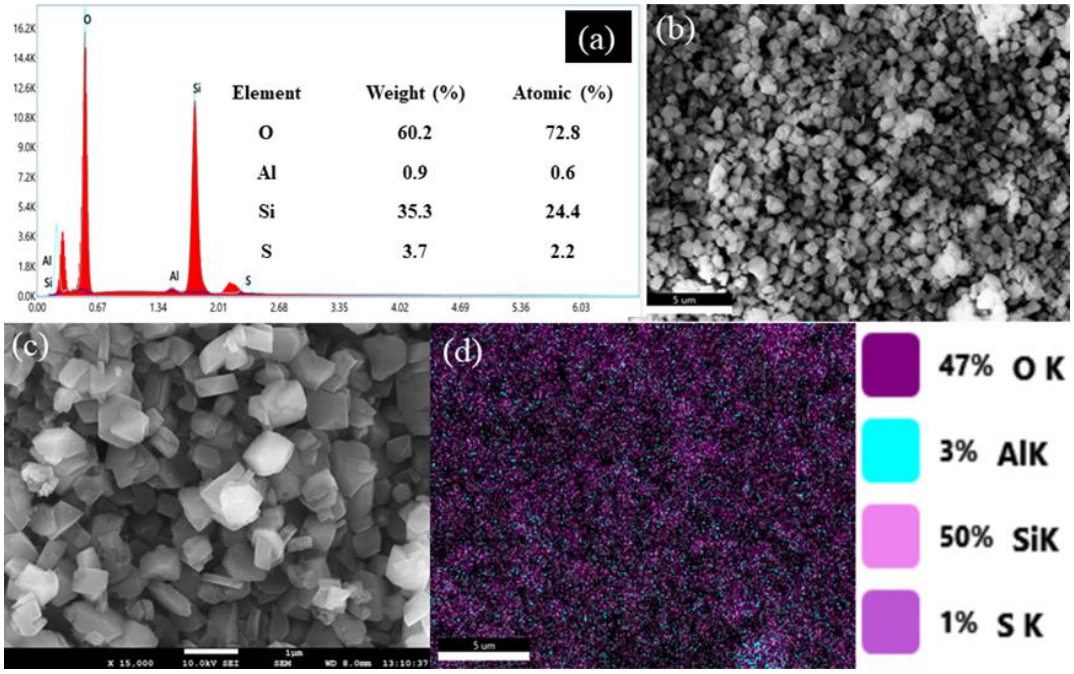

Figure 2.10. (a) EDS spectra, (b), (c) SEM images of HY and SY zeolites, and (d) elemental mapping of oxygen, aluminum, silicon, and sulfur in SY zeolite.

Figure 2.11 illustrates the morphological images created by FE-SEM of the parent zeolite beta, as well as the Li, Mg, and K-modified zeolite beta. The figure displays the spherical shapes of parent zeolite beta which becomes slightly distorted after modification with Li, Mg and K illustrated in **Figure 2.11(b),(c),(d)**. The particles have spherical shapes but do not have well-defined edges. The metal modified zeolites also show spherical structure confirming that the basic morphology of the zeolite remains the same even after modification. The EDS spectra of metal (Li, Mg, K) modified zeolite is shown in the **Figure 2.12**. The spectra cleared that a good amount of metal is loaded on the zeolite beta. Li cannot be detected in SEM/EDS, so no peak of Li is observed in EDS spectra of $Li_{20}\beta$ zeolite.

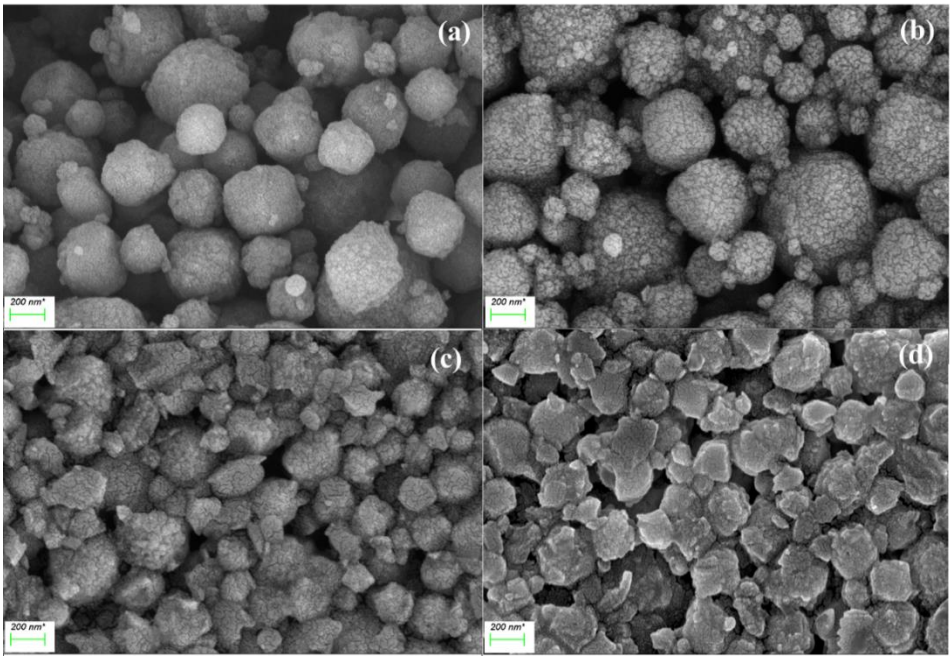

Figure 2.11. FE-SEM images of (a) parent zeolite beta and (b) Li modified (c) Mg modified, and (d) K-modified zeolite beta.

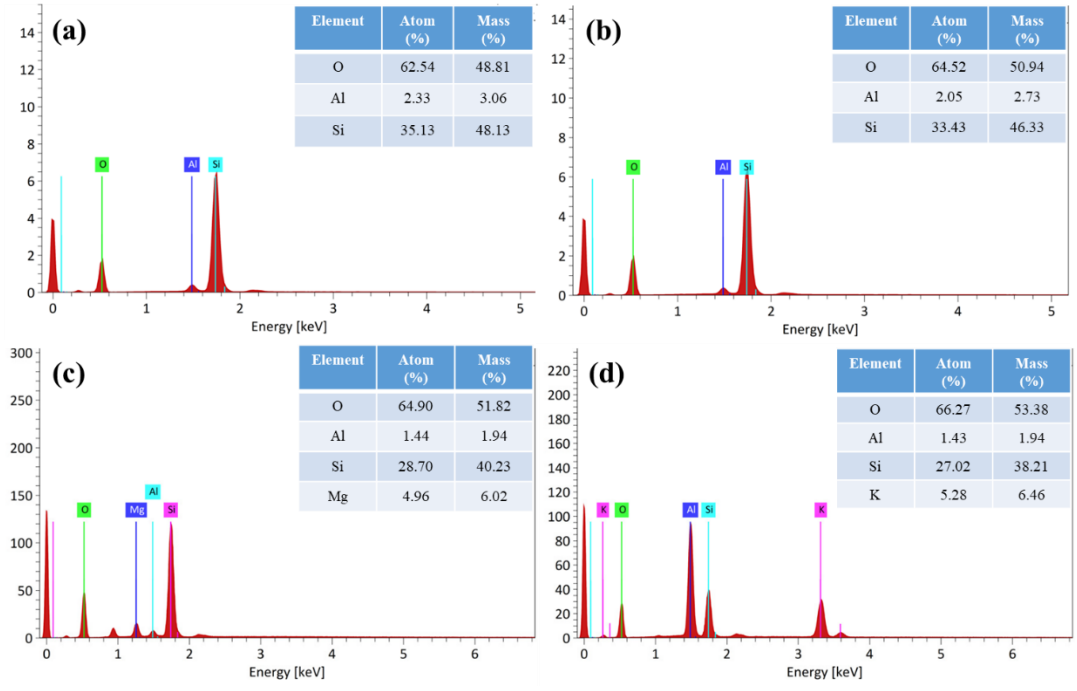

Figure 2.12. EDS graphs of (a) parent zeolite beta, (b) Li, (c) Mg, and (d) K modified zeolite beta.

FE-SEM analysis studied the morphology of pure and sulfuric acid-treated zeolites. **Figure 2.13(a),(b)** show the same morphologies indicating that the zeolite structure remains

unchanged after modification. The intergrown lath shape crystals are formed in the FE-SEM images of pure mordenite and SO_3H@Mor zeolites. The figure shows FE-SEM pictures, which reveal that plates are the most common type of crystal with irregular sizes. Due to the significant amount of silica, flat and prismatic crystals were formed.

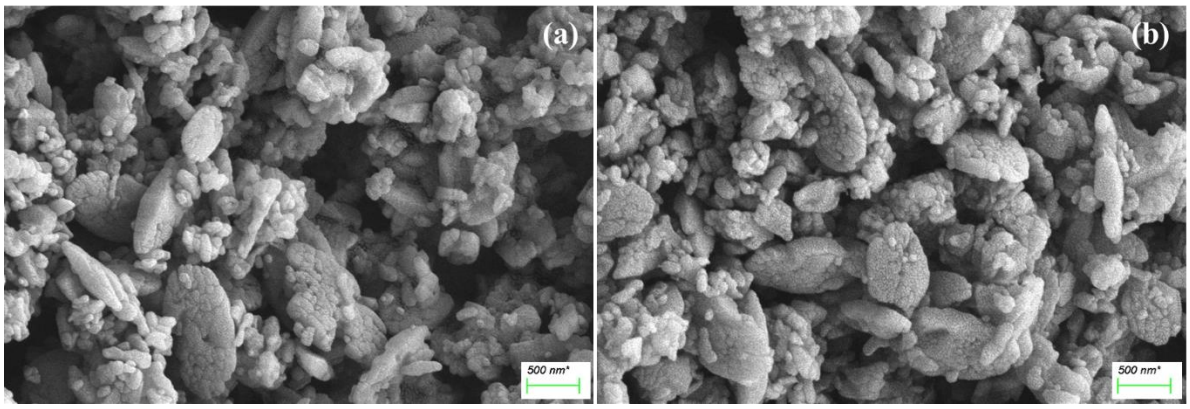

Figure 2.13. FE-SEM images of (a) pure and (b) sulfuric acid-treated mordenite zeolite at 500 nm.

The EDS technique explained the elemental composition of the catalyst's surface. In EDS, the region below the peaks provides information on the elemental structure of zeolite. The color mapping of every element revealed that each element was distributed equally across the surface of SO_3H@Mor zeolite. **Figure 2.14** displays the EDS and mapping of all the present elements. Also, **Table 2.1** explains the atom and mass percentage of the elements.

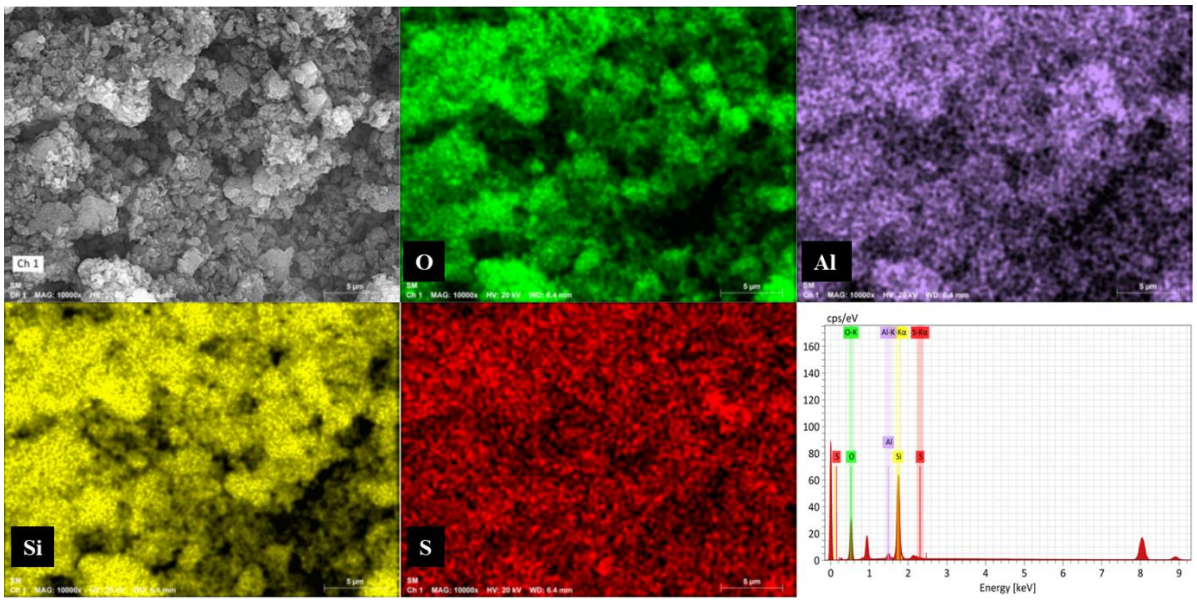

Figure 2.14. EDS-mapping of SO_3H@Mor zeolite.

Table 2.1. Percentage composition of all the elements present in the SO_3H@Mor zeolite.

Element	Mass (%)	Atom (%)
O	58.06	70.84
Al	2.18	1.30
Si	35.94	24.37
S	3.82	3.49
Total	**100**	**100**

2.6.3. High-Resolution Transmission Electron Microscopy

The images of $Li_{20}\beta$ catalyst obtained from the High-Resolution Transmission Electron Microscopy are shown in the **Figure 2.15**. It is clearly visible from the figure that $Li_{20}\beta$ catalyst possesses some distortion in its spherical structure, forming irregular shapes. The same results are observed in the FE-SEM images. The average grain diameter and the average spacing between the two grains are determined to be 500 nm and 24.28 nm, respectively.

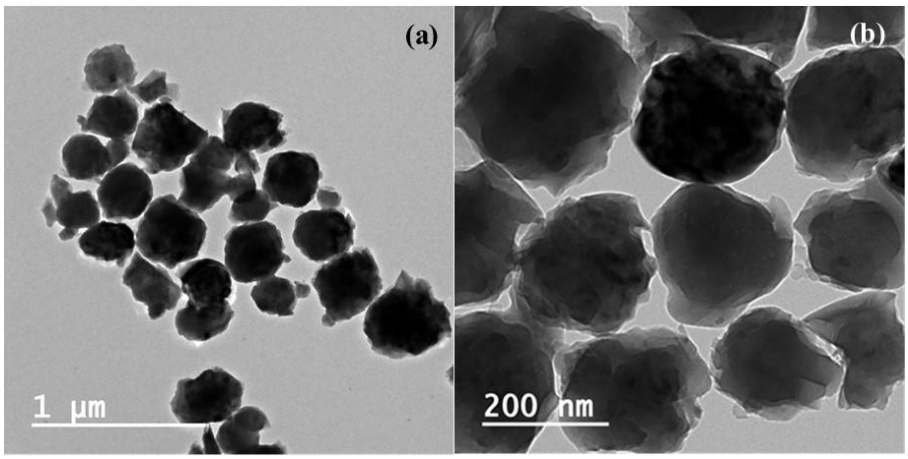

Figure 2.15. HR-TEM images of Li-modified zeolite beta at (a) Lower (b) Higher magnifications.

2.6.4. Fourier Transform Infrared Spectroscopy Analysis

The Fourier Transform Infrared Spectroscopy (FTIR) was performed in the range of 4000-450 cm^{-1} to study the surface characteristics of the HY and SY zeolite catalysts. Zeolites possess two types of group vibration frequency: internal vibrations of T-O where T represents SiO_4 and AlO_4 tetrahedron, and vibration of external linkages between tetrahedral. The FTIR spectra frequency ranging from 450-1300 cm^{-1} corresponds to the lattice cell of zeolite. The bands in the 400-500 cm^{-1} range represent the Si-O-Si vibrations, from 600-900 cm^{-1} attributed to symmetric and from 900-1250 cm^{-1} asymmetric stretching of Si-O-T. The peak at 1056.94 cm^{-}

[1] confirmed the presence of sulfonic group[12] due to S=O symmetric stretching[7] shown in **Figure 2.16**.

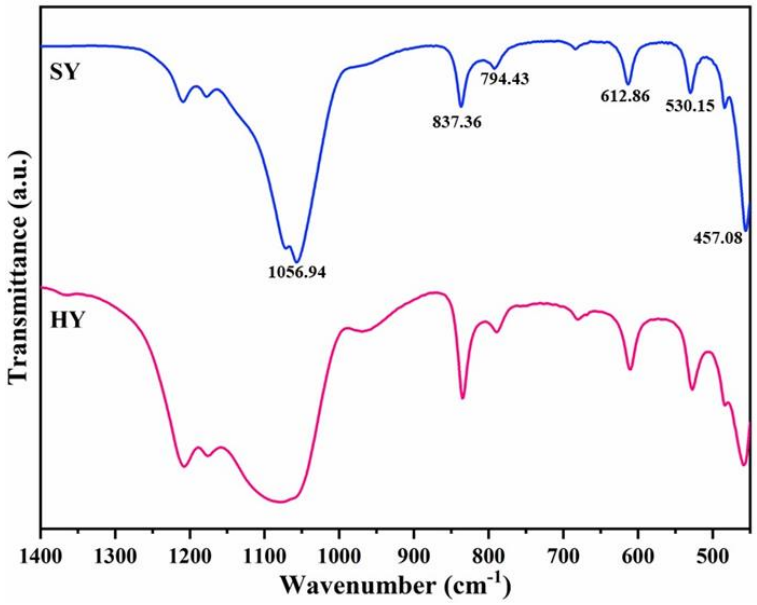

Figure 2.16. FTIR spectra of HY and SY zeolites.

2.6.5. X-ray Photoelectron Spectroscopy Analysis

X-ray photoelectron spectroscopy (XPS) was performed to study the quantitative measurements of the elemental composition of the sulphuric acid-modified zeolite Y. The service spectrum shows the photoelectronic lines of the O 1s, Si 2p, and S 2p in **Figure 2.17(a)**, confirming sulphurs' presence.[8] **Figure 2.17(b)** shows the binding energy of Si 2p at 103.6 eV which corresponds to Si-O linkage. The XPS data explains that the S 2p peak has two deconvoluted peaks, at 162.4 eV and 163.3 eV, due to S $2p_{3/2}$ and S $2p_{1/2}$ respectively, as shown in **Figure 2.17(c)**. The spectrum of O 1s has been further divided into three peaks with 532 eV, 532.5 eV, and 533.1 eV binding energies. The peak at 532 eV can be assigned to oxygen of sulphonate group, peak at 532.5 eV is responsible for the lattice form of oxygen of the zeolite Y structure, whereas the peak at 533.1 eV represents the hydroxyl group (C-OH) shown in **Figure 2.17(d)**.

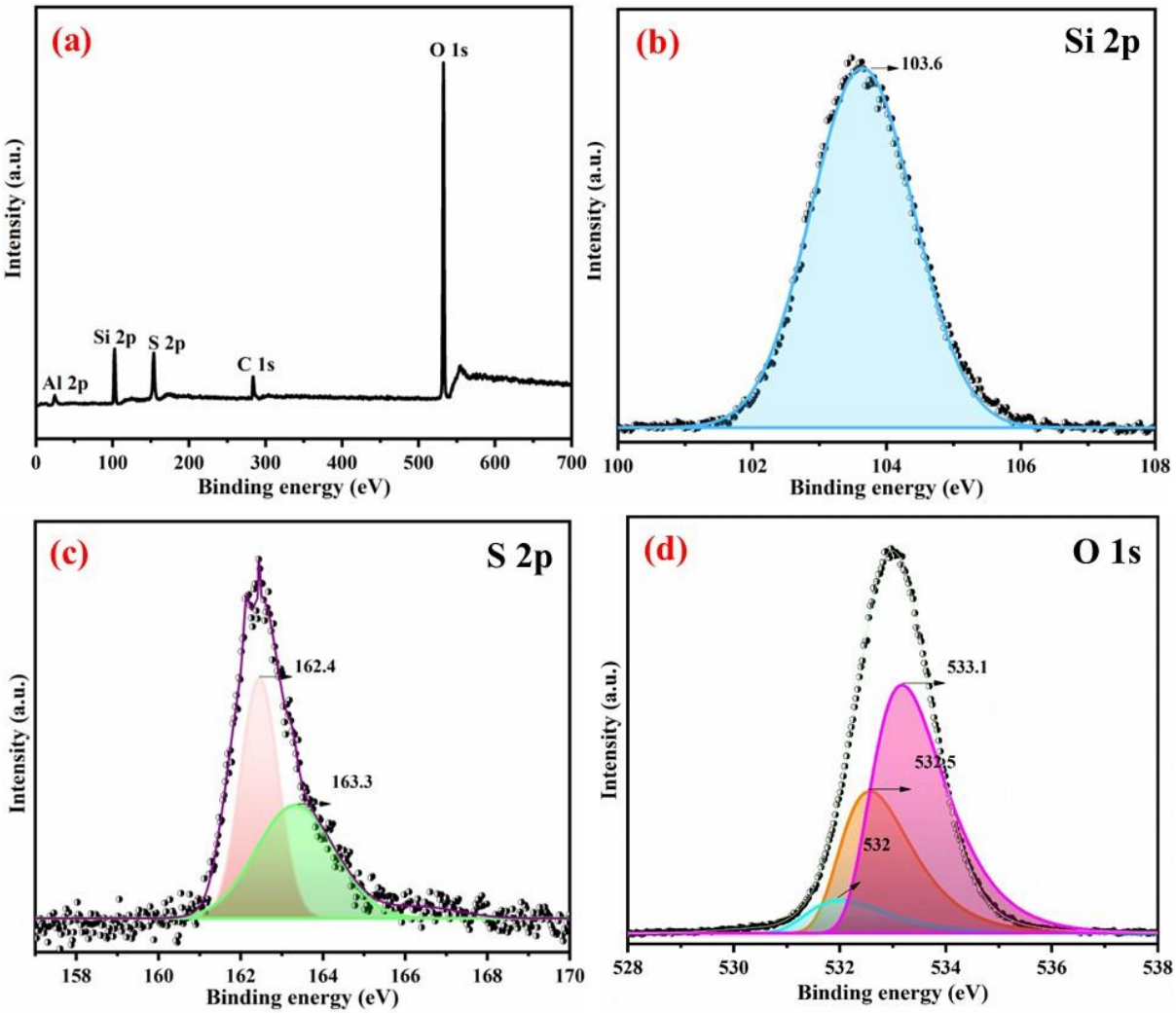

Figure 2.17. XPS service spectrum (a), the spectrum of Si 2p (b), S 2p (c), and O 1s (d).

XPS of the catalyst ($Li_{20}\beta$) was carried out to study its quantitative elemental composition measurements. The service spectrum of $Li_{20}\beta$ catalyst shown in **Figure 2.18(a)** depicts the characteristic peaks of Li (1s), O (1s), and Si (2p). The Li 1s has two deconvoluted peaks with binding energies at 53.9 eV and 54.9 eV as shown in **Figure 2.18(b)**. The peak at 53.9 eV confirms the Li-O linkage and peak at 54.9 eV confirms the Li-O-Si linkage. The spectrum of O 1s has been subdivided into three peaks having binding energies of 530.6, 531.2 and 532.1 eV shown in **Figure 2.18(c)**. The peak at 530.6 eV corresponds Li-O linkage, peak at 531.2 eV confirms the presence of lattice form of oxygen of the zeolite and peak at 532.1 eV corresponds to hydroxyl group. The peaks in **Figure 2.18(d)** at 102.1 and 102.6 eV are the lattice form of Si 2p which corresponds to Li_xSiO_y and Si-O-Si linkage respectively.

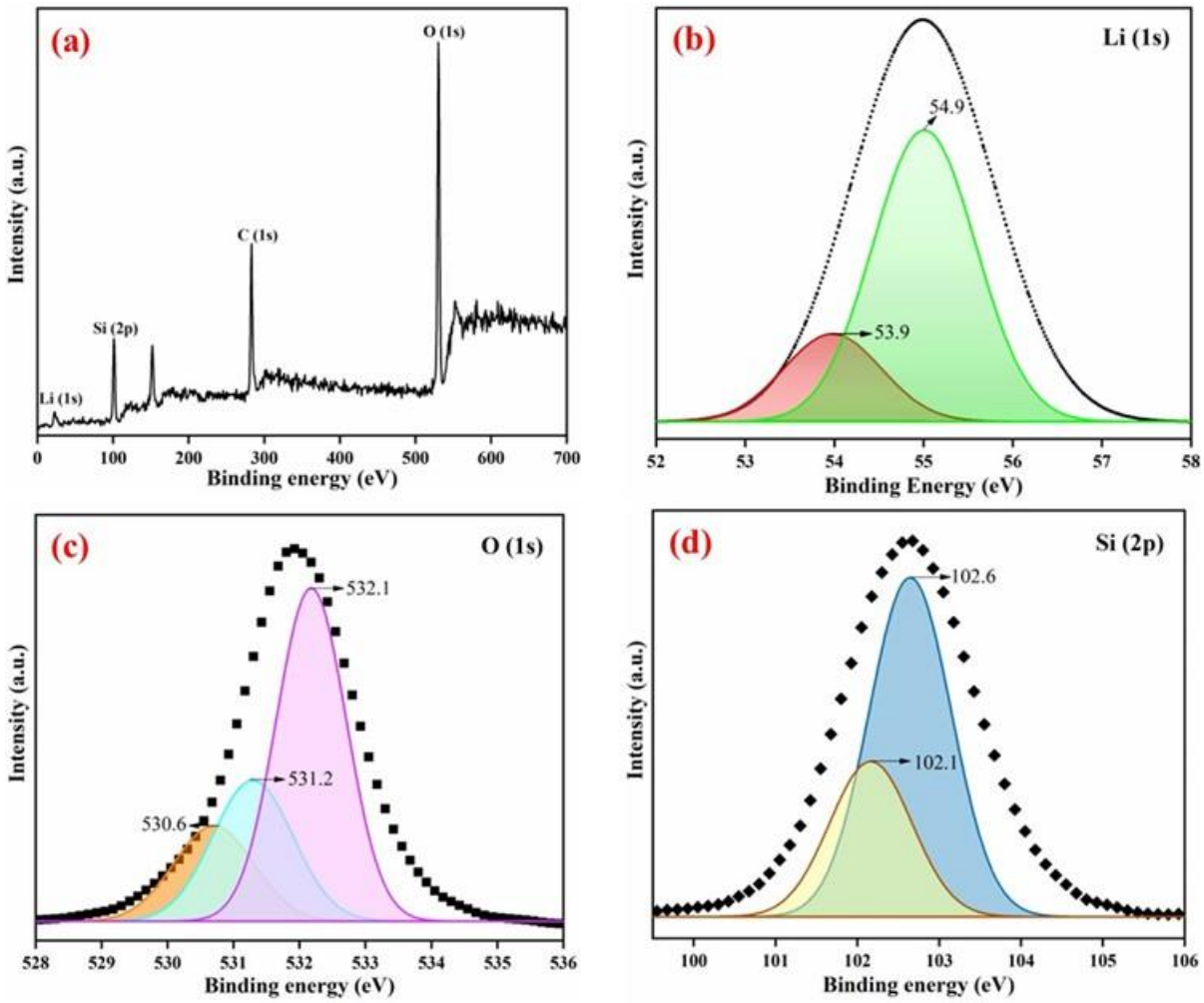

Figure 2.18. XPS (a) service spectrum, (b) Li (1s), (c) O (1s), and (d) Si (2p).

The elemental composition of the sulfuric acid-treated mordenite zeolite was quantitatively measured using X-ray photoelectron spectroscopy (XPS). **Figure 2.19(a)** shows the photoelectronic lines of the C 1s, O 1s, Si 2p, and S 2p in the service spectrum, confirming the presence of sulfur. According to the XPS results, the O 1s spectra have been subdivided into three portions with binding energies of 532.2 eV, 532.8 eV, and 533.1 eV. Peak at 532.2 eV is the linkage of oxygen with the sulphonate group, the lattice form of oxygen in the mordenite zeolite structure is represented by the peak at 532.86 eV, whereas the hydroxyl group displayed in **Figure 2.19(b)** is represented by the peak at 533.10 eV. The S 2p peak has two deconvoluted peaks at 162.3 eV and 163.4 eV, which corresponds to S $2p_{3/2}$ and S $2p_{1/2}$ respectively, as seen in **Figure 2.19(c)**. **Figure 2.19(d)** depicts the Si 2p binding energy of Si-O linkage at 103.22 eV.

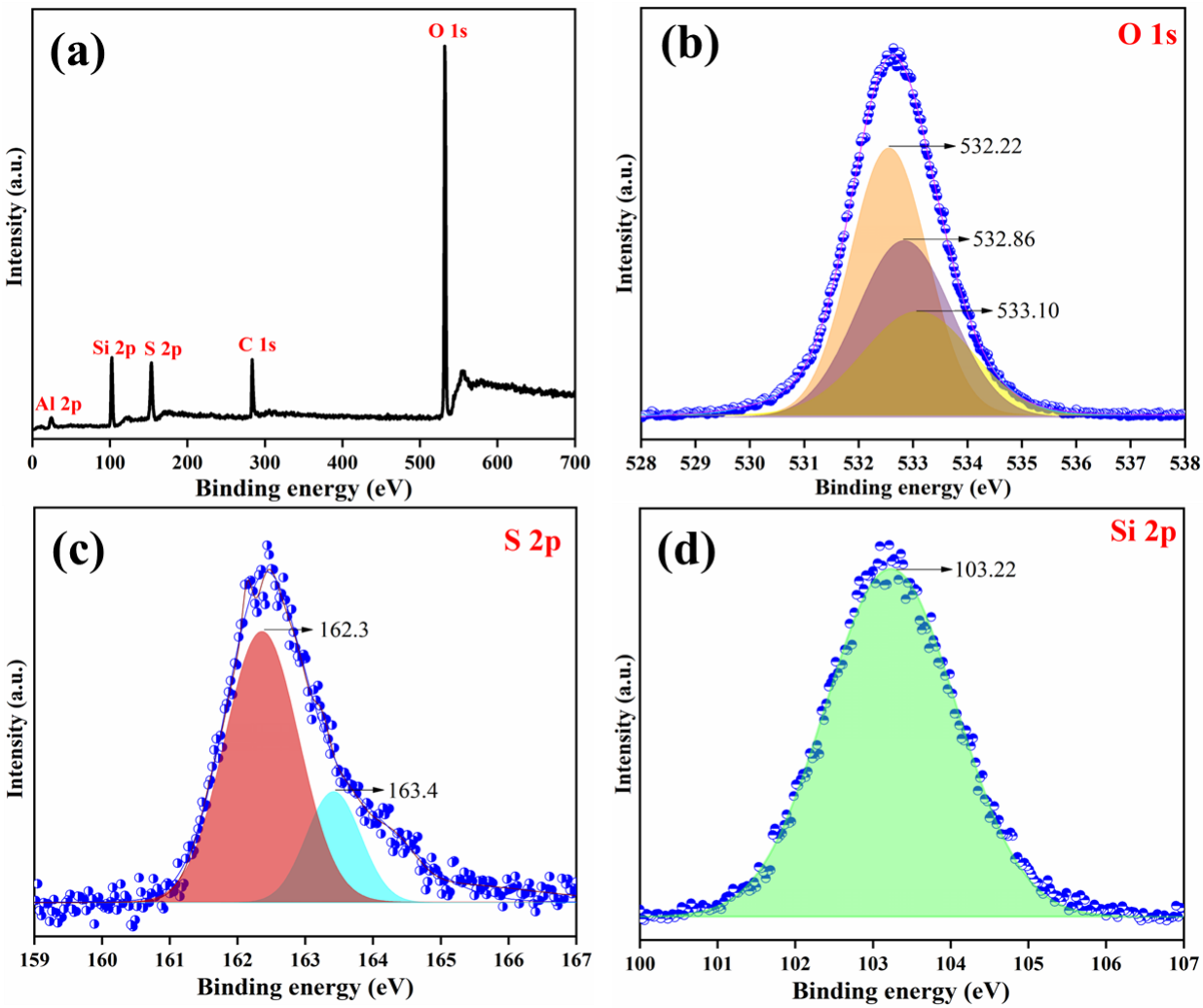

Figure 2.19. XPS (a) service spectrum, (b) O 1s, (c) S 2p, and (d) Si 2p

2.6.6. Ammonia- Temperature Programmed Desorption

Figure 2.20 shows the temperature-programmed desorption profile of ammonia in the zeolite samples. The desorption profiles indicate that CeZSM-5 exhibits higher acidity compared to HZSM-5. The zeolites are composed mainly of two types of acid sites with different strengths. Desorption from the weak acid sites in a TPD peak at lower temperatures (175 °C for HZSM-5 and 185 °C for CeZSM-5), while desorption from strong acid sites yields TPD peaks at higher temperatures (400 °C for HZSM-5 and 405 °C for CeZSM-5). Moreover, an increase in zeolite acidity causes a slight shift of the desorption peaks towards higher temperatures.[13] Therefore, the cerium exchange leads to an enhancement in both the quantity and strength of the acid sites in the zeolite. The zeolite acidity was measured to be 0.519 mmol/g of CeZSM-5 and 0.457 mmol/g of HZSM-5 zeolite.[14]

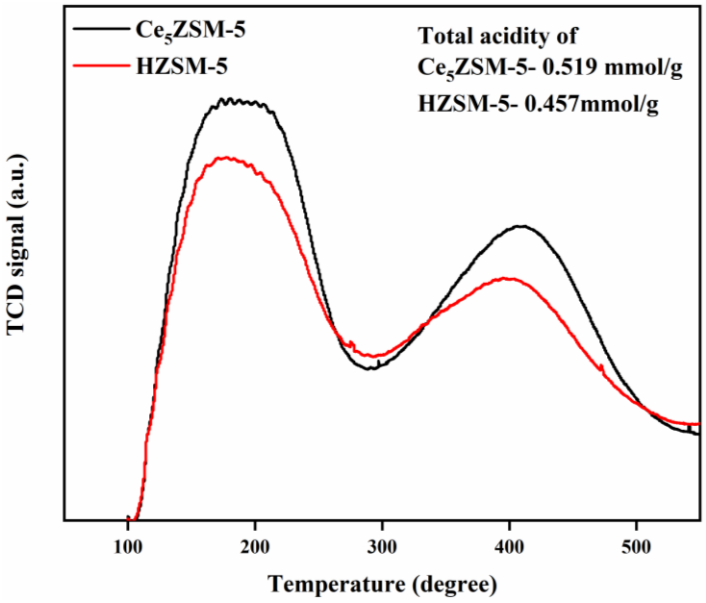

Figure 2.20. TPD of HZSM5 and Cerium-modified HZSM-5.

2.6.7. Dynamic Light Scattering

DLS graph of beta and $Li_{20}\beta$ zeolite is shown in the **Figure 2.21**. DLS was performed to determine the size distribution of the catalyst in a suspension. The hydrodynamic size of beta and $Li_{20}\beta$ zeolite from DLS comes out to be 531.326 nm and 605.699 nm respectively. The increase in the hydrodynamic size of $Li_{20}\beta$ is due to the impregnation of Li metal over the surface of the zeolite beta which increases in its size.

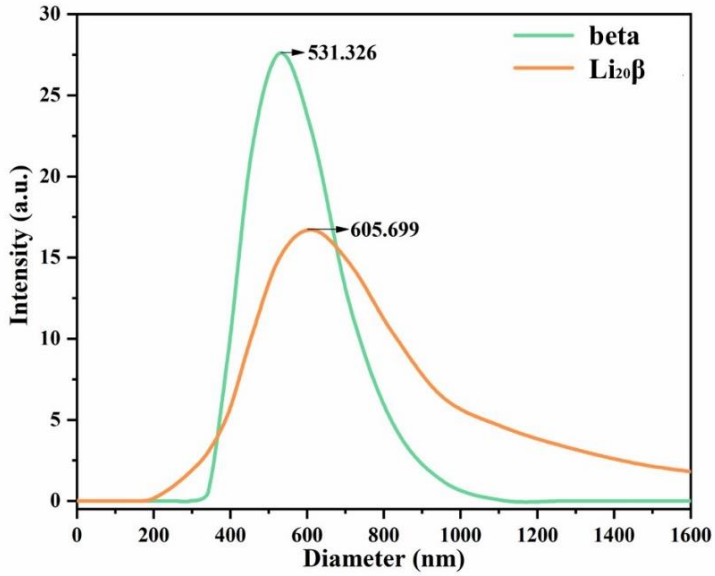

Figure 2.21. DLS graph of parent and Li-modified zeolite beta.

2.6.8. BET Analysis

The Brunauer, Emmett, and Teller (BET) methods were used to calculate surface area. Pore distribution was measured by the Barrett-Joyner-Halenda (BJH) plot shown in **Figure 2.22**. It has been seen that no such change is observed in the physicochemical properties after modification with sulphuric acid. Sulphuric acid-modified zeolite Y (SY) was found to have a BET surface area, 179 m^2/g and pore diameter, 2.35 nm, whereas unmodified zeolite Y was found to have BET surface area and pore diameter, 113 m^2/g and 3.43 nm respectively. The increase in the external surface area of the catalyst after modification was observed and this is due to the blockage of pores by sulfate ions. The modified zeolite (SY) showed an H1 hysteresis loop having type IV isotherm, responsible for its mesoporous structure shown in **Figure 2.22(f)**. The BJH plot shown in **Figure 2.22(a),(d)** clearly showed that the mesoporous material lies in the 3-30 nm range. The surface properties of HY and SY zeolites are summarized in **Table 2.2**.

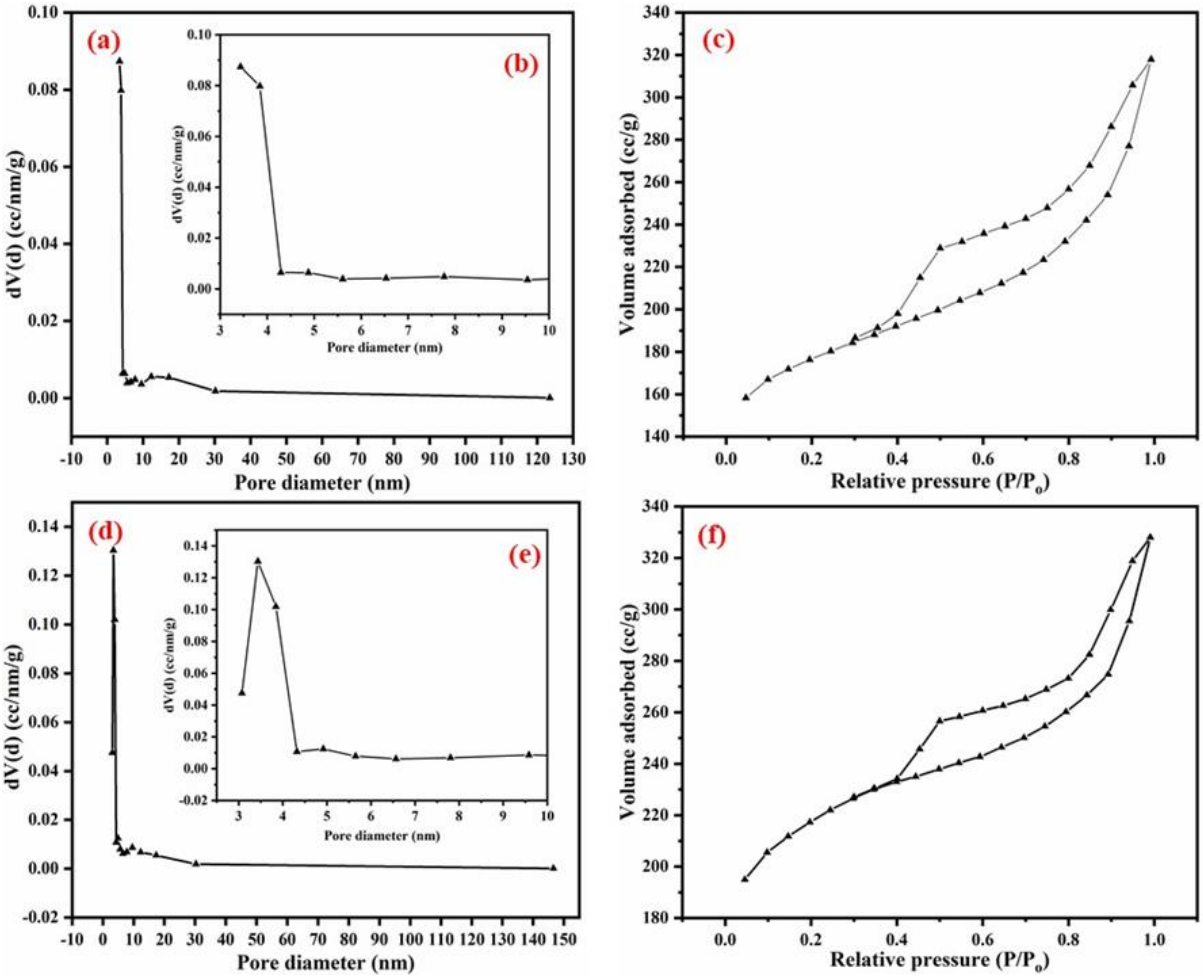

Figure 2.22. Pore size distribution of HY (a,b) and SY (d,e), Nitrogen adsorption-desorption isotherms for HY (c), SY (f)

Table 2.2. Surface properties of the catalysts

Sample	Surface area (m^2/g)	Total pore volume (cc/g)	Pore diameter (nm)	Micropore area (m^2/g)	Micropore volume (cc/g)
HY	113.1	0.201	3.43	599.638	0.274
SY	179.2	0.28	2.35	435.658	0.198

References

1 P. Gautam, S. Barman and A. Ali, *Int. J. Chem. React. Eng.*, , DOI:10.1515/ijcre-2020-0081.

2 P. Gautam, S. Barman and A. Ali, *ChemistrySelect*, 2022, **7**, 1–9.

3 A. Kaur and A. Ali, *Ind. Eng. Chem. Res.*, 2020, **59**, 2667–2679.

4 R. Saharan, G. Halder and S. Barman, *Int. J. Chem. React. Eng.*, 2019, **17**, 1–12.

5 Y. Cheng, J. S. Li, L. J. Wang, X. Y. Sun and X. D. Liu, *Sep. Purif. Technol.*, 2006, **51**, 210–218.

6 G. Afreen, T. Patra and S. Upadhyayula, *Mol. Catal.*, 2017, **441**, 122–133.

7 Y. Tian, R. Zhang, W. Zhao, S. Wen, Y. Xiang and X. Liu, *Catal. Letters*, 2020, **150**, 3553–3560.

8 X. Wang, K. Wang, C. A. Plackowski and A. V. Nguyen, *Appl. Surf. Sci.*, 2016, **367**, 281–290.

9 G. Jaya Rao, R. Mazumder, D. Dixit, C. Ghoroi, S. Bhattacharyya and P. Chaudhuri, *Ceram. Int.*, 2019, **45**, 4022–4034.

10 S. Dinda, P. Murge and B. Chakravarthy Paruchuri, *Bull. Mater. Sci.*, 2019, **42**, 1–9.

11 D. H. Morawala, A. K. Dalai and K. C. Maheria, *Catal. Letters*, 2020, **150**, 1049–1060.

12 A. G. Khiratkar, K. R. Balinge, M. Krishnamurthy, K. K. Cheralathan, D. S. Patle, V. Singh, S. Arora and P. R. Bhagat, *Catal. Letters*, 2018, **148**, 680–690.

13 S. Barman, S. K. Maity and N. C. Pradhan, *Chem. Eng. J.*, 2005, **114**, 39–45.

14 F. Momayez, J. Towfighi Darian and S. M. Teimouri Sendesi, *J. Anal. Appl. Pyrolysis*, 2015, **112**, 135–140.

CHAPTER 3

CATALYTIC PERFORMANCE OF CERIUM-MODIFIED ZSM-5 ZEOLITE FOR THE ESTERIFICATION OF GLYCEROL WITH ACETIC ACID

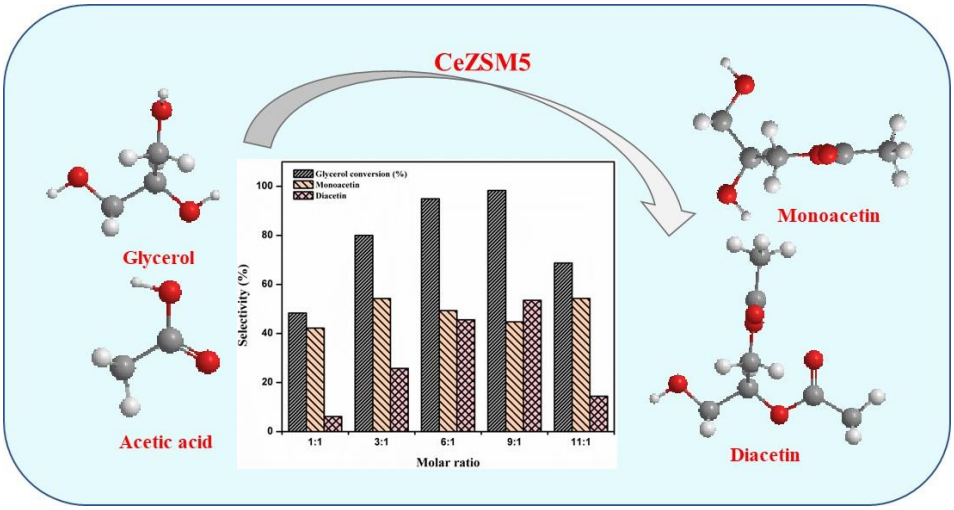

The current chapter explores the esterification of GLY with AcA utilizing cerium-modified HZSM-5 zeolite as the catalyst. In this chapter, the influence of various reaction parameters, such as the AcA to GLY mole ratio, reaction temperature, and catalyst weight on the yield and selectivity of the products was explored.

3.1. Introduction

Currently, global warming stands as a critical concern, leading to numerous initiatives to curtail greenhouse gas emissions, such as CO_2, in the atmosphere.[1] Biodiesel has emerged as a prominent alternative fuel source, garnering considerable attention worldwide.[2–4] However, a significant challenge in biodiesel production lies in the generation of approximately 10 wt% of glycerol as a by-product. With the rapid increase in glycerol production, the conversion of this low-valued glycerol into high-value product has become imperative.[5] This transformation of glycerol to high-valued chemicals is getting much attention these days. By 2020, global glycerol production is predicted to be about 37 million tons in the biodiesel market.[6]

In recent years, many reactions like dehydration, oxidation, esterification, fermentation, etherification, etc. have been introduced to decrease the amount of glycerol as a by-product in the world.[7] One of the significant derivatives of glycerol is acetins.[8] These acetins, including monoacetin, diacetin, and triacetin, find wide-ranging industrial applications, and are produced through the esterification of glycerol with acetic acid, employing acid catalysts with Lewis and/or Bronsted acid sites.[9] Monoacetin is employed in various sectors, such as the manufacturing of explosives, treatment of animal skin in the leather industry, as food additives, and as a solvent in tanning agents.[10] Additionally, diacetyl glycerol (DAG) serves as a softening agent, solvent, and intermediate in the synthesis of structural lipids.[11] Both are used as raw materials for biodegradable polyester production and can be applied in low-temperature processes (cryogenics).[12] In a gasoline engine, triacetin glycerol (TAG) is utilized as a fuel additive to reduce knocking. TAG is one of the antimicrobial agents used in pharmaceuticals and the production of cigarette filters.[13] It is also used to reduce tailpipe emissions.

In the past, the esterification reactions were commonly conducted using homogeneous catalysts like hydrofluoric, sulphuric acid, nitric acid, hydrochloric acid, p- toluene sulfonic acid.[14] Nevertheless, these liquid acids have drawbacks due to their hazardous nature, corrosiveness, and challenging removal from liquid products. Besides these, a liquid catalyst is not environment-friendly and not suitable for reactors due to its corrosive nature. To address these limitations, numerous solid acid catalysts have been documented in the literature for the

esterification reactions including molecular sieves, ion-exchanged resins, transition metals oxides, and Amberlyst-36, as well as Amberlyst-15, zeolites, zirconia-based acid catalyst,[15–17] cesium phosphotungstate catalyst,[13] microcrystalline cellulose, propyl sulfonic acid functionalized SBA-15, sulfonic acid functionalized SBA-15 catalysts, etc.[6,18–23] However, these heterogeneous catalysts have not exhibited satisfactory performance. Zeolites have attracted increasing attention due to their adjustable acidity, pore size, and capability to incorporate additional metals within the framework. Their shape and size selectivity characteristics have become highly relevant in the chemical industries as heterogeneous catalysts.[24,25] In the current study, the commercially available HZSM-5 zeolite has been modified with cerium ammonium nitrate solution to enhance its catalytic activity in glycerol esterification with acetic acid (**Scheme 3.1**).

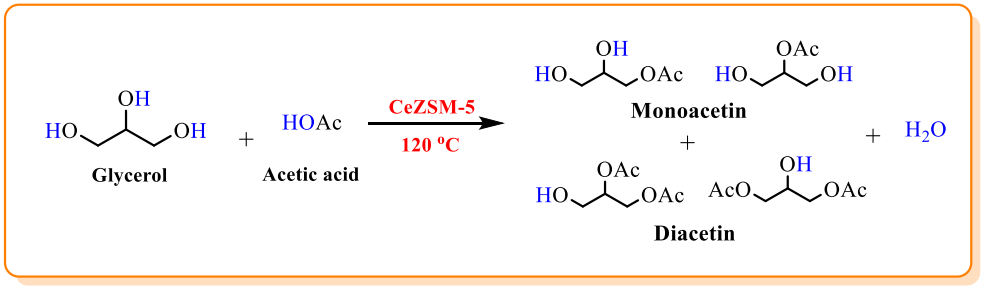

Scheme 3.1. Esterification of glycerol with acetic acid using CeZSM-5 zeolite.

3.2. Results and Discussion

3.2.1. Activity of catalyst in the esterification reaction

The esterification reaction of glycerol with acetic acid was performed without a catalyst. This reaction shows a maximum of 40.59 % glycerol conversion in 5 h of reaction time. The same reaction was then carried out with the HZSM-5 zeolite catalyst which shows 76.43 % glycerol conversion. The HZSM-5 zeolite showed much better conversion than a blank reaction as shown in **Figure 3.1(a)**. To achieve a higher conversion the catalyst was modified with cerium refluxing with 1 %, 3 %, 5 %, and 7 % ceric ammonium nitrate solution. These zeolites are designated as Ce_1ZSM-5, Ce_3ZSM-5, Ce_5ZSM-5, and Ce_7ZSM-5 respectively. The activity of modified catalysts was evaluated at a constant catalyst weight of 8 wt%, mole ratio of 9, at a temperature of 120 °C, and reaction time of 1 to 5 h. In **Figure 3.1(b)**, Ce_5ZSM-5 showed the maximum conversion of 98.32 % in 5 h reaction time whereas Ce_1ZSM-5 gives 35.82 %

conversion, Ce_3ZSM-5 gives 63.54 % conversion and Ce_7ZSM-5 gives 95.21 % conversion. Therefore, Ce_5ZSM-5 was taken to carry out all other reactions.

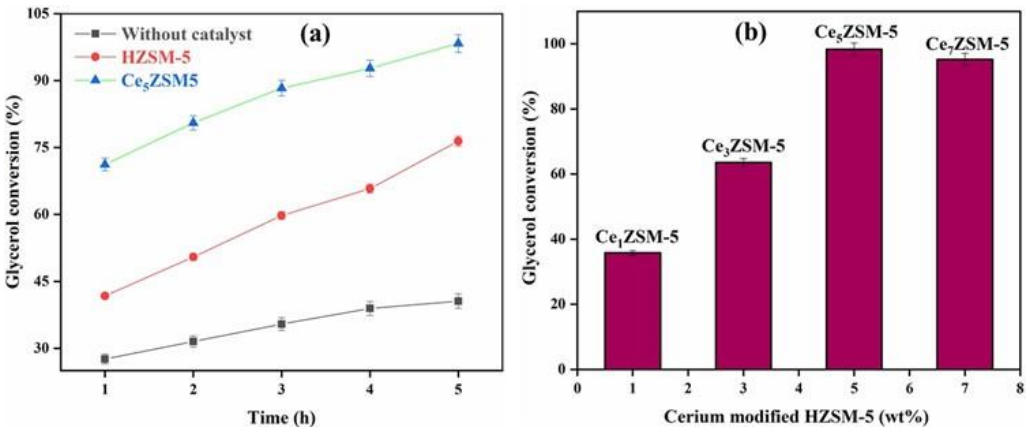

Figure 3.1. (a) Effect of catalyst, (b) Effect of cerium loading on glycerol conversion.

Conditions: Catalyst 8 wt%, temperature 120 ℃, mole ratio 9:1, reaction time 5 h.

3.2.2. Effect of acetic acid to glycerol mole ratio on glycerol conversion

The experiments aimed to optimize the mole ratio of glycerol to acetic acid. The esterification was carried out at a constant temperature of 120 ℃ while varying the mole ratio of acetic acid to glycerol from 1 to 11, as shown in **Figure 3.2**. As the acetic acid to glycerol mole ratio increased from 1 to 9, there was a corresponding increase in glycerol conversion, reaching a maximum conversion of 98.32 % at mole ratio 9. However, beyond this ratio, the glycerol conversion decreased to 48.35 %. With the increase in mole ratio, the selectivity of monoacetin gradually decreases from 82 % to 45.52 % whereas diacetin selectivity gradually increases from 12.24 % to 54.48 %.

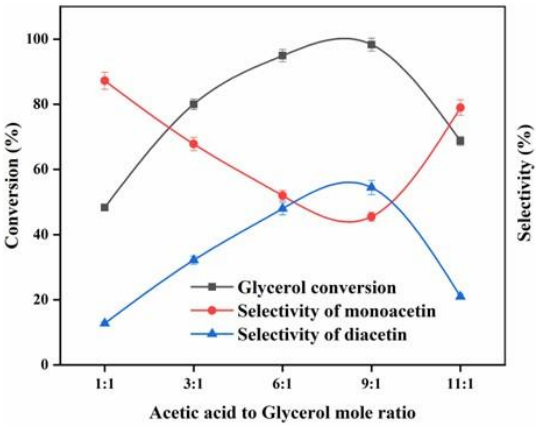

Figure 3.2. Effect of glycerol to acetic acid mole ratio on glycerol conversion.

Conditions: 8 wt% Ce_5ZSM-5 catalyst, temperature 120 ℃, reaction time 5 h.

Above the reactant ratio of 9:1, monoacetin selectivity increases to 79.01 % whereas diacetin selectivity decreases to 20.99 %. These results show that the mole ratio of reactants has an important role in glycerol conversion and product selectivity. As the mole ratio increases to 11, a sharp and significant decrease in glycerol conversion is observed which is due to the decrease in the concentration of glycerol in the reaction mixture and also to the blockage of active sites of zeolite by excess reactant at higher mole ratio.

3.2.3. Effect of catalyst loading on glycerol conversion

Experiments were conducted to investigate the impact of catalyst loading on glycerol conversion. The study explored the effect of catalyst weight on glycerol conversion at 120 ℃ with a reactant mole ratio of 9. The catalyst weight ranged from 2 to 8 wt%. **Figure 3.3** shows that the glycerol conversion significantly increased from 34 % to 98.32 % when the catalyst loading was increased from 2 to 8 wt%. The increase in catalyst weight leads to a higher number of active sites available for the reaction, resulting in greater conversion of the reactants. The larger the number of active sites higher is the conversion of the reactants. Finally, glycerol conversion reaches its maximum of 98.32 % over an 8 wt% catalyst. The selectivity of monoacetin decreases from 76.62 % to 45.52 % with the increase in catalyst weight but diacetin selectivity increases from 23.38 % to 54.48 % over an 8 wt% catalyst.

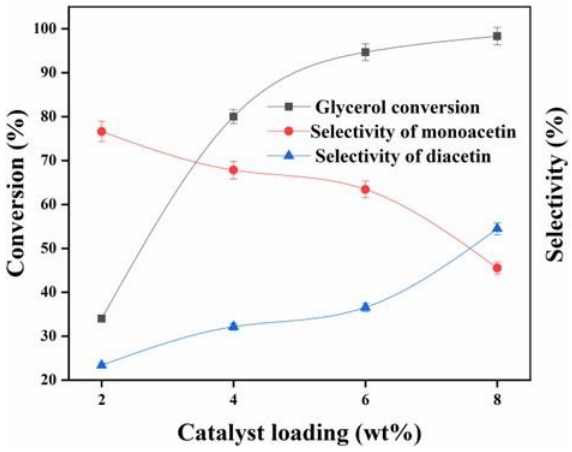

Figure 3.3. Effect of catalyst loading on glycerol conversion.

Conditions: Ce_5ZSM-5, catalyst 8 wt%, temperature 120 ℃, molar ratio 9:1, reaction time 5 h.

3.2.4. Effect of temperature on glycerol conversion

The effect of reaction temperature on glycerol conversion was studied by varying the temperature from 30 ℃ to 120 ℃ and shown in **Figure 3.4** at constant catalyst weight 8 wt%,

mole ratio 9, and reaction time 1 to 5 h. It is observed that with the increase in temperature from 30 ℃ to 120 ℃, the conversion of glycerol increases. A maximum glycerol conversion of 98.32 % is obtained at 120 ℃, 5 h of reaction time. At 30 ℃ temperature, 5 h reaction time, 11.46 % conversion of glycerol was achieved. It is seen that with an increase in reaction time, conversion increases as in higher contact time interaction of the reactant molecules increases. 120 ℃ was taken as the optimum temperature as a maximum conversion is obtained at this temperature.

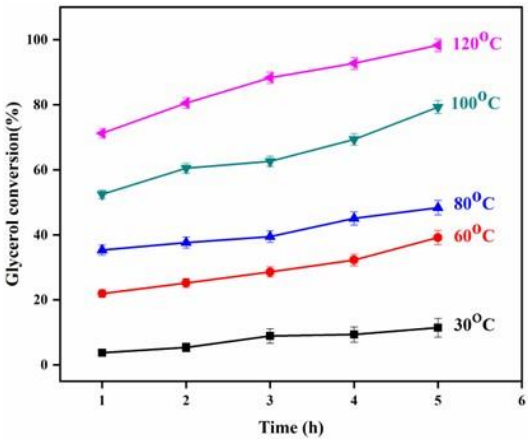

Figure 3.4. Effect of temperature on glycerol conversion.

Conditions: Ce_5ZSM-5, catalyst 8 wt %, molar ratio 9:1, reaction time 5h.

3.2.5. Catalyst Reusability and stability test

The catalyst reusability test was investigated at a temperature of 120 ℃, 8 wt% Ce_5ZSM-5 catalyst, the mole ratio of reactants 9:1, and a reaction time of 5 h. Before every cycle, the catalyst was separated from the reaction mixture either by centrifugation or by filtration method followed by washing and drying overnight at 333 K, and finally, the catalyst was calcined at 823 K for 4 h before every reaction. Four cycles were performed to check the renewability of the catalyst. The obtained results are shown in **Figure 3.5.** It is clear from the figure that there is no significant decrease in glycerol conversion. Product selectivity was also consistent for the four cycles. Glycerol conversion was reduced to 88.25 % in the 4^{th} cycle from 98.32 % in the 1^{st} cycle. The decrease in the glycerol conversion could be due to the leaching of cerium from HZSM-5 which decreases the activity of the catalyst and also deactivation of the catalyst for the blockage of the active sites by reactants and products. However, with a decrease in conversion in every recycle diacetin selectivity decreases from 54.48 % to 52.72 % whereas monoacetin selectivity increases from 45.52 % to 47.28 %.

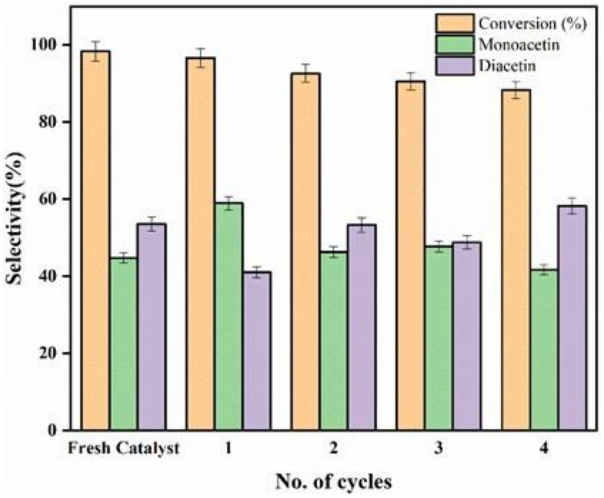

Figure 3.5. Reusability of zeolite catalyst in the esterification reaction.

3.3. Kinetic modelling

The reaction kinetics of the esterification of GLY with AcA is scarcely reported in the literature. Kinetic runs were performed at five different temperatures ranging from 60-120 °C. The product samples were collected after every hour at each temperature. All the kinetic runs were conducted at optimized parameters like catalyst 8 wt%, glycerol to acetic acid mole ratio 9:1, and reaction time 5 h.

The elementary steps of esterification reactions are given below.

$$\text{Glycerol} + \text{Acetic acid} \xrightarrow{k_1} \text{Monoacetin} + \text{Water}$$

$$\text{Monoacetin} + \text{Acetic acid} \xrightarrow{k_2} \text{Diacetin} + \text{Water}$$

The overall reaction

$$\text{Glycerol} + \text{Acetic acid} \xrightarrow{K} \text{Monoacetin} + \text{Diacetin}$$

Langmuir-Hinshelwood-Hougen-Watson (LHHW) model was tried to fit the kinetic data for the esterification reaction of GLY with AcA with the surface reaction as a rate-controlling step. Model equations followed by single-site as well as dual-site mechanisms were derived and tried to fit the kinetic data but were discarded due to negative values of rate constants. The following rate expression using the L-H-H-W model.

For the Dual-site mechanism,

rate of disappearance of GLY $r_G = \frac{Ct^2\,(k_1 K_G K_{AA} C_G C_{AA} - k_2 K_M K_D C_M C_D)}{Z^2}$.....(1)

Where, $Z = 1+K_G C_G+K_{AA} C_{AA}+K_M C_M+K_D C_D$

k_1 and k_2 are reaction rate constants. K_G, K_{AA}, K_M, & K_D are the adsorption constants and C_G, C_{AA}, C_M & C_D are the concentrations of GLY, AcA, MA, and DA respectively.

Now, for the Single-site mechanism:

$$r_G = \frac{kC_G}{Z} \text{.....(2)}$$

Where, $Z = 1+K_G C_G+K_M C_M+K_D C_D$

The model parameters were estimated using non-linear regression by Polymath 6.10. But due to the negative rate constant values in both cases, the models were not considered

The generalized rate of the reaction is expressed as:

$$-r_G = -\frac{dCg}{dt} = kC_g C_a \text{.....(3)}$$

Where k is the rate constant and C_g and C_a are the concentration of GLY and AcA respectively. In the esterification reaction, AcA was taken as an excess reactant, so the concentration of AcA was assumed to be constant for the overall reaction. Since AcA is present in excess amounts in the reaction, the rate of the reaction was expressed based on limiting reactant GLY only. Thus, the rate of reaction was expressed as:

$$-r_G = -\frac{dCg}{dt} = kC_g$$

Now, the order of the reaction was calculated by plotting zero, first, and second-order rate equations as shown in **Figure 3.6**. Among all the plotted graphs, the R^2 value is maximum which is 0.94 for **Figure 3.6 (b)**. So, The linear nature of the plot of $-\ln(1-X_{gly})$ *versus* reaction time was observed in the first-order reaction rate.

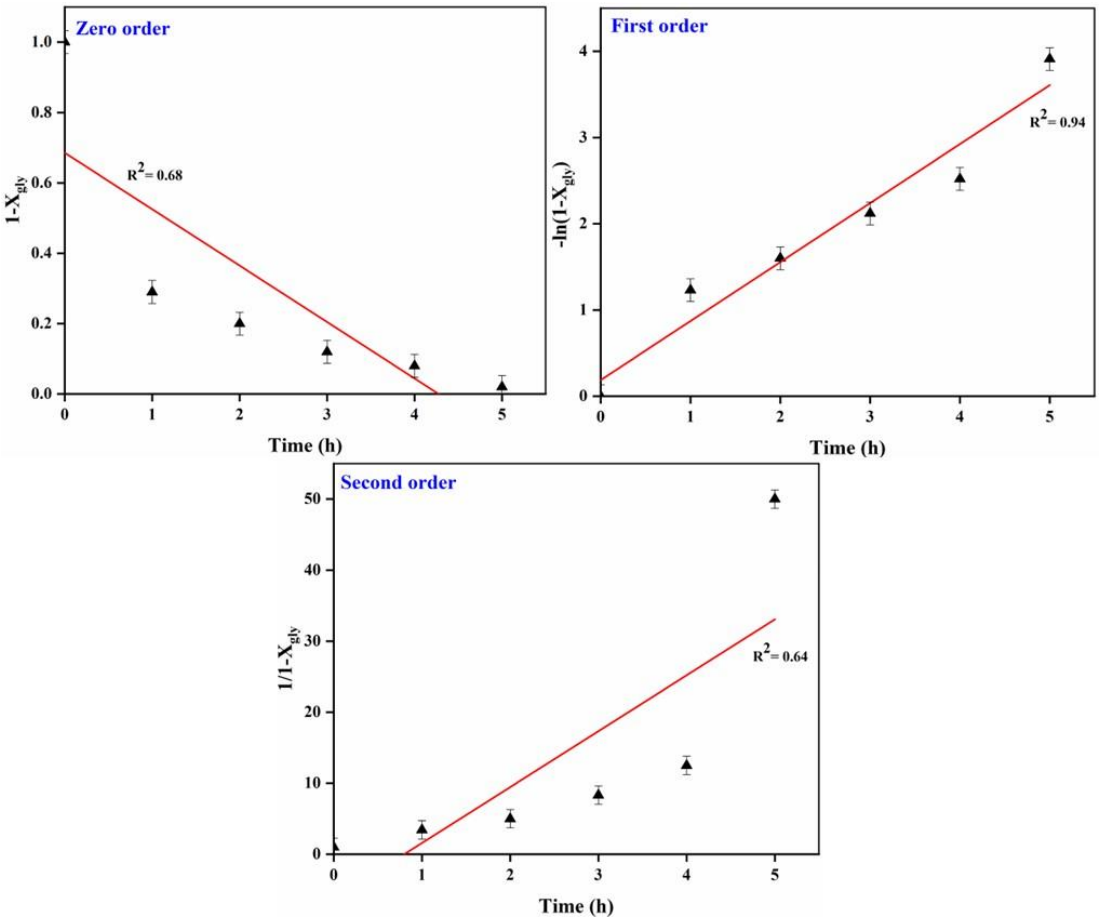

Figure 3.6. A plot of (a) 1-X_{gly}, (b) -ln(1-X_{gly}), and (c) 1/1-X_{gly} *versus* reaction time (h) for zero, first, and second order reaction.

Table 3.1 shows the effect of temperature on the reaction rate constant. It is also clear from **Table 3.1** that with an increase in temperature value of k increases. The first-order kinetics is shown in **Figure 3.7 (a)** at different reaction temperatures. Different k values were estimated by the different slopes of this graph. Arrhenius equation was employed to find the activation energy of esterification and the plot is shown in **Figure 3.7 (b)**.

$$K = Ae^{\frac{-Ea}{RT}}$$

$$\ln K = lnA - \frac{Ea}{RT}$$

Where k is the rate constant, A is the Arrhenius constant, E_a is the activation energy, R is the universal gas constant and T is the temperature. The activation energy (E_a) and pre-exponential factors (A) were 63.720 kJmol^{-1} and 6.56×10^7 respectively shown in **Table 3.2**.[26]

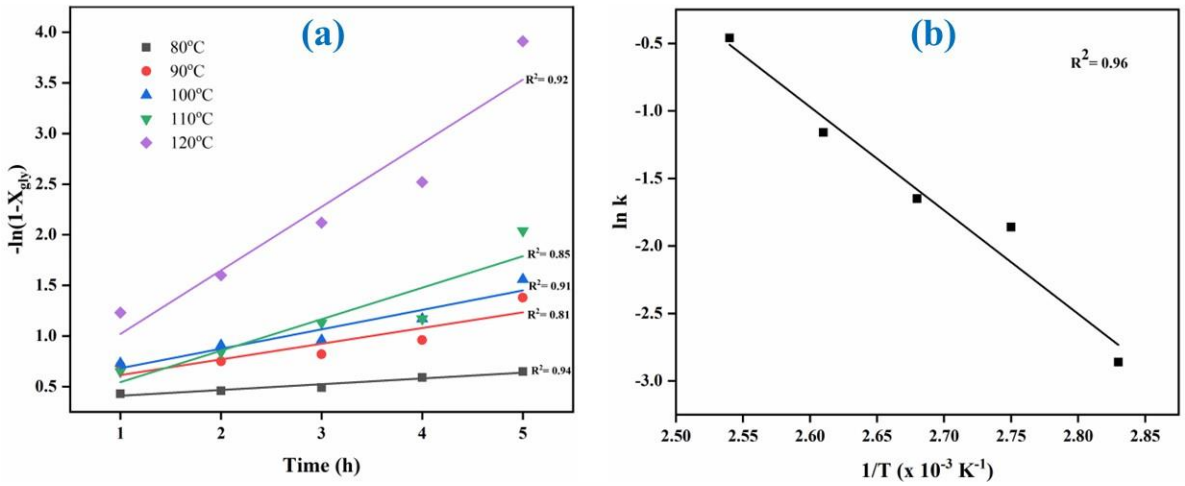

Figure 3.7. (a) A plot of -ln(1-X_{gly}) *versus* reaction time (h), (b) Arrhenius plot for esterification of GLY.

Table 3.1. Effect of temperature on the rate constant of the reaction

Temperature (°C)	Rate constant, k (h^{-1})
80	0.057
90	0.155
100	0.192
110	0.311
120	0.628

Table 3.2. Activation energy and pre-exponential factor

Activation Energy, E_a (kJmol^{-1})	Pre-exponential factor, A
63.72	6.56×10^{7}

3.4. Plausible mechanism

The acidic sites of the catalyst play a crucial role in determining the selectivity of the products. **Scheme 3.2** presents a plausible mechanism of the esterification of glycerol (GLY) with acetic acid (AcA), initiated by the activation of the carbonyl group of AcA through the CeZSM-5 catalyst. This activation leads to an increase in the electrophilicity of the carbonyl carbon. Subsequently, the oxygen atom of one of the hydroxyl groups of GLY attacks the same carbonyl carbon. Following this, a proton transfer occurs from this intermediate to the other hydroxyl group of the GLY, leading to the formation of the water molecule. The loss of water ultimately results in the synthesis of monoacetin. This same mechanism continues in the

reaction of monoacetin with AcA, leading to the synthesis of diacetin. The catalyst is regenerated by centrifugation for further reaction.

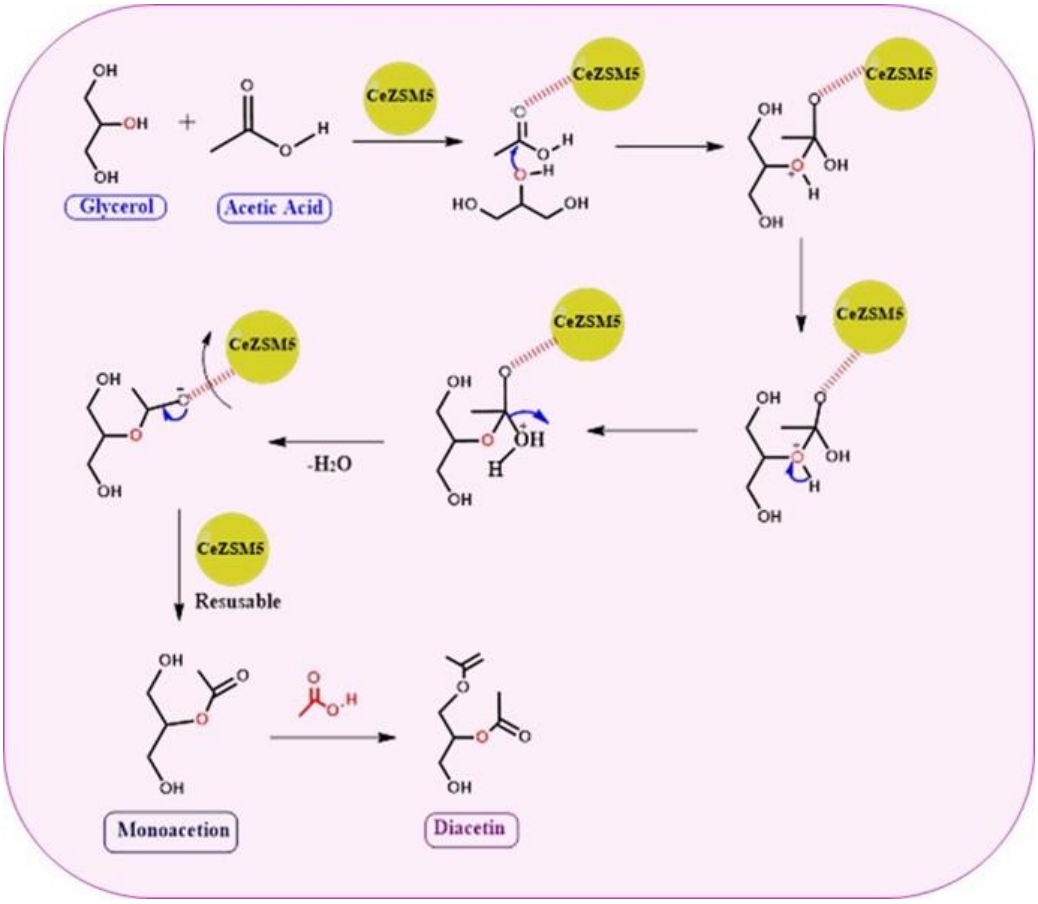

Scheme 3.2. Plausible reaction mechanism for the esterification reaction.

3.4. Conclusion

The HZSM-5 zeolite was successfully modified with cerium, and various characterization techniques were used. The resulting catalyst, Ce_5ZSM-5 zeolite, proved to be highly effective for the esterification reaction of GLY with AcA, leading to the synthesis of MA and DA. The reaction was conducted at different temperatures, catalyst weights, and the mole ratios of reactants. At 120 ℃, using 8 wt% of the catalyst and 9:1 molar ratio of acetic acid to glycerol, a maximum GLY conversion of 98.32% was achieved. This condition resulted in a mixture of products, specifically Ma and DA, with no formation of TA. This selectivity indicates that the catalyst is quite specific to the synthesis of MA and DA only. The catalyst's regenerability was also evaluated, and it showed no significant decrease in the GLY conversion for up to four cycles of use. The reaction was found to follow pseudo-first-order kinetics. Activation energy and pre-exponential factor for this reaction were estimated to be 63.72 $kJmol^{-1}$ and 6.56×10^{7} respectively.

References

1 V. L. C. Gonçalves, B. P. Pinto, J. C. Silva and C. J. A. Mota, *Catal. Today*, 2008, **133**–**135**, 673–677.

2 J. Liu, Z. Wang, Y. Sun, R. Jian, P. Jian and D. Wang, *Chinese J. Chem. Eng.*, 2019, **27**, 1073–1078.

3 H. Wepoh, 2015, 3–10.

4 M. Zhang, J. Shi, Y. Sun, W. Ning and Z. Hou, *Catal. Commun.*, 2015, **70**, 72–76.

5 S. Kale, U. Armbruster, S. Umbarkar, M. Dongare and A. Martin, *10th Green Chem. Conf.*, 2013, **70–71**.

6 S. Kale, S. B. Umbarkar, M. K. Dongare, R. Eckelt, U. Armbruster and A. Martin, *Appl. Catal. A Gen.*, 2015, **490**, 10–16.

7 M. Pagliaro, R. Ciriminna, H. Kimura, M. Rossi and C. Della Pina, *Angew. Chemie - Int. Ed.*, 2007, **46**, 4434–4440.

8 J. Liu, Z. Wang, Y. Sun, R. Jian, P. Jian and D. Wang, *Chinese J. Chem. Eng.*, 2019, **27**, 1073–1078.

9 L. Setyaningsih, F. Siddiq and A. Pramezy, *MATEC Web Conf.*, 2018, **154**, 2–5.

10 W. Hu, Y. Zhang, Y. Huang, J. Wang, J. Gao and J. Xu, *J. Energy Chem.*, 2015, **24**, 632–636.

11 A. B. S. Neto, A. C. Oliveira, E. Rodriguez-Castellón, A. F. Campos, P. T. C. Freire, F. F. F. Sousa, J. M. Filho, J. C. S. Araujo and R. Lang, *Catal. Today*, 2018, **349**, 57.

12 S. A. Rane, S. M. Pudi and P. Biswas, *Chem. Biochem. Eng. Q.*, 2016, **30**, 33–45.

13 S. Sandesh, P. Manjunathan, A. B. Halgeri and G. V. Shanbhag, *RSC Adv.*, 2015, **5**, 104354–104362.

14 S. Karnjanakom, P. Maneechakr, C. Samart and G. Guan, *Energy Convers. Manag.*, 2018, **173**, 262–270.

15 H. Rastegari, H. S. Ghaziaskar and M. Yalpani, *Ind. Eng. Chem. Res.*, 2015, **54**, 3279–3284.

16 P. S. Reddy, P. Sudarsanam, G. Raju and B. M. Reddy, *Catal. Commun.*, 2010, **11**, 1224–1228.

17 R. B. Cahyono, Z. Mufrodi, A. Hidayat and A. Budiman, *ARPN J. Eng. Appl. Sci.*, 2016, **11**, 5194–5197.

18 M. Y. Huang, X. X. Han, C. Te Hung, J. C. Lin, P. H. Wu, J. C. Wu and S. Bin Liu, *J. Catal.*, 2014, **320**, 42–51.

19 B. Mallesham, P. Sudarsanam and B. M. Reddy, *Ind. Eng. Chem. Res.*, 2014, **53**, 18775–18785.

20 K. Jagadeeswaraiah, M. Balaraju, P. S. S. Prasad and N. Lingaiah, *Appl. Catal. A Gen.*, 2010, **386**, 166–170.

21 M. Popova, Á. Szegedi, A. Ristić and N. N. Tušar, *Catal. Sci. Technol.*, 2014, **4**, 3993–4000.

22 L. Zhou, E. Al-Zaini and A. A. Adesina, *Fuel*, 2013, **103**, 617–625.

23 B. O. Dalla Costa, H. P. Decolatti, M. S. Legnoverde and C. A. Querini, *Catal. Today*, 2017, **289**, 222–230.

24 B. Yilmaz and U. Müller, *Top. Catal.*, 2009, **52**, 888–895.

25 N. Fattahi, K. Triantafyllidis, R. Luque and A. Ramazani, *Catalysts*, 20.19, **9,** 758.

26 L. Zhou, T. H. Nguyen and A. A. Adesina, *Fuel Process. Technol.*, 2012, **104**, 310–318.

CHAPTER 4

CATALYTIC SYNTHESIS OF ENERGY-RICH FUEL ADDITIVE LEVULINATE ESTERS FROM LEVULINIC ACID USING MODIFIED ULTRA-STABLE ZEOLITE Y

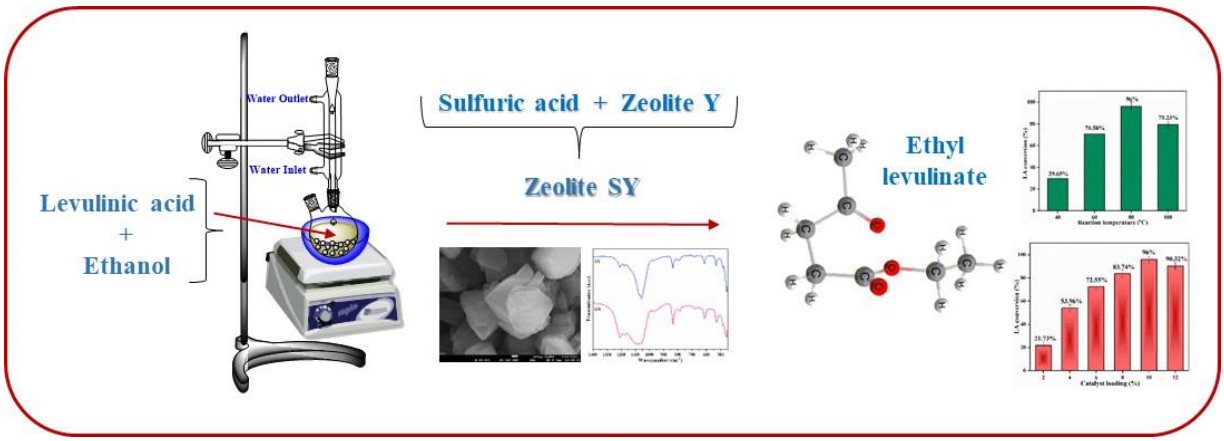

4.1. Introduction

In the present scenario, due to the increase in the worldwide population, modernization, and living standards, non-renewable energy resources (coal, diesel, petrol, natural gases, etc.) are insufficient to fulfill the global future energy demands.[1–3] This leads to the continued rise in the cost of fossil fuels. Also, the burning of these fossil fuels affects the environment like global warming, smog formation, the overall increase in the temperature, etc.[4,5] Global researchers are trying alternative renewable energy resources that would be used as energy demand in the future.[6,7] According to the studies, in 2015, the obtained energy from renewable sources was 6.7%, and in 2017, it was 7.2%. So, it becomes necessary to develop bio-based technology to synthesize renewable fuels.[8]

Biomass is a renewable resource consisting of carbon-based matter found in plants, agricultural, forest, and municipal residues, both in fresh and waste forms. Approximately 3.33% of this biomass is utilized by humans and animals, either directly through food consumption or non-food applications. Its annual production amounts to about 2.0×10^{11} tons.[9–11] Additionally, biomass serves as a primary source of renewable energy, with applications in the synthesis of carbon-based fuels, chemicals, and other value-added products, contributing to a greener future.[5] In recent years, significant research efforts have been focused on converting biomass into valuable chemicals and biofuels, getting much more attention.[12,13]

Levulinic acid contains ketone and carboxylic acid groups, making it suitable for synthezing various compounds such as levulinate esters, δ-amino levulinic acid, 1,4- pentanediol, α-angelica lactone, β-acetylacrylic acid, γ-valerolactone, etc.[14–16] Among all, levulinic acid (LA) and its esters are highly valuable materials derived from biomass and find applications as platform chemicals in green solvents, fragrances, biofuels, pharmaceutical intermediates, monomers in polymers, fuel additives, flavoring agents and resin precursors.[17–21] For instance, ethyl levulinate can serve as amiscible biofuel in regular diesel car engines, with a potential use of up to 5 wt%.[22,23] Additionally, n-butyl levulinate finds applications in organic process industries as plasticizing agents, odorous substances, solvents, and fuel-additive compounds.[24]

Esters of levulinic acid can be synthesized through catalytic esterification with alkyl alcohols like methanol, ethanol, and butanol. This reaction yield methyl levulinate, ethyl levulinate, and butyl levulinate respectively utilizing an acidic catalyst.[23,25–28] Liquid- phase esterification of levulinic acid can be accomplished using acidic catalysts, such as sulphuric acid, phosphoric acid or hydrochloric acid, polyphosphoric acid, or p-toluenesulfonic acid.[29–31] However, the

use of homogeneous catalysts causes significant environmental issues, including handling and transportation challenges, toxicity, equipment corrosion, disposal, and regeneration. To address these drawbacks, researchers have developed environmentally friendly heterogeneous catalysts, which exhibit considerable catalytic activity, renewability and stability in the reaction medium.[32–36] Some examples of such heterogeneous catalysts include resins,[26,37-40] silica-based,[27,41-46] heteroployacids,[23,37,38,47,48,39–46] zirconia-based,[27,28,49–53] zeolites,[12,24,25,38,54–58] bio-catalysts,[59–62] etc. which are utilized for various reactions.

Zeolites, in particular, are crystalline, microporous three-dimensional aluminosilicates interconnected by the oxygen atoms, possessing channels, cages and well-defined molecular dimensions known as pores.[63,64] Due to these unique characteristics, zeolites find wide-ranging applications in the production of petrochemicals, water purification, wastewater treatment, oil-refining plants, and various organic reactions, such as isomerization, alkylation, cracking, esterification. They serve as solid-acid catalysts, material adsorbents, and ion-exchangers.[56,57] The choice of zeolite as a catalyst in a specific reaction depends on the desired properties required for that particular reaction. Therefore, zeolites can be designed and modified to enhance their catalytic properties based on the specific reaction requirements.[12,38,54–56]

Various zeolites like H-BEA, H-ZSM-5, H-MOR, H-Y,[24] zeolites and sulfated oxides,[25] dodecatungstophosphoric acid modified DH-ZSM-5,[38] descilicated H-ZSM-5,[55] mesoporous H-ZSM-5,[54] micro-mesoporous H-BEA,[57] micro/ mesoporous H-ZSM-5,[56] micro/meso H-Z5,[65] hierarchical H-ZSM-5,[12] Al-containing zeolite MCM-41,[66] hierarchical ZSM-12,[67] Micromesoporous beta,[68] were reported in the literature performing esterification of levulinic acid with different alochols. Various zeolites have been used earlier for this reaction but very scarce work is done with the modified form of zeolite in this field. Various homogeneous and heterogeneous catalysts were used, and kinetics were also studied. In this work, ethyl levulinate is synthesized by esterifying levulinic acid with ethanol, using sulfuric acid-modified zeolite as catalyst.

4.2. Results and Discussion

4.2.1. The activity of the catalyst in the esterification reaction

The esterification of levulinic acid and ethanol were performed at optimum conditions like levulinic acid to ethanol mole ratio 1:11, catalyst concentration of 10 wt% at 80 ℃ having reaction run time of 5 h. The esterification can be performed even in the absence of any acidic catalyst as levulinic acid can stabilize the reaction on its own. Three different reactions were

performed, one without catalyst, the other with a parent hydrogen form of ultra-stable zeolite (HY), and the third with sulfuric acid-modified zeolite (SY), shown in the **Figure 4.1**. The highest conversion of 96% in case of SY catalyst due to the presence of maximum acid sites present on the surface of the catalyst which are responsible for the maximum conversion which is less for HY zeolite.

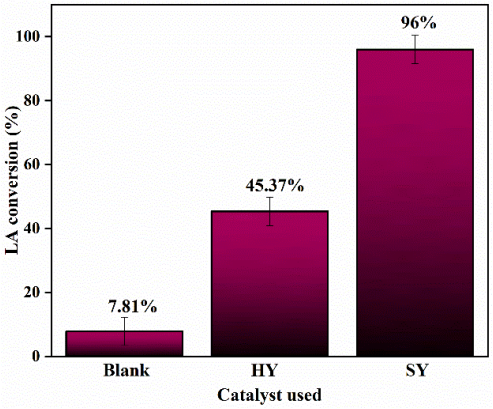

Figure 4.1. Effect of catalyst on LA conversion (Reaction conditions: Catalyst 10 wt%, temperature 80 °C, a mole ratio of LA: ethanol 1:11, reaction time 5 h).

4.2.2. Effect of catalyst amount on conversion of levulinic acid

The optimization of catalyst weight was performed and shown in **Figure 4.2**. It is visible from the figure that levulinic acid conversion increases from 21.73% to 96% as the amount of catalyst loading increases from 2 wt% to 12 wt%. The higher the catalyst, the more the availability of active sites, the availability of active sites, so the conversion of reactants to product formation is also more. Also, at 12 wt% catalyst loading, conversion showed some decrement to 90.32%. This is due to the increase in the catalyst's available sites, which proceeds the reaction in the reverse direction. The 10 wt% catalyst loading was used for further experiments.[70]

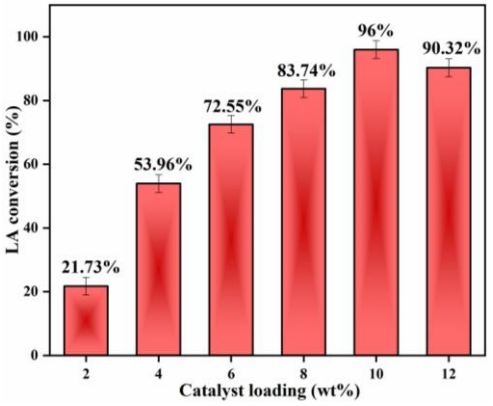

Figure 4.2. Effect of catalyst loading on LA conversion (Reaction conditions: temperature 80 °C, a mole ratio of LA: ethanol 1:11, reaction time 5 h).

4.2.3. Effect of levulinic acid/ethanol mole ratio on conversion of levulinic acid

The effect of the mole ratio of levulinic acid and ethanol was investigated by varying the mole ratio from 1:1 to 1:13 at optimized reaction conditions with 10 wt% catalyst loading, reaction time, 5 h, and temperature 80 °C. The effect of the mole ratio from 1:1 to 1:13 is depicted in Figure 8. It is seen from **Figure 4.3** that with increase in mole ratio, Levulinic acid conversion increases which is due to the more driving force in the direction of the formation of ethyl levulinate.[69] The percentage conversion of levulinic acid is increased from 25.9% to 96% which is maximum at the mole ratio of 1:11, above this ratio, conversion decreases because an excessive amount of ethanol blocks the active sites of catalyst reducing conversion. Hence 1:11 mole ratio was selected to carry out reactions throughout the experiments.

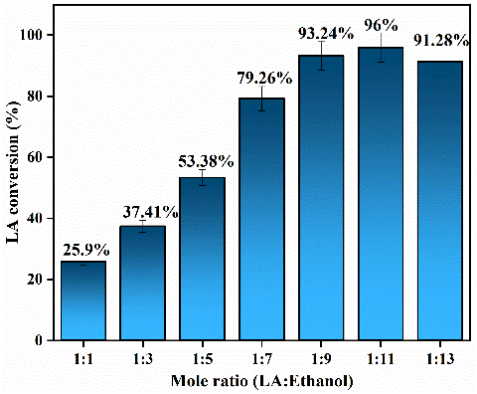

Figure 4.3. Effect of mole ratio on LA conversion (Reaction conditions: Catalyst 10 wt%, temperature 80 °C, reaction time 5 h).

4.2.4. Effect of reaction time on conversion of levulinic acid

The effect of reaction time on the esterification of levulinic acid was studied at catalyst loading 10 wt%, the mole ratio of levulinic acid: ethanol 1:11 , reaction temperature 80 °C and 96% of levulinic acid conversion was obtained at 5 h of reaction time. After that, the conversion starts decreasing due to the formation of water molecules that take the reaction in the reverse direction, which is held due to the hydrolysis of the ester (**Figure 4.4**).

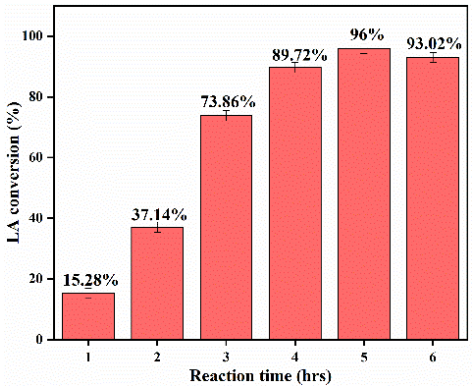

Figure 4.4. Effect of reaction time on LA conversion (Reaction conditions: Catalyst 10 wt%, temperature 80 °C, a mole ratio of LA: ethanol 1:11).

4.2.5. Effect of reaction temperature on conversion of levulinic acid

The effect of reaction temperature on esterification reactions was observed in the temperature range of 40 ℃ - 100 ℃ at mole ratio of levulinic acid to ethanol of 1:11, 10 wt% catalyst loading at a reaction time of 5 h. The results shown in **Figure 4.5** explain that higher temperature increases the reaction rate, and conversion also increases. The maximum conversion was obtained at 80 ℃, and this is due to the maximum successful collisions between the reactants, which are responsible for the sufficient energy required for the formation of the product.

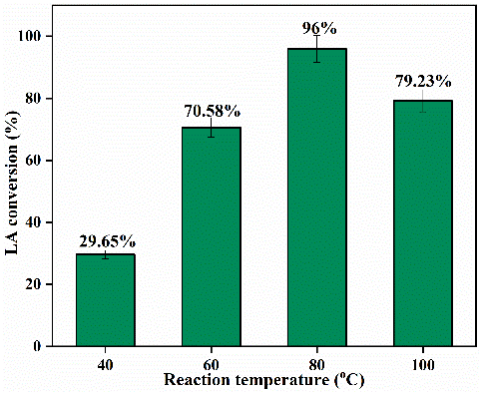

Figure 4.5. Effect of reaction temperature on LA conversion **(**Reaction conditions: Catalyst 10 wt%, a mole ratio of LA: ethanol 1:11, reaction time 5 h).

4.2.6. Effect of different alcohols on esterification of levulinic acid

The esterification of levulinic acid were carried out with ethanol, isopropanol and n-butanol. Esterification with ethanol over sulfuric acid-modified zeolite (SY) showed 96% conversion of levulinic acid at optimized reaction conditions: 10 wt% catalysts, the reactants mole ratio of

1:11, reaction time of 5 h and reaction temperature 80 ℃ shown in **Figure 4.6**. The esterification with ethanol, propanol, and butanol gives 96%, 77.33%, and 40.64% of levulinic acid conversion, respectively. It is clear from the conversion that shorter carbon chain alcohols showed higher conversion for the esterification reaction. It is due to the steric effect of using longer chain alcohols that resist the conversion of intermediate to levulinate ester.[70] Siva Sanker et al., 2016, also explained that long-chain alcohol resulted in the formation of γ-valerolactone, which is intermediate, and this is because the hydrogen of long-chain alcohol is more prone to get transferred from alcohol to levulinic acid to form γ-valerolactone.

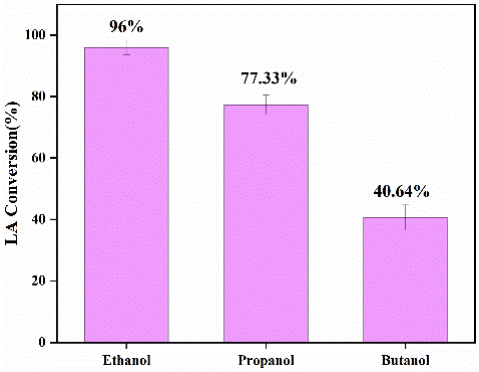

Figure 4.6. Effect of different alcohols on LA conversion (Reaction conditions: Catalyst 10 wt%, temperature 80 °C, a mole ratio of LA: alcohol 1:11, reaction time 5 h).

4.2.7. Catalyst reusability

The catalyst's reusability was evaluated through four cycles under optimized reaction conditions: a mole ratio of levulinic acid to ethanol 1:11, 10 wt% of catalyst loading, a reaction temperature of 80 °C, and a reaction run of 5 hours. After each cycle, the catalyst was separated from the reaction mixture using either by filtration or centrifugation. However, during filteration process, some catalyst loss occurred. The separaed catalyst was then washed, dried overnight at 100 ℃, and finally calcined at 500 ℃ for 2 hours. **Figure 4.7** illustrates the levulinic acid conversion during the four cycles. The conversion decreased from 96% to 11.52% in the 4^{th} cycle. This reduction in conversion may be attributed to the leaching of sulfate ions, or other species strongly adsorbed on the catalyst's active sites, leading to the deactivation of the catalyst over prolonged use.[25,51]

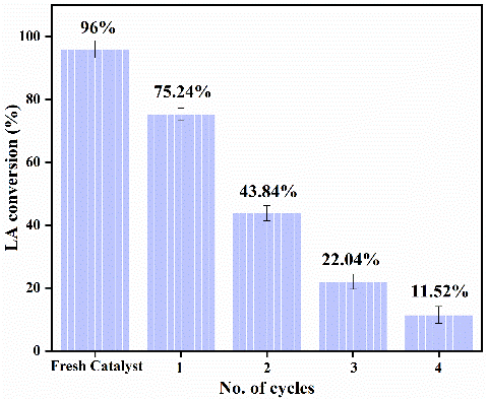

Figure 4.7. Reusability of modified zeolite in the esterification reaction of levulinic acid.

4.3. Kinetic study

The kinetic run for the reaction was carried out at four different temperatures i.e. 50 °C, 60 °C, 70 °C, and 80 °C respectively at optimized reaction parameters like catalyst 10 wt%, levulinic acid to ethanol mole ratio 1:11, reaction time 5 h. The aliquots were collected after each hour for every temperature. **Scheme 4.1** shows chemical reaction for the esterification reaction of levulinic acid with ethanol in the presence of sulfuric acid modified zeolite Y as heterogeneous catalyst.

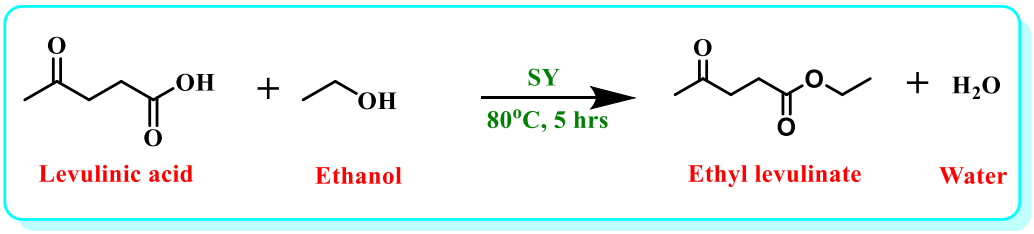

Scheme 4.1. Esterification of levulinic acid with ethanol at optimum conditions using SY zeolite as a catalyst.

In the esterification reaction of levulinic acid with ethanol, ethanol is taken in excess amount in the reaction mixture. Hence, its concentration is considered to be constant in the overall reaction. This is the reason that the reaction rate was expressed in terms of limiting reactant which is levulinic acid only. Thus, the expression for the rate of the reaction was:

$$-r_{LA} = -\frac{dC_{LA}}{dt} = kC_{LA} \qquad \text{Equation (1)}$$

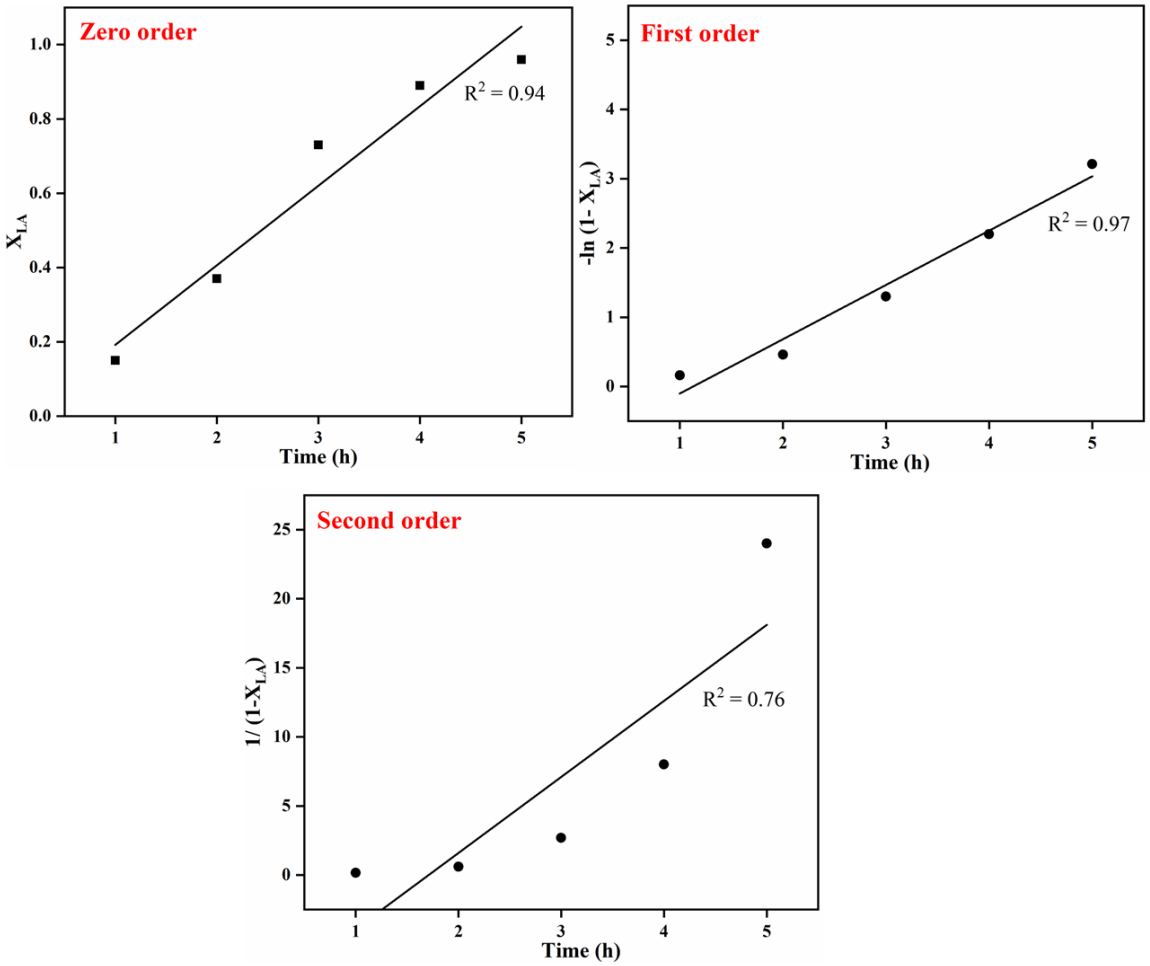

Figure 4.8. A plot of (a) X_{LA}, (b) $-\ln(1-X_{LA})$, and (c) $1/1-X_{LA}$ versus reaction time (h) for zero, first, and second order reaction.

The first step is to calculate the order of the reaction. So, the order was calculated by plotting the graph for zero, first, and second-order rate equations shown in **Figure 4.8**. The $R^2 = 0.97$ value is the maximum for the first-order reaction shown in **Figure 4.8(b)**. This confirms that the esterification reaction of levulinic acid with ethanol follows a first-order reaction.

The effect of the temperature on the rate constant for the reaction is shown in **Table 4.1**. **Table 4.1** clears that the rate constant value increases as the temperature increases. The kinetic study at different temperatures for the first-order reaction is shown in **Figure 4.9(a)**. Four different values of rate constant were calculated for four different temperatures. The activation energy was calculated using the Arrhenius equation as shown in **Figure 4.9(b)**.

$$k = Ae^{\frac{-Ea}{RT}} \qquad \text{Equation (2)}$$

$$\ln k = \ln A - \frac{E_a}{RT} \qquad \text{Equation (3)}$$

Where, k is the rate constant for the reaction, A is Arrhenius constant, E_a is the activation energy, R is the universal gas constant, and T is the temperature for the reaction. The activation energy (E_a) and pre-exponential factor (A) come out to be 19.570 $kJmol^{-1}$ and 1563.997 respectively.[71]

Table 4.1 Effect of temperature on the reaction rate

Temperature (°C)	Rate constant, k (h^{-1})
50	0.162
60	0.213
70	0.415
80	0.784

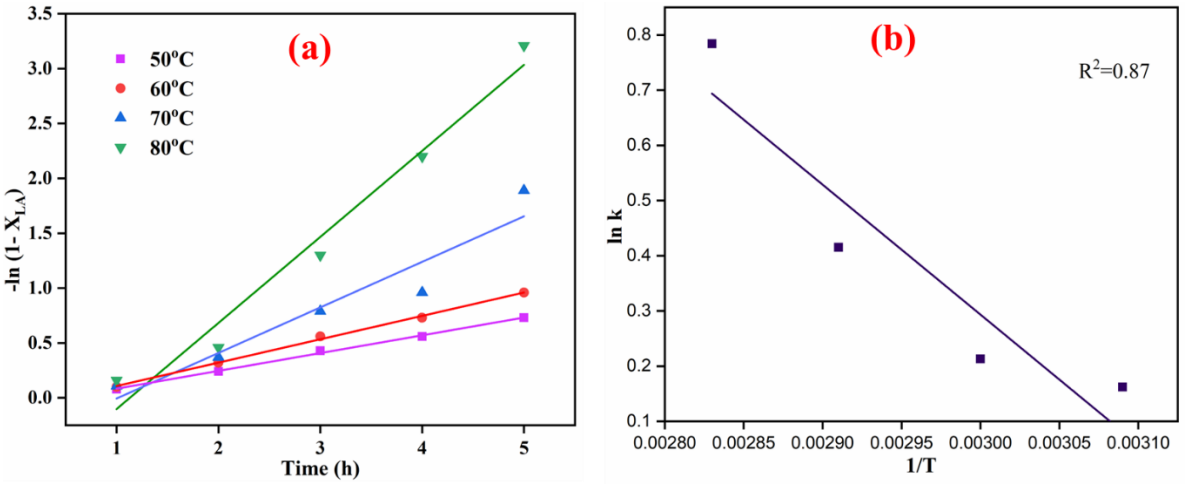

Figure 4.9. (a) A plot of $-\ln(1-X_{LA})$ vs reaction time (h) for the esterification reaction, (b) Arrhenius plot for esterification of levulinic acid.

4.3. Plausible mechanism

The high yield and selectivity of the product can be attributed to the presence of acidic sites. A plausible mechanism for the esterification of levulinic acid with various alcohols is presnted in the **Scheme 4.2**. The reaction initiates with the nucleophilic attack of zeolite to the oxygen of the carbonyl group in levulinic acid. Subsequently, the hydroxyl group performs anucleophilic attack on the positively charged carbonyl carbon. Proton transfer follows, resulting in the generation of the water molecule and the synthesis of the levulinate ester, ultimately leading to the removal of the catalyst.[43,69,72]

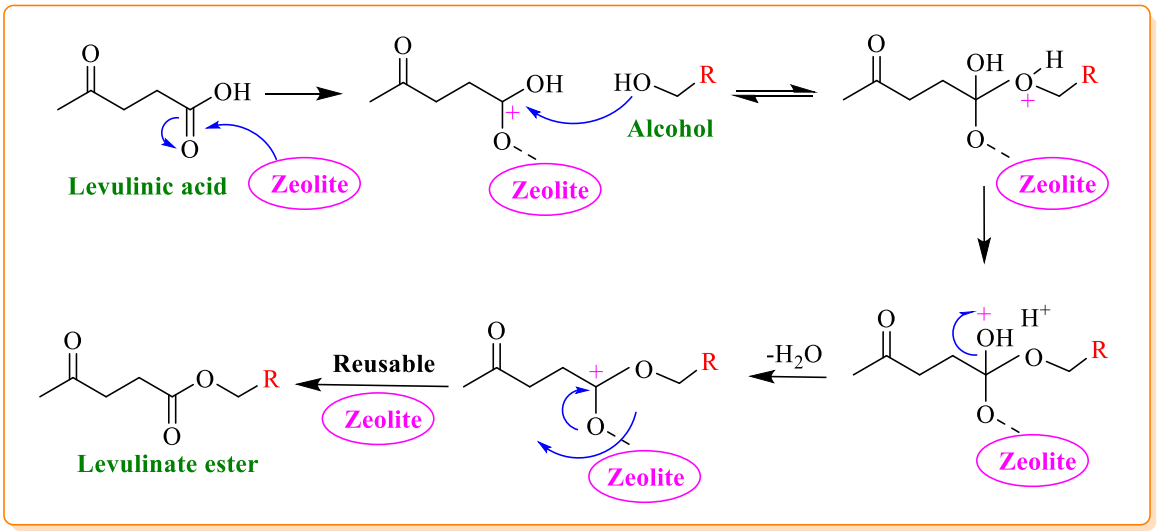

Scheme 4.2. A plausible mechanism for the esterification of levulinic acid with ethanol.

4.4. Conclusion

The H form of ultra-stable zeolite Y was modified with sulfuric acid, and characterization was performed to prove that zeolite Y has successfully modified. The reaction was carried out at different catalyst concentrations, the mole ratio of reactants, temperature, and reaction run time. The maximum levulinic acid conversion obtained was 96% which was at catalyst 10 wt%, reaction temperature 80 °C, a mole ratio of LA: ethanol 1:11, reaction time 5 hrs with 100% selectivity. The reusability of the catalyst was also examined and it shows a signification fall in the conversion for 4 cycles. The kinetic study of the reaction was also studied and the reaction comes out to be a pseudo-first-order reaction with activation energy and pre-exponential factor 19.570 kJmol^{-1} and 1563.997 respectively.

Reference

1 K. C. Badgujar, V. C. Badgujar and B. M. Bhanage, *Fuel Process. Technol.*, 2020, **197**, 106213.

2 V. Dhyani and T. Bhaskar, *Renew. Energy*, 2018, **129**, 695–716.

3 I. M. Atadashi, M. K. Aroua, A. R. Abdul Aziz and N. M. N. Sulaiman, *J. Ind. Eng. Chem.*, 2013, **19**, 14–26.

4 Y. Sun and J. Cheng, *Bioresour. Technol.*, 2002, **83**, 1–11.

5 M. A. Hossain, M. A. Mohamed Iqbal, N. M. Julkapli, P. San Kong, J. J. Ching and H. V. Lee, *RSC Adv.*, 2018, **8**, 5559–5577.

6 V. C. Badgujar, K. C. Badgujar, P. M. Yeole and B. M. Bhanage, *Bioprocess Biosyst. Eng.*, 2019, **42**, 47–61.

7 H. F. Liu, F. X. Zeng, L. Deng, B. Liao, H. Pang and Q. X. Guo, *Green Chem.*, 2013, **15**, 81–84.

8 K. C. Badgujar and B. M. Bhanage, *Bioresour. Technol.*, 2015, **178**, 2–18.

9 K. Tadele, S. Verma, M. A. Gonzalez and R. S. Varma, *Green Chem.*, 2017, **19**, 1624–1627.

10 D. W. Rackemann and W. O. Doherty, *Biofuels, Bioprod. Biorefining*, 2011, **5**, 198–214.

11 K. C. Badgujar and B. M. Bhanage, *Waste biorefinery*, Elsevier B.V., 2018, **3-38**.

12 K. Y. Nandiwale and V. V. Bokade, *Process Saf. Environ. Prot.*, 2016, **99**, 159–166.

13 Y. Xiao, G. Xiao and A. Varma, *Ind. Eng. Chem. Res.*, 2013, **52**, 14291–14296.

14 R. A. Sheldon, *Green Chem.*, 2014, **16**, 950–963.

15 K. C. Maheria, A. Lodhi, H. Lankapati and R. Krishna, *Catalysis for Clean Energy and Environmental Sustainability*, 2021, **1**, 345-382.

16 S. V. Vassilev, D. Baxter, L. K. Andersen and C. G. Vassileva, *Fuel*, 2010, **89**, 913–933.

17 H. J. Zhang, X. Y. Niu, J. Hu, C. L. Ren, H. L. Chen and X. G. Chen, *Catal. Sci. Technol.*, 2014, **4**, 3013-3024.

18 E. Christensen, J. Yanowitz, M. Ratcliff and R. L. McCormick, *Energy and Fuels*, 2011, **25**, 4723–4733.

19 J. C. Serrano-Ruiz, D. Wang and J. A. Dumesic, *Green Chem.*, 2010, **12**, 574–57.

20 M. Hartweg and C. R. Becer, *Green Chem.*, 2016, **18**, 3272–3277.

21 C. Leibig, B. Mullen, T. Mullen, L. Rieth and V. Badarinarayana, *ACS Symp. Ser.*, 2011, **1063**, 111–116.

22 A. Démolis, N. Essayem and F. Rataboul, *ACS Sustain. Chem. Eng.*, 2014, **2**, 1338–1352.

23 N. A. S. Ramli, D. Sivasubramaniam and N. A. S. Amin, *Bioenergy Res.*, 2017, **10**, 1105–1116.

24 K. C. Maheria, J. Kozinski and A. Dalai, *Catal. Letters*, 2013, **143**, 1220–1225.

25 D. R. Fernandes, A. S. Rocha, E. F. Mai, C. J. A. Mota and V. Teixeira Da Silva, *Appl. Catal. A Gen.*, 2012, **425**–**426**, 199–204.

26 G. Pasquale, P. Vázquez, G. Romanelli and G. Baronetti, *Catal. Commun.*, 2012, **18**, 115–120.

27 G. D. Yadav and A. R. Yadav, *Chem. Eng. J.*, 2014, **243**, 556–563.

28 M. M. Zainol, N. Aishah, S. Amin and M. Asmadi, *Renew. Energy*, 2019, **130**, 547–557.

29 P. L. Boey, S. Ganesan, G. P. Maniam, M. Khairuddean and J. Efendi, *Energy Convers. Manag.*, 2013, **65**, 392–396.

30 C. Liu, K. Zhang, Y. Liu and S. Wu, 2019, **14**, 2186–2196.

31 C. Chang, G. Xu and X. Jiang, *Bioresour. Technol.*, 2012, **121**, 93–99.

32 P. Gupta and S. Paul, *Catal. Today*, 2014, **236**, 153–170.

33 A. Yamaguchi, O. Sato, N. Mimura and M. Shirai, *Catal. Today*, 2016, **265**, 199–202.

34 L. Hu, L. Lin, Z. Wu, S. Zhou and S. Liu, *Appl. Catal. B Environ.*, 2015, **174**–**175**, 225–243.

35 R. K. Sharma, R. Gaur, M. Yadav, A. Goswami, R. Zbořil and M. B. Gawande, *Sci. Rep.*, 2018, **8**, 1–12.

36 Y. Tian, F. Zhang, J. Wang, L. Cao and Q. Han, *Bioresour. Technol.*, 2021, **342**, 125977.

37 M. Wu, X. Zhang, X. Su, X. Li, X. Zheng, X. Guan and P. Liu, *Catal. Commun.*, 2016, **85**, 66–69.

38 K. Y. Nandiwale, S. K. Sonar, P. S. Niphadkar, P. N. Joshi, S. S. Deshpande, V. S. Patil and V. V. Bokade, *Appl. Catal. A Gen.*, 2013, **460–461**, 90-98.

39 X. Zhou, Z. X. Li, C. Zhang, X. P. Gao, Y. Z. Dai and G. Y. Wang, *J. Mol. Catal. A Chem.*, 2016, **417**, 71–75.

40 M. Wu, Q. Q. Zhao, J. Li, H. Y. Wu, X. C. Zheng, X. X. Guan and P. Liu, *J. Exp. Nanosci.*, 2016, **11**, 1331–1347.

41 X. C. Zheng, N. Li, M. Wu, X. X. Guan and X. L. Zhang, *Res. Chem. Intermed.*, 2017, **43**, 6651–6664.

42 M. Wu, Q. Q. Zhao, J. Li, X. L. Su, H. Y. Wu, X. X. Guan and X. C. Zheng, *J. Porous Mater.*, 2016, **23**, 1329–1338.

43 Q. jie Luan, L. jun Liu, S. wen Gong, J. Lu, X. Wang and D. mei Lv, *Process Saf. Environ. Prot.*, 2018, **117**, 341–349.

44 S. Dharne and V. V. Bokade, *J. Nat. Gas Chem.*, 2011, **20**, 18–24.

45 C. B. Vilanculo, L. C. de Andrade Leles and M. J. da Silva, *Waste and Biomass Valorization*, 2020, **11**, 1895–1904.

46 K. Manikandan and K. K. Cheralathan, *Appl. Catal. A Gen.*, 2017, **547**, 237–247.

47 N. Lucas, L. Gurrala and A. Athawale, *J. Porous Mater.*, 2019, **26**, 1335–1343.

48 K. Yan, G. Wu, J. Wen and A. Chen, *Catal. Commun.*, 2013, **34**, 58–63.

49 M. M. Zainol, N. A. S. Amin and M. Asmadi, *Fuel Process. Technol.*, 2017, **167**, 431–441.

50 F. Su, L. Ma, D. Song, X. Zhang and Y. Guo, *Green Chem.*, 2013, **15**, 885–890.

51 Y. Kuwahara, W. Kaburagi, K. Nemoto and T. Fujitani, *Appl. Catal. A Gen.*, 2014, **476**, 186–196.

52 F. Su, Q. Wu, D. Song, X. Zhang, M. Wang and Y. Guo, *J. Mater. Chem. A*, 2013, **1**, 13209–13221.

53 D. Unlu, O. Ilgen and N. Durmaz Hilmioglu, *Chem. Eng. Res. Des.*, 2017, **118**, 248–258.

54 K. Y. Nandiwale, S. K. Yadava and V. V. Bokade, *J. Energy Chem.*, 2014, **23**, 535–541.

55 K. Y. Nandiwale, P. S. Niphadkar, S. S. Deshpande and V. V. Bokade, *J. Chem. Technol. Biotechnol.*, 2014, **89**, 1507–1515.

56 K. Y. Nandiwale and V. V. Bokade, *Chem. Eng. Technol.*, 2015, **38**, 246–252.

57 C. R. Patil, P. S. Niphadkar, V. V. Bokade and P. N. Joshi, *Catal. Commun.*, 2014, **43**, 188–191.

58 P. Dugkhuntod, T. Imyen, W. Wannapakdee, T. Yutthalekha, S. Salakhum and C. Wattanakit, *RSC Adv.*, 2019, **9**, 18087–18097.

59 H. M. Salvi and G. D. Yadav, *Biocatal. Agric. Biotechnol.*, 2019, **18**, 101038.

60 G. D. Yadav and I. V. Borkar, *Ind. Eng. Chem. Res.*, 2008, **47**, 3358–3363.

61 A. Lee, N. Chaibakhsh, M. B. A. Rahman, M. Basri and B. A. Tejo, *Ind. Crops Prod.*, 2010, **32**, 246–251.

62 K. C. Badgujar and B. M. Bhanage, *Fuel Process. Technol.*, 2015, **138**, 139–146.

63 B. Yilmaz and U. Müller, *Top. Catal.*, 2009, **52**, 888–895.

64 S. Rayalu, S. U. Meshram and M. Z. Hasan, *J. Hazard. Mater.*, 2000, **77**, 123–131.

65 P. Parthasarathy and S. K. Narayanan, *Environ. Prog. Sustain. Energy*, 2014, **33**, 676–680.

66 A. Najafi Chermahini and M. Nazeri, *Fuel Process. Technol.*, 2017, **167**, 442–450.

67 T. Imyen, K. Saenluang, P. Dugkhuntod and C. Wattanakit, *Microporous Mesoporous Mater.*, 2020, 110768.

68 D. H. Morawala, A. K. Dalai and K. C. Maheria, *Catal. Letters*, 2020, **150**, 1049–1060.

69 A. G. Khiratkar, K. R. Balinge, M. Krishnamurthy, K. K. Cheralathan, D. S. Patle, V. Singh, S. Arora and P. R. Bhagat, *Catal. Letters*, 2018, **148**, 680–690.

70 K. Anjali, A. Vijayan, N. J. Venkatesha and A. Sakthivel, *Inorg. Chem. Commun.*, 2021, **123**, 108302.

71 M. M. Zainol, M. Asmadi and N. A. S. Amin, *Chem. Eng. Sci.*, 2022, **247**, 117079.

72 M. Varkolu, V. Moodley, F. S. W. Potwana, S. B. Jonnalagadda and W. E. van Zyl, *React. Kinet. Mech. Catal.*, 2017, **120**, 69–80.

CHAPTER 5

SYNTHESIS OF GLYCEROL CARBONATE USING LITHIUM-MODIFIED ZEOLITE BETA: A KINETIC STUDY

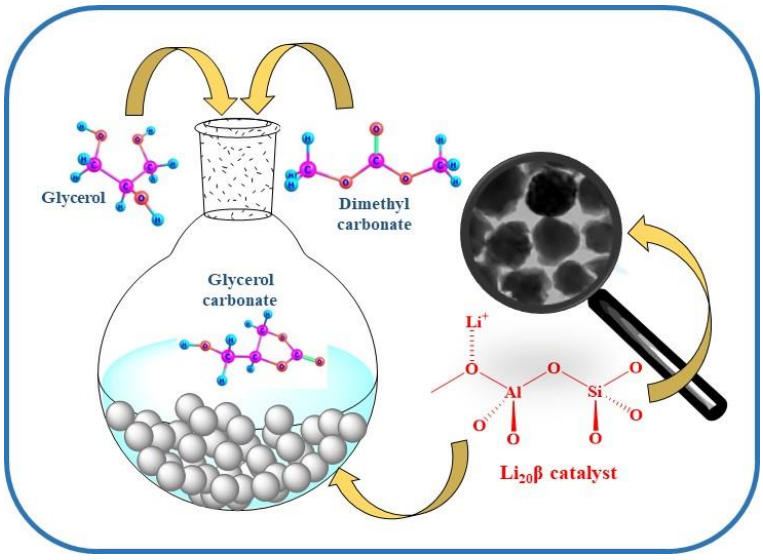

5.1. Introduction

The increasing consumption of fossil fuels leads to increased global warming. This increase needs to be controlled, and many countries all over the world have taken many serious steps to minimize this global warming threat. Renewable fuels can be used to replace the usage of fossil fuels in our day-to-day life. Biodiesel (BD) is the best substitute among all renewable resources. The growth of BD capacity has increased 5 times from 2006 to 2020.[1] BD, at a commercial scale, is obtained by transesterifying a variety of triglycerides, such as jatropha curcas, used cooking oils, yellow grease, animal fats, etc., with methanol or ethanol. This reaction, along with fatty acid methyl esters (FAME), commonly known as BD, also yielded crude glycerol (GLY) as a by-product[2–7] which is around 10 wt% of the BD production.[8]

The largest GLY manufacturer is in Europe, producing nearly about 2.5 million tons of GLY per year, which is estimated to triple by 2030.[9] The estimated global market is predicted to be around US $150 billion by the end of the year 2024.[10] The rapid increase in the production of BD in the last few years has dropped the global price of GLY from US$ 0.27-0.41 per pound to US$ 0.04-0.09 per pound.[11] Thus, it becomes crucial to convert this crude GLY to value-added chemicals and fuel additives like esters, ethers, acrolein, glyceric acid, propanediol, acetins, glycerol carbonate (GC), etc.[12,13] Out of all the GLY derivatives, GC (4-hydroxymethyl-1,3-dioxolane-2-one) has got more attention as it is a green compound of the century, biodegradable, less toxic with high boiling point, and low flammable properties. It is extensively used in the manufacturing of plastic, paint, biological lubricant, fibers, as a solvent in the cosmetic industries, and as an electrolyte for lithium-ion batteries.[14] Moreover, it plays significant role in the synthesis of polymers and glycidol.[15] Transparency Market Research report says that the global market for GC will hike at around 7% per year and reach US$ 2.4 billion by 2030.

Various direct and indirect catalytic pathways have been designed to convert GLY to value-added products shown in **Scheme 5.1.**[16] Among all the pathways, the indirect synthesis pathway involved carboxylation of phosgene and transesterification using alkylene and dialkyl carbonate.[17] GC synthesized via these pathways showed a high yield as nucleophilic carbon of the carbonate group reacts with the hydroxyl group of the GLY. The direct synthesis pathways were used earlier and were stopped due to the hazardous nature of the carbon monoxide. These days, Huntsman Corporation is using oxidative carbonylation for the production of GC. Carbonates like alkyl carbonates and dimethyl carbonates (DMC) can also be used as a source of carbonate for the reaction. Direct carboxylation of GLY with DMC is the potential pathway

for GC synthesis under mild reaction conditions. This pathway not only gives maximum conversion of GLY and yield of GC but also it provides easy separation as there is quite large difference in the boiling point of reactants and product obtained.[18]

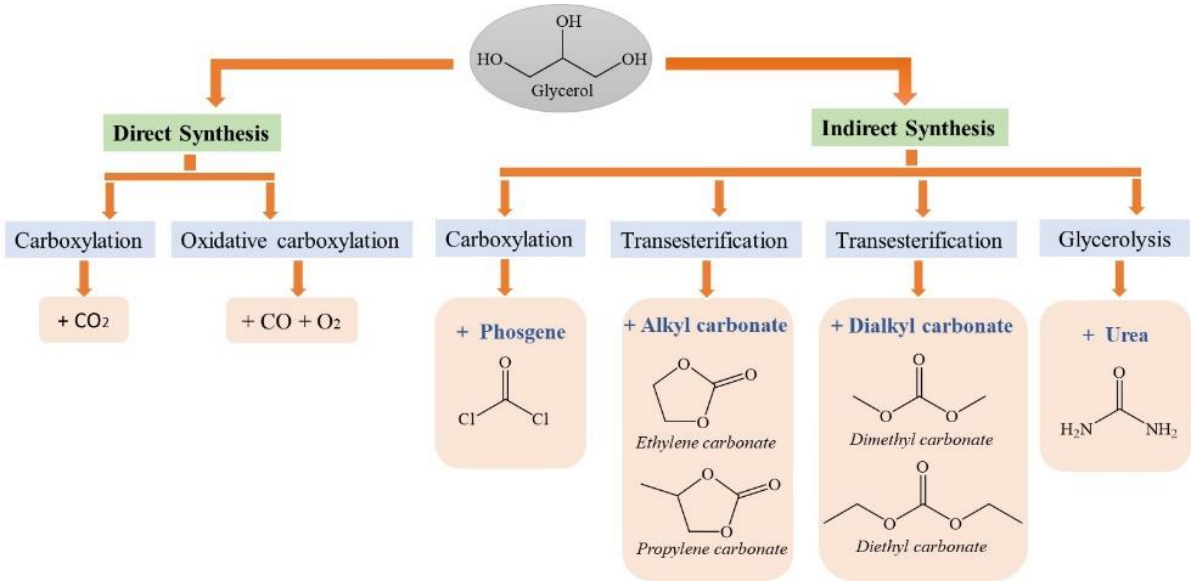

Scheme 5.1. Various pathways for the synthesis of GC.

A basic homogeneous as well as heterogeneous catalyst is required to synthesize GC from GLY via transesterification reaction.[19] Many homogeneous catalytic systems are reported in the literature, *viz.*, K_2CO_3,[20] trimethylamine,[21] ionic liquids,[22] alkali and alkali earth metals hydroxides.[23] Although excellent results are obtained from these catalysts but they also have disadvantages like difficulty in the separation from the reaction mixture and its reusability is not possible. To conquer these drawbacks, heterogeneous catalysts were adopted in the transesterification reaction. It is very simple to remove these catalysts from the reaction medium and reuse them multiple times. A variety of basic heterogeneous catalysts have been used by researchers in the past few decades *viz.*, MgO,[24,25] CaO,[26] CaO-ZrO_2,[27] Mg/ZnO,[28] Ca-Al hydrocalumite,[29] mixed oxides,[30–34] $NaAlO_2$ doped CaO,[35] Na_2SiO_3,[36] oil palm empty fruit bunch ash,[37] Ti-SBA-15,[38] Ni/FA,[39] K-TUD-1,[40] Co/MCM-41,[41] Mo/MCM-41,[42] K-zeolite,[43] anion exchange resins,[44] Na- based zeolites,[45] etc. Catalysts like metal oxides and mixed metal oxides show high GC yield but also leaching problems that decrease their reusability property. Basic sites of the catalyst are responsible for the initiation of the reaction. The catalyst made with metals like lithium (Li), sodium (Na), potassium (K), cerium (Ce), molybdenum (Mo) etc. gives a good yield of GC. Lithium nitrate shows strong ion size effect of all alkali metals, which is responsible for creating strong basic sites. Literature shows some catalyst with lithium metal such as alkali metal silicates (Li, Na, K),[46] Li/CaO-La_2O_3,[47] Li/Mg composite,[48]

$LiNO_3/Mg_4AlO_{5.5}$,[49] Li/ZnO,[50] Li/MCM-41,[51] Li/CFA,[52] Li_4SiO_4,[53] Li-oil palm ash zeolite,[54] Li/ZrO_2,[12] used for the transesterification reaction of GLY and DMC. Very less literature is available on the transesterification reaction using zeolite and modified zeolite.[55] The present work is focused on the alkali and alkaline earth metals like Li, Mg, and K modified zeolite beta for synthesizing GC via the transesterification reaction of GLY and DMC under mild conditions. The main purpose of using alkali and alkaline earth metals with zeolite provides several benefits like it reduces support acidity, improving physiochemical properties, increases basicity of oxygen atoms in the zeolite framework. Various Li modified zeolite beta catalysts were synthesized using wet-impregnation method, and the best performed Li modified zeolite was compared with Mg and K modified zeolite beta. ^{1}H-NMR spectroscopy was performed for the quantification of GC formed and left out GLY in the reaction.[13] The kinetic study of the reaction was also performed.

5.2. Results and Discussion

5.2.1. Selection of metals loading on zeolite beta

In this study, the zeolite beta catalyst was prepared using various alkali and alkaline earth metals such as Li, K, and Mg. In order to determine the catalytic performance of the prepared catalysts, the transesterification reaction of GLY and DMC having a molar ratio of 1:5 was performed for 5 h at 95 ℃ (**Figure 5.1**). The prepared catalysts exhibited 100% selectivity towards GC without the formation of side products. Among all the prepared catalysts Li and K-modified beta, zeolite exhibited higher activity. Although, while comparing the stability of Li and K-modified zeolite Li modified zeolite showed better catalytic activity. Li, K, and Mg modified zeolite beta gives 81.48%, 76.71%, and 59.35% yield of GC respectively. So, Li/beta zeolite containing 20 wt% Li was selected for all the reactions for the purpose of obtaining the highest GC yield.

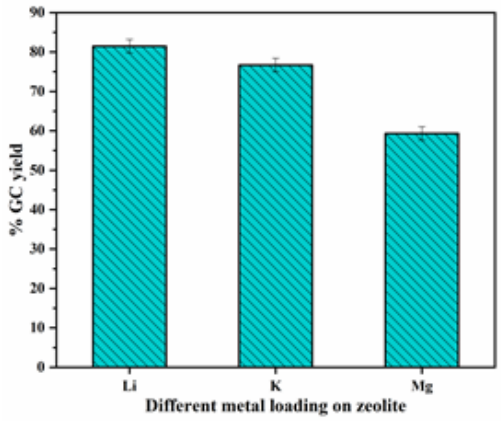

Figure 5.1. Effect of different metal content in zeolite on yield of GC (Reaction conditions: GLY:DMC mole ratio 1:5, $Li_{20}\beta$ dosage 10 wt% w.r.t. GLY, temperature 95 °C, time 5 h).

5.2.2. Li impregnation over the surface of zeolite

To achieve the maximise yield of GC, zeolite beta was treated with different concentrations of lithium-nitrated solutions using the wet impregnation method. The catalytic activity of the modified zeolite was examined at a dosage of 10 wt%, reactants mole ratio 1:5 at a temperature of 95 °C having 5 hours reaction time. In **Figure 5.2**, it is clearly visible that the 20 wt% loading of Li on zeolite beta gives the maximum GC yield, which is 81.48%. An increase in the Li metal concentration, it increases the catalytic activity of the zeolite. An increase of GC yield is observed with 5 to 20 wt% Li loading and at 25 wt% catalyst dosage, a decrement in the yield is observed owing to excessive Li clogging the active basic sites present on the zeolite surface thereby decreasing the yield of the GC. Therefore, a 20 wt% Li-loaded zeolite beta named $Li_{20}\beta$ zeolite was taken for further reactions to achieve the maximum GC yield.

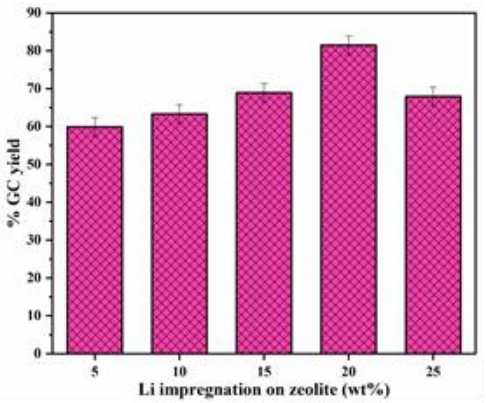

Figure 5.2. Effect of Li metal on GC yield (Reaction conditions: GLY:DMC mole ratio 1:5, $Li_{20}\beta$ dosage 10 wt% w.r.t. GLY, temperature 95 °C, time 5 h).

5.2.3. Effect of $Li_{20}\beta$ catalyst dosage on GC yield

The transesterification reaction depends on the presence of the active sites of the basic catalyst which further depends on the type of metal loading on the surface. The more active sites present more would be the interaction of active sites with the reactants which leads to high conversion. A negligible reaction occurs in the absence of the catalyst. This is the reason for choosing a good basic catalyst that can cross the activation energy barrier easily. To achieve maximum GC yield, various catalytic reactions were carried out by changing the catalyst concentration w.r.t. GLY. $Li_{20}\beta$ catalysts with different concentrations i.e. from 5 to 25 wt% were used and

it has been seen that a maximum yield of 81.48% was achieved at 10 wt% (**Figure 5.3**). However, when the catalyst loading is further increased, it shows a decrement to 64.48% and after that, no noticeable change was found in the yield. This could be due to the accumulation of the catalyst molecules which inhibit the mass transfer to actives sites of the catalyst.[41] Hence, 10 wt% catalyst dosage comes out to be the best dosage out of all for the GC synthesis and is selected for optimizing the rest of the parameters for the transesterification reaction.

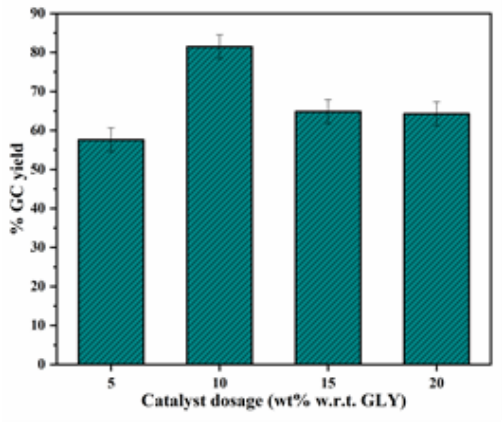

Figure 5.3. Effect of catalyst loading on GC yield (Reaction conditions: GLY:DMC mole ratio 1:5, $Li_{20}\beta$ dosage 10 wt% w.r.t. GLY, temperature 95 °C, time 5 h).

5.2.4. Effect of GLY/DMC mole ratio on GC yield

Mole ratio of reactants i.e. GLY/DMC is one the most important factor affecting the conversion and synthesis of GLY and GC respectively. In the present work, mole ratio is varied from 1:2 to 1:6 to for the yield of GC shown in **Figure 5.4**. Initially, as the mole ratio increases, GC yield increases up to 1:5 from 50.71 % to 81.48 %. After that, reduction in the GC yield is observed of 67.76 % which may be due to the increase in the immiscibility of the reactants. As

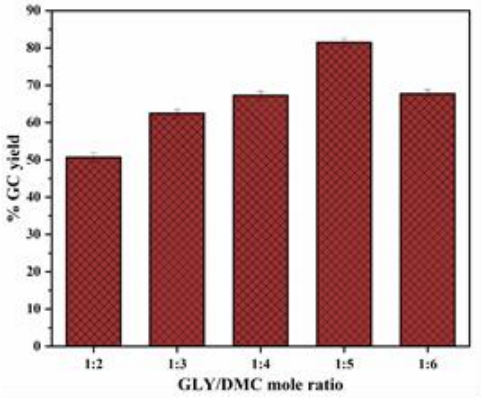

Figure 5.4. Effect of GLY/DMC mole ratio on GC yield (Reaction conditions: GLY:DMC mole ratio 1:5, $Li_{20}\beta$ dosage 10 wt% w.r.t. GLY, temperature 95 °C, time 5 h).

we know, GLY is hydrophilic and DMC is hydrophobic in nature, hence, due to high concentration of DMC in the reaction, the formation of these two phases makes the reaction difficult to proceed which ultimately decreases the yield of the GC.[35]

5.2.5. Effect of reaction temperature on GC yield

Generally, transesterification is a reversible reaction and thus, temperature has a significant impact in the progress of a reaction. In general, higher the reaction temperature, higher would be the rate of the reaction and hence higher would be the GC yield. To obtain the highest yield of the GC, the reaction temperature was varied from 65 ℃ to 105 ℃ at the 10 wt% catalyst loading with mole ratio of 1:5 in 5 hours reaction time shown in the Figure 13. The **Figure 5.5** representing the prominent rise in the yield of GC from 65 ℃ to 95 ℃. At 95 ℃, 81.48% yield of GC was obtained. The reason being the maximum successful collisions occurred between both the reactants at highest temperature. Beyond this temperature, a slight reduction in the yield was observed which could be attributed to the decarboxylation of the GC into glycidol which leads to ring opening of GC structure and hence decreasing the yield of GC.[50]

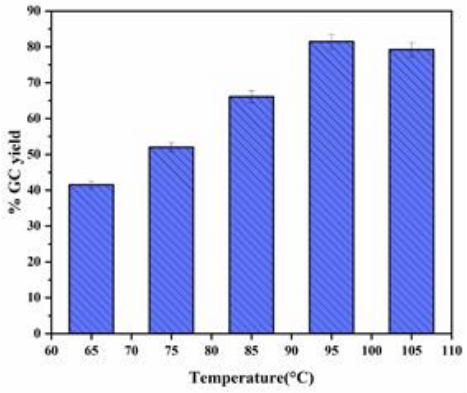

Figure 5.5. Effect of reaction temperature on GC yield (Reaction conditions: GLY:DMC mole ratio 1:5, $Li_{20}\beta$ dosage 10 wt% w.r.t. GLY, temperature 95 ℃, time 5 h).

5.2.6. Effect of reaction time on GC yield

To study the effect of reaction time, the reaction was performed for 6 hours and the observations are shown in the **Figure 5.6**. The maximum GC yield was observed in 5 hours at a reaction condition of 10 wt% catalyst dosage, GLY:DMC mole ratio of 1:5 at 95 ℃. The yield of GC increases from 31.1% to 81.48% in the first five hours of reaction run. After this, a slight decrement is observed for the sixth hour of the reaction run which may be due to the excessive basic active sites on the $Li_{20}\beta$ catalyst surface being used to decarboxylate the GC molecule.[51]

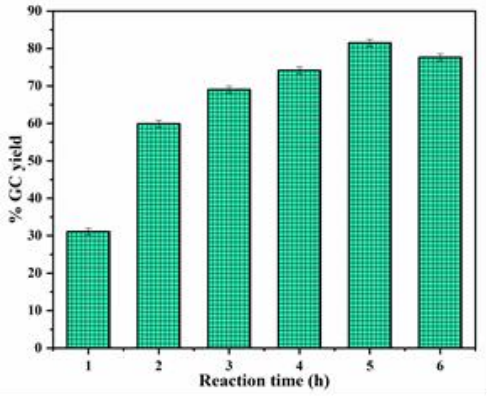

Figure 5.6. Effect of reaction time on GC yield (Reaction conditions: GLY:DMC mole ratio 1:5, $Li_{20}\beta$ dosage 10 wt% w.r.t. GLY, temperature 95 ℃, time 5 h).

5.2.7. Regeneration of catalyst

The key benefit of using heterogeneous catalyst is its reusability which makes them more useful at large scale by lowering the price of the product. The transesterification reaction of GLY with DMC was performed using the catalyst $Li_{20}\beta$ at an optimal reaction conditions like GLY:DMC mole ratio 1:5, 10 wt% $Li_{20}\beta$ catalyst, 95 ℃ reaction temperature and 5 hours reaction time. The catalyst was regenerated after every cycle. Catalyst was washed with methanol and after then it was oven dried overnight. After that it is recalcined at 700 ℃. The reactions were performed using the regenerated catalyst and **Figure 5.7** showing the FE-SEM images of $Li_{20}\beta$ catalyst before and after the transesterification reaction GLY with DMC.

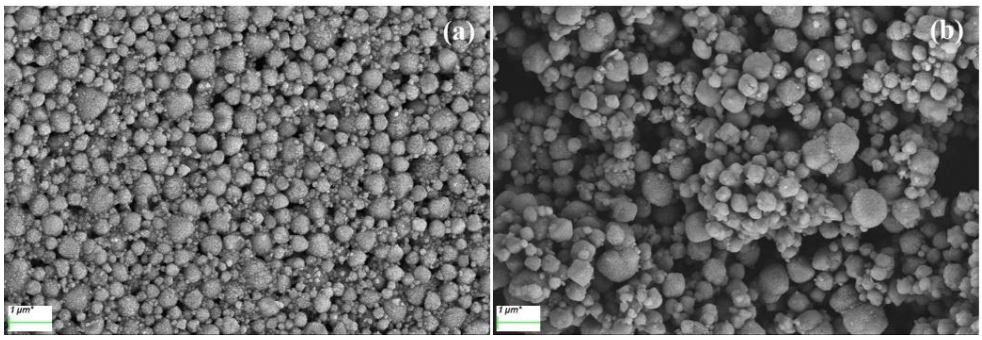

Figure 5.7. Comparison of the $Li_{20}\beta$ zeolite (a) before, (b) after the transesterification reaction.

5.2.8. Recyclability of catalyst

The recyclability of the $Li_{20}\beta$ zeolite catalyst was performed by regenerating it in the above discussed section using the procedure (ii) under the optimal conditions. The $Li_{20}\beta$ zeolite was reused up to five catalytic cycles at the optimal reaction conditions. The gradual decrement in

the GC yield was observed from 81.48% to 59.88% for the five cycles and this is shown in the **Figure 5.8**. Although, decrement is observed but no side product formation is observed during the reusability process up-to five cycles.

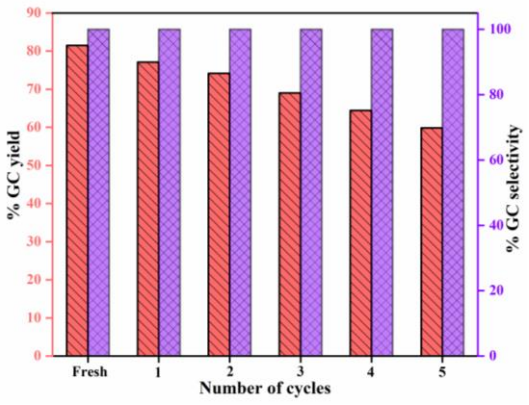

Figure 5.8. Reusability of $Li_{20}\beta$ zeolite (Reaction conditions: GLY:DMC 1:5, $Li_{20}\beta$ dosage 10 wt% w.r.t. GLY, temperature 95 ℃, time 5 h).

5.3. Reaction kinetics

The kinetics for the transesterification of GLY and DMC is scarcely reported in the literature shown in Table 1. To study the reaction kinetics of transesterification of GLY and DMC, it was studied in the presence of 10 wt% of $Li_{20}\beta$ zeolite as best performed catalyst at temperatures ranging from 65 ℃ to 95 ℃ having 1:5 mole ratio of GLY:DMC for 5 hours reaction time. The aliquots were collected after each hour during the reaction time for all the four temperatures. The transesterification reaction of GLY and DMC over $Li_{20}\beta$ zeolite is shown in the Scheme 2.

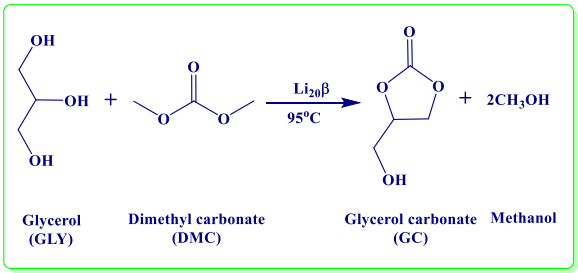

Scheme 5.2. Synthesis of GC using $Li_{20}\beta$ zeolite.

The reaction order was found by plotting rate equations for zero, first and second-order which is shown in the **Figure 5.9**. From all the graphs that were plotted, the relative higher value of R^2 which is 0.98, for the second order reaction rate suggested the transesterification reaction of GLY and DMC over $Li_{20}\beta$ zeolite followed second-order kinetics as shown in the **Figure 5.9(c).**

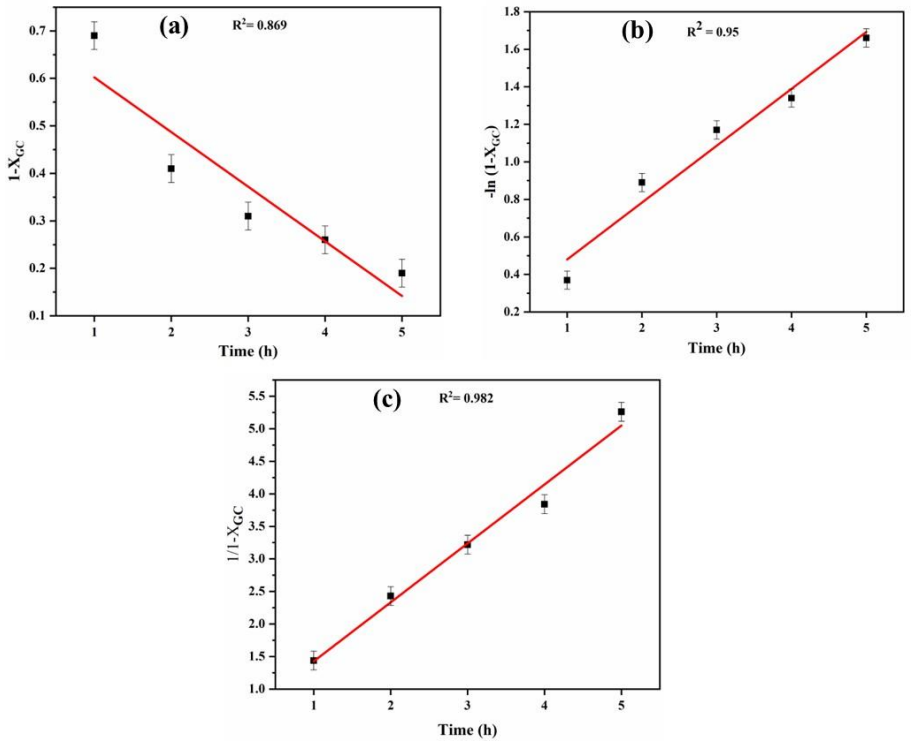

Figure 5.9. A plot of (a) 1-X_{GC}, (b) -ln(1-X_{GC}), and 1/1-X_{GC} *versus* reaction time (h) for zero, first, and second-order reaction.

Table 5.1. Effect of rate constant with reaction temperature

Reaction temperature (°C)	Rate constant, k (h^{-1})
65	0.328
75	0.576
85	0.705
95	0.905

Table 5.1 showing the temperature effect on the rate of the reaction and it was confirmed that the k value increases with an increase in temperature of the reaction. The second-order kinetics at various reaction temperatures has been shown in **Figure 5.10(a)**. The slope of this graph gives different k values for the reaction which further applied on Arrhenius equation to find the activation energy and plot for lnk against 1/T is shown in **Figure 5.10(b)**.

$$k = Ae^{\frac{-Ea}{RT}} \qquad \text{Equation (1)}$$

$$\ln k = \ln A - \frac{E_a}{RT} \qquad \text{Equation (2)}$$

Where, k represents the reaction rate constant, Eα represents the activation energy, A represents Arrhenius constant, T represents the temperature and R represents the universal gas constant for the reaction.

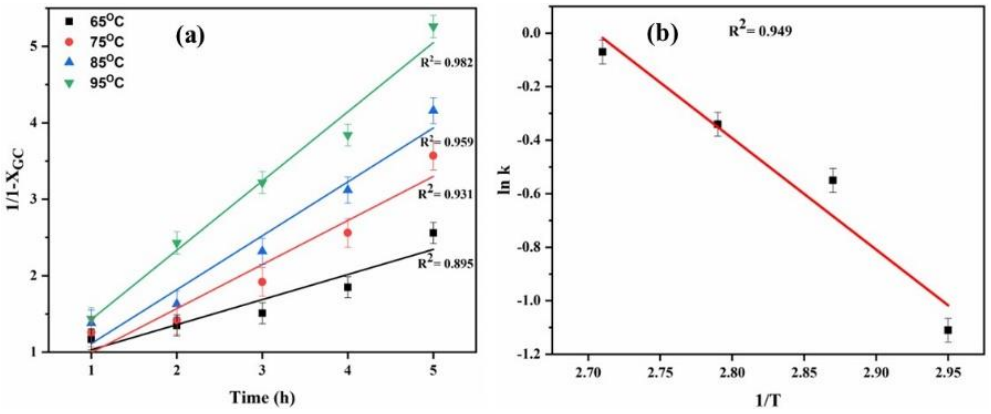

Figure 5.10. (a) A plot of $1/(1-X_{GC})$ *vs* reaction time (h) for the transesterification reaction, (b) lnk vs 1/T plot for transesterification of GLY with DMC.

From the **Figure 5.10(b),** the activation energy (Eα) comes out to be 34.60 $kJmol^{-1}$ and pre-exponential factor (A) comes out be 7.76×10^4 for the transesterification reaction (**Table 5.2**). According to the literature, the activation energy has been reported in the range of 22.012 to 53.77 kJ/mol.

Table 5.2. Activation energy and pre-exponential factor

Activation energy, Eα (kJ/mol)	Pre-exponential factor, A
34.60	7.76×10^4

5.4. Plausible mechanism

$Li_{20}\beta$ zeolite catalyzed transesterification reaction of GLY with DMC comprise of interaction of catalyst with both the substrates (**Scheme 5.3**). Firstly, the basic sites present on the $Li_{20}\beta$ zeolite withdraws the primary hydroxy group of GLY and at the same time it accompanied the interaction between O of DMC and Si present on the surface of catalyst. Moreover, DMC gets triggered by Lewis acidic sites of Si present in zeolite. Furthermore, the carbonyl group present on DMC was nucleophilically attacked by the primary hydroxy group of GLY, followed by the alcohol elimination to form an intermediate.[54] The intermediate undergoes intramolecular nucleophilic substitution to synthesize GLC by eliminating another alcohol molecule.

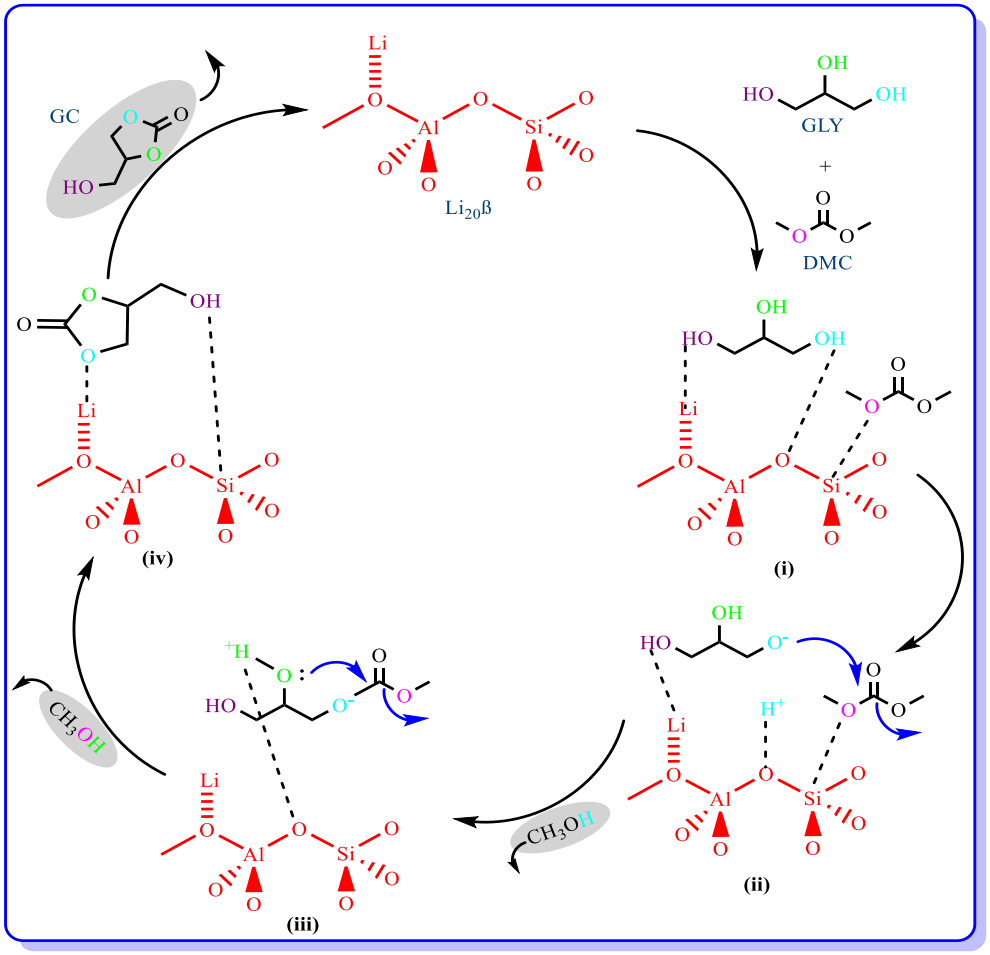

Scheme 5.3. Plausible mechanism presenting the interaction between GLY, DMC and $Li_{20}\beta$ zeolite.

5.5. Conclusion

In the present work, zeolite beta was successfully modified with different alkali and alkaline earth metals using wet-impregnation method. Under optimal reaction conditions (GLY:DMC 1:5, catalyst dosage 10 wt% w.r.t. GLY, temperature 95℃, time 5 h), $Li_{20}\beta$ zeolite performed to be the optimum catalyst for the transesterification reaction. A maximum GC yield of 81.48% was observed and the reaction showed a second-order reaction kinetics having activation energy 34.60 kJ/mol. The stability and performance of $Li_{20}\beta$ was experimented by reusing it for five reaction cycles which shows the decrement in the GC yield to 59.9% but imparting 100% selectivity towards GC.

Reference

1 S. Nomanbhay, R. Hussein and M. Y. Ong, *Green Chem. Lett. Rev.*, 2018, **11**, 135–157.

2 N. Rozulan, S. A. Halim, N. Razali and S. S. Lam, *Biomass Convers. Biorefin.*,2022, **12**, 4665-4682.

3 L. C. Meher, D. Vidya Sagar and S. N. Naik, *Renew. Sustain. Energy Rev.*, 2006, **10**, 248–268.

4 Z. Ullah, M. A. Bustam and Z. Man, *Renew. Energy*, 2015, **77**, 521–526.

5 Sahar, S. Sadaf, J. Iqbal, I. Ullah, H. N. Bhatti, S. Nouren, Habib-ur-Rehman, J. Nisar and M. Iqbal, *Sustain. Cities Soc.*, 2018, **41**, 220–226.

6 N. Mansir, S. H. Teo, I. Rabiu and Y. H. Taufiq-Yap, *Chem. Eng. J.*, 2018, **347**, 137–144.

7 C. Delesma, P. Okoye, M. Castellanos-López, A. Longoria and J. Muñiz, *Fuel*, 2022, **307**, 121874.

8 J. Li and T. Wang, *J. Chem. Thermodyn.*, 2011, **43**, 731–736.

9 W. Praikaew, W. Kiatkittipong, F. Aiouache, V. Najdanovic-Visak, M. Termtanun, J. W. Lim, S. S. Lam, K. Kiatkittipong, N. Laosiripojana, S. Boonyasuwat and S. Assabumrungrat, *Int. J. Energy Res.*, 2022, **46**, 1646–1658.

10 D. Procopio and M. L. Di Gioia, *Catalysts*, 2022, **12**, 50.

11 J. Keogh, G. Deshmukh and H. Manyar, *Fuel*, 2022, **310**, 122484.

12 A. Kaur and A. Ali, *Ind. Eng. Chem. Res.*, 2020, **59**, 2667–2679.

13 K. Abida, B. Chudasama and A. Ali, *New J. Chem.*, 2020, **44**, 9365–9376.

14 W. K. Teng, G. C. Ngoh, R. Yusoff and M. K. Aroua, *Energy Convers. Manag.*, 2014, **88**, 484–497.

15 S. Nomanbhay, M. Y. Ong, K. W. Chew, P. L. Show, M. K. Lam and W. H. Chen, *Energies*, 2020, **13,** 1483.

16 J. R. Ochoa-Gómez, O. Gómez-Jiménez-Aberasturi, C. Ramírez-López and M. Belsué, *Org. Process Res. Dev.*, 2012, **16**, 389–399.

17 A. Galadima and O. Muraza, *Waste and Biomass Valorization*, 2017, 8, 141–152.

18 M. O. Sonnati, S. Amigoni, E. P. Taffin De Givenchy, T. Darmanin, O. Choulet and F. Guittard, *Green Chem.*, 2013, **15**, 283–306.

19 P. U. Okoye, A. Z. Abdullah and B. H. Hameed, *Energy Convers. Manag.*, 2017, **133**, 477–485.

20 G. Rokicki, P. Rakoczy, P. Parzuchowski and M. Sobiecki, *Green Chem.*, 2005, **7**, 529–539.

21 F. Paquin, J. Rivnay, A. Salleo, N. Stingelin and C. Silva, *J. Mater. Chem. C*, 2015, **3**,

10715–10722.

22 Z. I. Ishak, N. A. Sairi, Y. Alias, M. K. T. Aroua and R. Yusoff, *Catal. Rev. - Sci. Eng.*, 2017, **59**, 44–93.

23 A. O. Esan, A. D. Adeyemi and S. Ganesan, *J. Clean. Prod.*, 2020, **257**, 120561.

24 M. Manikandan and P. Sangeetha, *ChemistrySelect*, 2019, **4**, 6672–6678.

25 F. Paquin, J. Rivnay, A. Salleo, N. Stingelin and C. Silva, *J. Mater. Chem. C*, 2015, **3**, 10715–10722.

26 W. Roschat, S. Phewphong, T. Kaewpuang and V. Promarak, *Mater. Today Proc.*, 2018, **5**, 13909–13915.

27 X. Zhang, S. Wei, X. Zhao, Z. Chen, H. Wu, P. Rong, Y. Sun, Y. Li, H. Yu and D. Wang, *Appl. Catal. A Gen.*, 2020, **590,** 117313.

28 G. Pradhan and Y. C. Sharma, *Fuel*, 2021, **284**, 118966.

29 L. Zheng, S. Xia, X. Lu and Z. Hou, *Cuihua Xuebao/Chinese J. Catal.*, 2015, **36**, 1759–1765.

30 M. Malyaadri, K. Jagadeeswaraiah, P. S. Sai Prasad and N. Lingaiah, *Appl. Catal. A Gen.*, 2011, **401**, 153–157.

31 G. Parameswaram, P. S. N. Rao, A. Srivani, G. N. Rao and N. Lingaiah, *Mol. Catal.*, 2018, **451**, 135–142.

32 Y. Li, H. Zhao, W. Xue, F. Li and Z. Wang, *Nanomaterials*, 2022, **12**, 1972.

33 S. E. Kondawar, C. R. Patil and C. V. Rode, *ACS Sustain. Chem. Eng.*, 2017, **5**, 1763–1774.

34 P. Zhang, Y. Chen, M. Zhu, C. Yue, Y. Dong, Y. Leng, M. Fan and P. Jiang, *Catal. Letters*, 2020, **150**, 2863–2872.

35 A. Chotchuang, P. Kunsuk, A. Phanpitakkul, S. Chanklang, M. Chareonpanich and A. Seubsai, *Catal. Today*, 2022, **388**–**389**, 351–359.

36 S. Wang, P. Hao, S. Li, A. Zhang, Y. Guan and L. Zhang, *Appl. Catal. A Gen.*, 2017, **542**, 174–181.

37 P. U. Okoye, S. Wang, L. Xu, S. Li, J. Wang and L. Zhang, *Energy Convers. Manag.*, 2019, **179**, 192–200.

38 P. Devi, U. Das and A. K. Dalai, *Chem. Eng. J.*, 2018, **346**, 477–488.

39 S. Bepari, N. C. Pradhan and A. K. Dalai, *Catal. Today*, 2017, **291**, 36–46.

40 S. Arora, V. Gosu and V. Subbaramaiah, *Mol. Catal.*, 2020, **496**, 111188.

41 S. Arora, V. Gosu, V. Subbaramaiah and T. C. Zhang, *Can. J. Chem. Eng.*, 2021, **100**, 1868–1883.

42 P. Sikarwar, U. K. A. Kumar, V. Gosu and V. Subbaramaiah, *J. Environ. Chem. Eng.*, 2018, **6**, 1736–1744.

43 Y. T. Algoufi and B. H. Hameed, *Fuel Process. Technol.*, 2014, **126**, 5–11.

44 A. V. Shvydko, S. A. Prihod ko and M. N. Timofeeva, *Catal. Ind.*, 2022, **14**, 181-188.

45 S. Pan, L. Zheng, R. Nie, S. Xia, P. Chen and Z. Hou, *Cuihua Xuebao/Chinese J. Catal.*, 2012, **33**, 1772–1777.

46 N. Hindryawati, G. P. Maniam, M. R. Karim and K. F. Chong, *Eng. Sci. Technol. an Int. J.*, 2014, **17**, 95–103.

47 H. Maleki, M. Kazemeini, A. S. Larimi and F. Khorasheh, *J. Ind. Eng. Chem.*, 2017, **47**, 399–404.

48 L, Zhenmin, L, Bin, Q. Fengrui, Z. Yan, W. Xiaoxiao, N. Ziyan, W. Jin, L. Haiqiang, S. Shen, P. Ruili, W. Yuanyang and X. Yongbing, *ACS Omega*, 2022, **7**, 5032-5038.

49 Z. Liu, J. Wang, M. Kang, N. Yin, X. Wang, Y. Tan and Y. Zhu, *J. Ind. Eng. Chem.*, 2015, **21**, 394–399.

50 X. Song, Y. Wu, F. Cai, D. Pan and G. Xiao, *Appl. Catal. A Gen.*, 2017, **532**, 77–85.

51 S. Arora, V. Gosu, U. K. A. Kumar and V. Subbaramaiah, *J. Clean. Prod.*, 2021, **295**, 126437.

52 S. Arora, V. Gosu, V. Subbaramaiah and B. H. Hameed, *J. Environ. Chem. Eng.*, 2021, **9**, 105999.

53 J. X. Wang, K. T. Chen, J. S. Wu, P. H. Wang, S. T. Huang and C. C. Chen, *Fuel Process. Technol.*, 2012, **104**, 167–173.

54 W. A. Khanday, P. U. Okoye and B. H. Hameed, *Energy Convers. Manag.*, 2017, **151**, 472–480.

55 S. Sahani, S. N. Upadhyay and Y. C. Sharma, *Ind. Eng. Chem. Res.*, 2021, **60**, 67–88.

CHAPTER 6

ALKYLATION OF INDOLE WITH METHYL VINYL KETONE USING SULFURIC ACID-MODIFIED ZEOLITE CATALYST

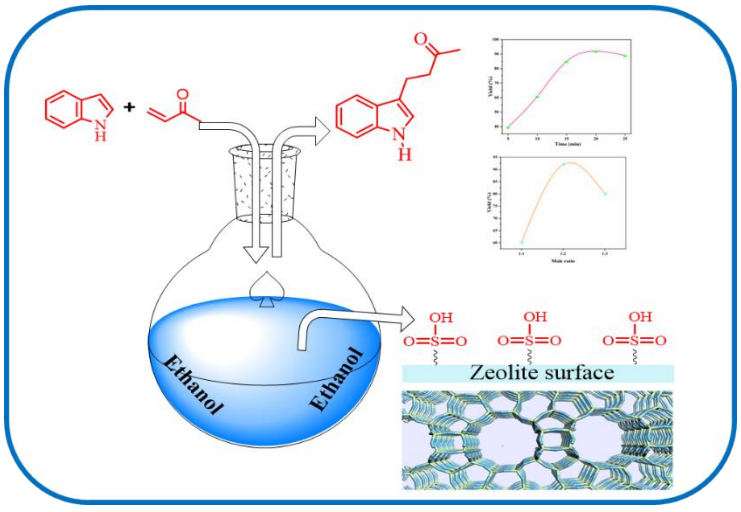

6.1. Introduction

Organic and medicinal chemists are focusing their efforts on simplifying or improving existing processes utilized in the production of pharmacological compounds. Some pharmacologically and biologically active chemicals primarily consist of nitrogen-containing heterocycles. The recent advances in the synthesis of heterocyclic molecules into a variety of derivatives have gained considerable interest.[1] Solid-support reactions, chemoenzymatic reactions, and microwave-induced reactions have already had a huge impact on modern science. Catalytic techniques have also made major contributions.[2]

Indole is one of the promising heterocyclic rings. Numerous chemicals and natural products have been discovered to be 3-substituted indoles. Since substituted indoles can bind to numerous receptors with high affinity, they have been termed "privileged structures."[3] As a result, active research has been concentrated on the synthesis and selective functionalization of indoles over the years.[4] 3-substituted indoles are useful intermediates for the synthesis of a wide range of indole derivatives because the 3-position of the indole is the appropriate site for the electrophilic attack. The 3-(3-oxoalkyl) indole or β-indolylketones produced by the Michael reaction of indole with α,β-unsaturated ketones by alkylation have received interest as one of the key carbon-carbon bond-building processes.[5] β-Indolylketones are useful synthetic scaffolds for medicinal and synthetic organic chemists, and they have gained a lot of attention as a building block for the synthesis of many natural products and biologically active compounds.

Numerous synthetic preparation techniques for these substances have been published during the past few years using various catalysts such as $Bi(Otf)_3$[6], bis(oxazolinyl)pyridine (pybox)-scandium (III) triflate complexes,[7] CAN,[8] $InBr_3$,[9,10] PTSA,[11] PVSA,[12] PDA,[13] FAP,[14] $Cu(Otf)_3$,[15] GaI_3,[16] $HfCl_4$ and $ScCl_3$,[17] $NO^+BF^-_4$,[18] $Zr(OtBu)_4$,[19] TCT,[20] Zn-HAP,[21] HPA,[22] bronsted acid ionic liquid,[23] $Sc(DS)_3$,[24] $InCl_3$,[25] $[Al(DS)_3]\cdot 3H_2O$,[26] Amine salt,[27] SmI_3,[28] sulfamic acid,[29] $Zn(OAc)_2$,[30] TiO_2,[31] Montmorillonite K10,[32] $CoCl_2$,[33] $KHSO_4$,[34] I_2,[2] alumina,[35] sulfated zirconia on silica tubes,[36] camphor sulfonic acid,[37] Fe^{3+}-mont[38] etc.

Actually, these processes are electrophilic substitutions of indoles that are catalyzed by acids. The acidity of the reaction medium needs to be carefully controlled in order to avoid side reactions like dimerization and polymerization. In reality, a lot of these procedures have been carried out in highly acidic environments which produced low yields of product at longer reaction times with costly reagents and thus difficult to handle.[22] Therefore, there is a great

need for novel, effective Lewis acid catalysts. As a result, superior catalytic systems that are inexpensive, easy to access, and ecologically friendly are desirable. Acetonitrile has been used as a solvent in the presence of Lewis acid in some of the reactions discussed in the literature.[3] No doubt, it gives a high yield of the expected product but the solvent is not environment friendly. So, the selection of a good heterogeneous catalyst along with an eco-friendly solvent is the challenge of this reaction system.

In the present work, mordenite zeolite has been treated with sulfuric acid (**Scheme 6.1**). To provide insight into its activity and reusability, it was thoroughly characterized using a variety of techniques including XRD, FE-SEM, EDS-mapping, XPS, and HR-TEM. The activity of SO_3H@Mor zeolite was compared to other catalysts in the reaction of methyl vinyl ketone with indole to produce β-indolylketone. The effect of various parameters on the yield of the product was thoroughly investigated in the present article.

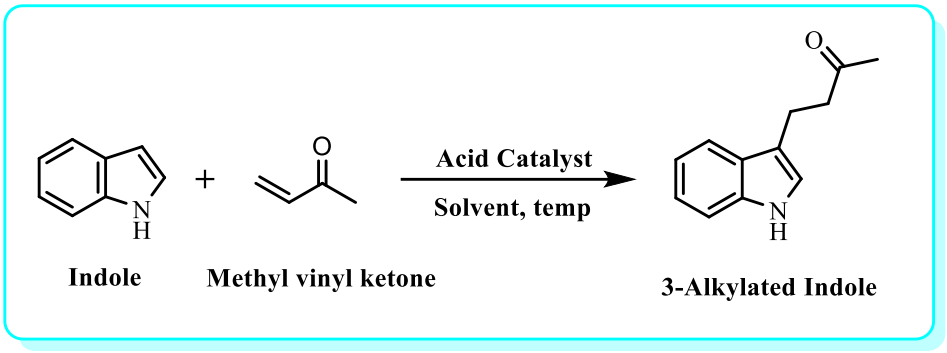

Scheme 6.1. Alkylation of indole with methyl vinyl ketone.

6.2 Results and Discussion

6.2.1. Efficacy of various catalysts

Alkylation of indole with methyl vinyl ketone was performed using various zeolites like HZSM-5, Beta, Mordenite, SO_3H@Z5, SO_3H@Beta, and SO_3H@Mor. It was observed that sulfuric acid-modified zeolites give higher yields as compared to parent zeolites shown in **Figure 6.1**. Out of all these catalysts, sulfuric acid-treated zeolite gives the highest yield of 92%. Hence, SO_3H@Mor is used as a heterogeneous catalyst for all the further alkylation reactions of indole with methyl vinyl ketone.

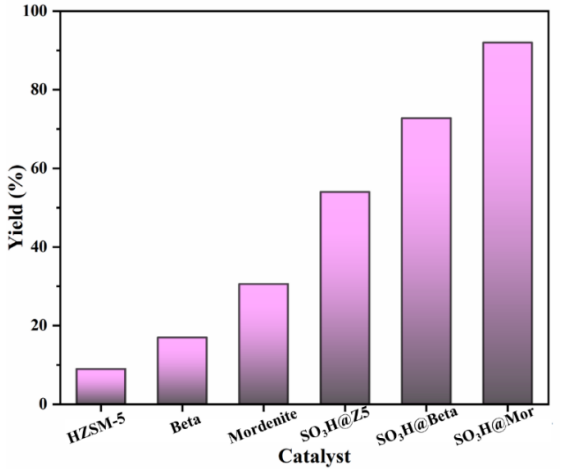

Figure 6.1. Efficacy of various catalysts on the yield of β-indolylketone (Reaction conditions: catalyst 7.5 wt%, indole:methyl vinyl ketone 1:2, reaction time 20 min, solvent- ethanol at rt)

6.2.2. Effect of catalyst concentration

The rate of the reaction is directly proportional to the catalyst concentration which was varied from 2.5 to 10 wt%. The conversion of reactants or product formation increases with an increase in the catalyst concentration due to a proportional increase in the number of active sites in the reaction mixture, as shown in Figure 6.2. However, there was no increase in the yield above the catalyst concentration of 7.5 wt% instead showed decrement up to 81% for 10 wt% and this is because the number of active sites available for the reaction was more than the number of molecules present for the reaction.

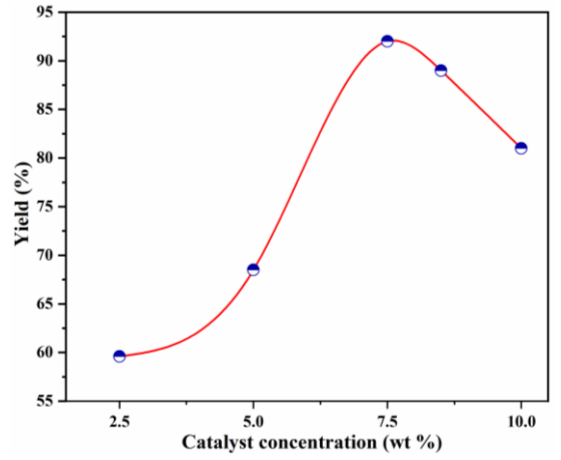

Figure 6.2. Effect of catalyst concentration on the yield of β-indolylketone (Reaction conditions: catalyst- SO_3H@Mor, indole:methyl vinyl ketone 1:2, reaction time 20 min, solvent- ethanol at rt)

6.2.3. Effect of mole ratio of reactants

To achieve the highest yield, the indole to methyl vinyl ketone mole ratio was varied from 1 to 3. The reaction rate increases with an increase in the reactant's mole ratio. The mole ratio increases from 1 to 2 and gave 92% isolated yield but for the 1:3 mole ratio, it shows a good decrement to 80% which confirms that the 1:2 mole ratio of indole to methyl vinyl ketone was selected for further experiments (Figure 6.3). A sharp and considerable decrease in the yield is related to a decrease in indole concentration in the reaction mixture as well as the blocking of zeolite active sites by excess reactant at a higher mole ratio.

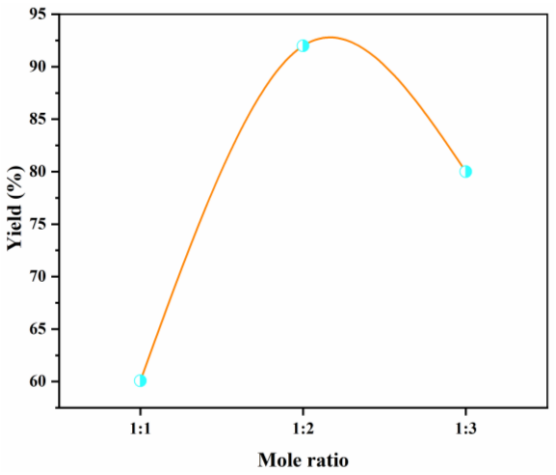

Figure 6.3. Effect of mole ratio on the yield of β-indolylketone (Reaction conditions: catalyst- 7.5 wt% SO_3H@Mor, reaction time 20 min, solvent- ethanol at rt)

6.2.4. Effect of reaction time

The reaction was run for 25 minutes to evaluate the influence of reaction time, and the results are presented in Figure 6.4. At 7.5 wt% SO_3H@Mor catalyst dose, indole:methyl vinyl ketone 1:2, solvent-ethanol at rt, a maximum indolylketone yield was observed in 20 minutes. The isolated yield increased from 39.6% to 92% after 20 minutes of reaction time, followed by a slight decline of yield to 89% in 25 minutes, which could be due to the formation of side products in the reaction.

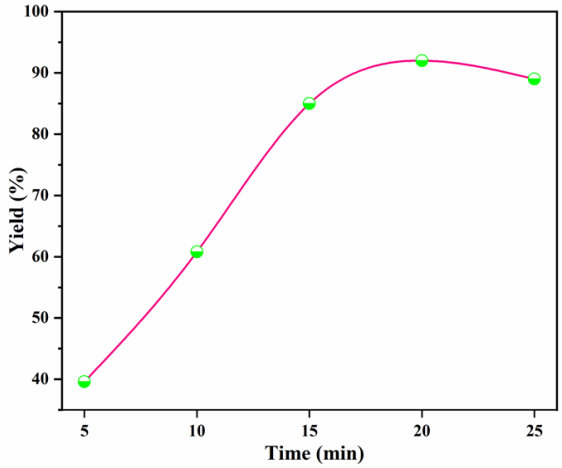

Figure 6.4. Effect of reaction time on the yield of β-indolylketone (Reaction conditions: catalyst- 7.5 wt% SO_3H@Mor, indole:methyl vinyl ketone 1:2, solvent- ethanol at rt)

6.2.5. Reusability of catalyst

The reusability of the catalyst was performed by carrying out the experiments for three cycles at optimized reaction conditions, 7.5 wt% SO_3H@Mor catalyst, indole:methyl vinyl ketone 1:2, reaction time 20 min, ethanol as solvent at rt. Each time the reaction was finished, the catalyst was removed from the reaction mixture using a centrifugation or filtration process. Every time the catalyst was filtered, a small quantity of the catalyst is lost. The catalyst was then washed, dried overnight in a 100 °C oven, and then calcined for two hours at 500 °C. The decrement in yield of β-indolylketone has been shown in **Figure 6.5**. The yield of β-indolylketone decreased from 92% to around 42% in the 3rd cycle of the reusability study. This decline may be caused by the leaching of sulfate ions or another strongly adsorbent species from the catalyst's active sites, which causes the catalyst to become inactive for a longer period of time.

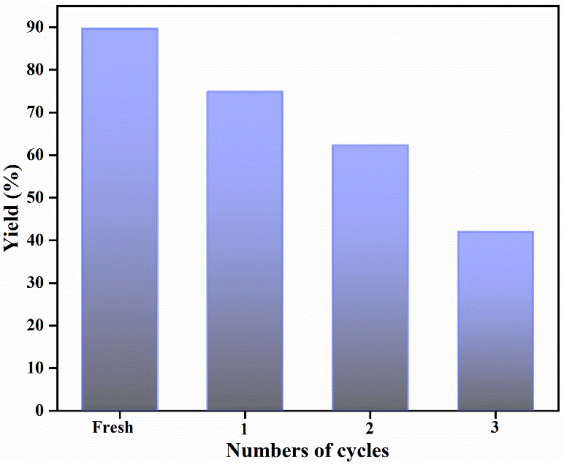

Figure 6.5. Reusability study on the yield of β-indolylketone (Reaction conditions: catalyst- 7.5 wt% SO_3H@Mor, indole:methyl vinyl ketone 1:2, reaction time 20 min, solvent- ethanol at rt)

6.3. Reaction kinetics

To investigate the reaction kinetics of alkylation of indole with methyl vinyl ketone, 7.5 wt% SO_3H@Mor zeolite was used as the best-performing catalyst at room temperature with a 1:3 mole ratio of indole:methyl vinyl ketone in the presence of ethanol as a solvent for a 20 minutes reaction time. During the reaction period, aliquots were taken every 5 minutes. **Scheme 6.2** depicts the alkylation of indole with methyl vinyl ketone in the presence of SO_3H@Mor zeolite as a heterogeneous catalyst at optimized conditions.

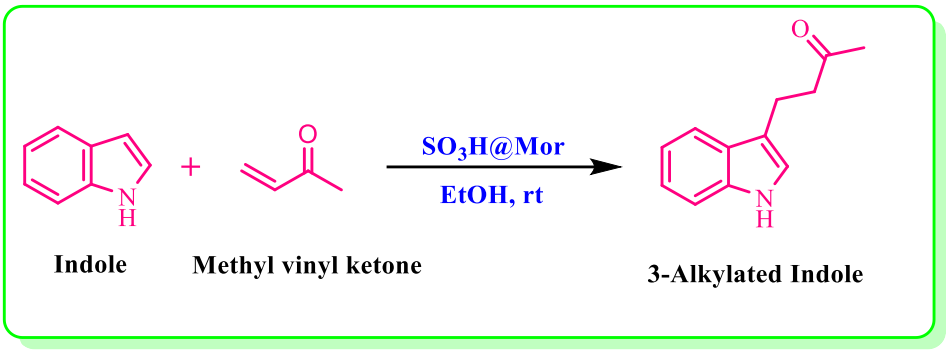

Scheme 6.2. Synthesis of 3-alkylated indole using SO_3H@Mor zeolite as a catalyst.

The reaction order was determined by analyzing rate equations for zero and first, as seen in **Figure 6.5**. The relatively higher value of R^2 for the first-order reaction rate, 0.98, indicates that the alkylation of indole with methyl vinyl ketone followed pseudo-first-order kinetics, as depicted in **Figure 6.5(b)**. The slope of this graph gives the rate constant, k value for the reaction which is 0.153 min^{-1} shown in **Figure 6.5(b)**.

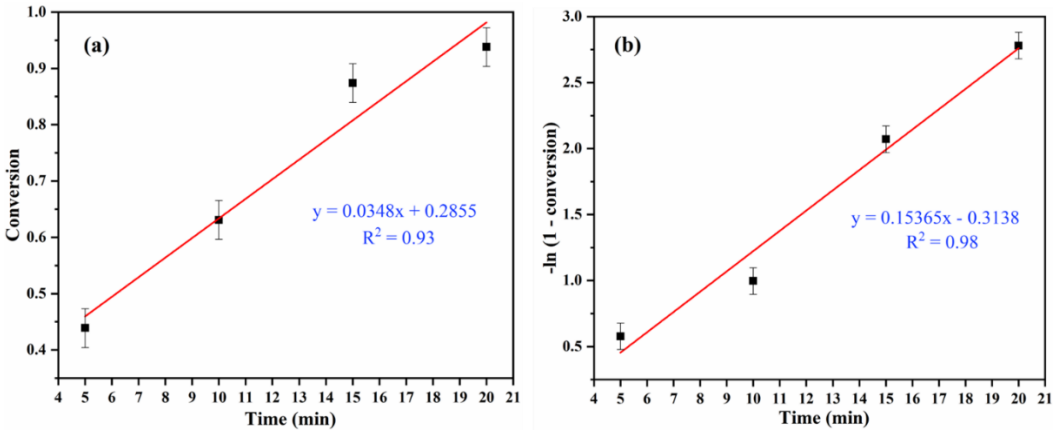

Figure 6.6. A plot of (a) Conversion, and (b) -ln (1 - conversion) *versus* reaction time (min) for zero, and first-order reactions.

6.4. Plausible mechanism

Scheme 6.3 suggested a plausible mechanism for the synthesis of β-indolylketone using indole and methyl vinyl ketone in the presence of SO_3H@Mor zeolite as a heterogeneous catalyst. The oxygen atom of methyl vinyl ketone (2) combines with SO_3H@Mor to produce intermediate 4. After attacking the electron-deficient conjugated carbon-carbon double bond of 4 to produce 5, the indole ring's electron-rich -position transfers a hydrogen atom to produce 6. Finally, 6 was rearranged to yield target compound 3, and the subsequent cycle was catalyzed by SO_3H@Mor zeolite.

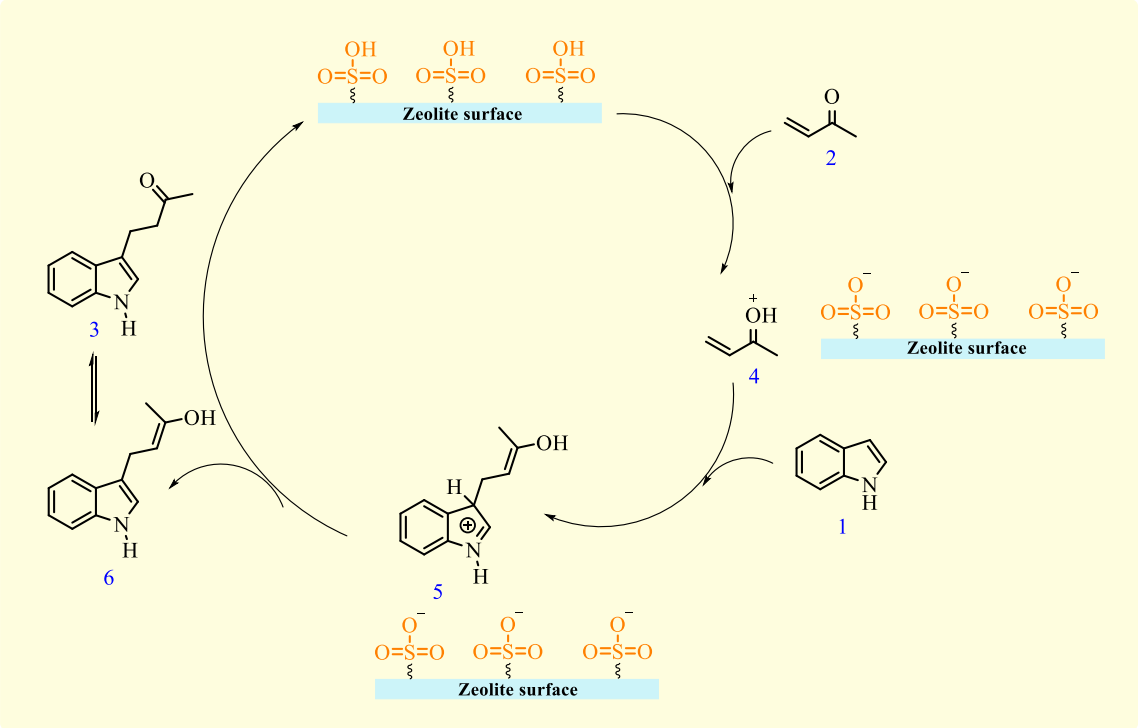

Scheme 6.3. A plausible mechanism of the synthesis of β-indolylketone.

6.5. Conclusion

In conclusion, 7.5 wt% of SO_3H@Mor zeolite as a heterogeneous catalyst has successfully catalyzed the Michael addition of indole and methyl vinyl ketone to give 3-alkylated indole with an excellent yield of 92%. The procedure used in the present work has many advantages such as high yield, reaction performed at room temperature, ethanol as solvent, and catalyst recyclability. The kinetic study confirmed that the reaction followed pseudo-first order reaction with rate constant 0.153 min^{-1}.

References

1 M. L. Deb and P. J. Bhuyan, *Tetrahedron Lett.*, 2007, **48**, 2159–2163.

2 B. K. Banik, M. Fernandez and C. Alvarez, *Tetrahedron Lett.*, 2005, **46**, 2479–2482.

3 M. J. Naim, O. Alam, J. Alam, F. Bano and P. Alam, *Int. J. Pharma Sci. Res.*, 2016, **7**, 51–62.

4 H. Firouzabadi, N. Iranpoor, M. Jafarpour and A. Ghaderi, *J. Mol. Catal. A Chem.*, 2006, **252**, 150–155.

5 M. Ad, K. Li, X. Lin, J. Wang, G. Li and Y. Wang, *JOL*, 2005, **13**, 2003-2006.

6 A. V. Reddy, K. Ravinder, T.V. Goud, P. Krishnaiah, T.V. Raju and Y. Venkateswarlu, *Tetrahedron Lett.,* 2003, **44**, 6257–6260.

7 D. A. Evans, K. A. Scheidt, K. R. Fandrick, H. W. Lam and J. Wu, *J. Am. Chem. Soc.*, 2003, **125**, 10780–10781.

8 S. Ko, C. Lin, Z. Tu, Y. Wang and C. Wang, *Tetrahedron Lett.,* 2006, **47**, 487–492.

9 M. Agnusdei, M. Bandini, A. Melloni and A. Umani-ronchi, *J. Org. Chem.,* 2003, **68**, 7126–7129.

10 M. Bandini, P. G. Cozzi, M. Giacomini, P. Melchiorre, S. Selva and A. Umani-ronchi, *J. Org. Chem.,* 2002, **67**, 3700–3704.

11 S. J. Ji and S. Y. Wang, *Ultrason. Sonochem.*, 2005, **12**, 339–343.

12 S. S. Ekbote, A. G. Panda, M. D. Bhor and B. M. Bhanage, *Catal. Commun.*, 2009, **10**, 1569–1573.

13 W. Zhou, L. Xu, L. Yang, P. Zhao and C. Xia, *J. Mol. Catal. A Chem.*, 2006, **249**, 129–134.

14 R. Tahir and K. Banert, *Appl. Catal. A-Gen.*, 2006, **315**, 147–149.

15 J. S. Yadav, B. V. S. Reddy, G. Baishya, K. V. Reddy and A. V. Narsaiah, *Tetrahedron*, 2005, **61**, 9541–9544.

16 Z. Huang, J. Zou and W. Jiang, *Tetrahedron Lett.*, 2006, **47**, 7965–7968.

17 M. Kawatsura, S. Aburatani and J. Uenishi, *Tetrahedron*, 2007, **63**, 4172–4177.

18 G. L. Wu and L. M. Wu, *Chin. Chem. Lett.*, 2008, **19**, 55–58.

19 G. Blay, I. Ferna, R. Pedro, C. Vila and F. De Quı, *Org. Lett.*, 2007, **9**, 9030–9031.

20 X. J. Yang and Y. Jing, *J. Chem.*, 2013, **2013**, 1–6.

21 R. Tahir, K. Banert, A. Solhy and S. Sebti, *J. Mol. Catal. A Chem.*, 2006, **246**, 39–42.

22 N. Azizi and M. R. Saidi, *Org. Biomol. Chem.*, 2006, **4**, 4275–4277.

23 C. J. Yu and C. J. Liu, *Molecules,* 2009, **14,** 3222-3228.

24 K. Manabe, N. Aoyama and S. Kobayashi, *ACS,* 2001, **343,** 174-176.

25 S. Abraham, B. V. S. Reddy and G. Sabitha, *Synthesis*, 2001, **14**, 2165–2169.

26 H. Firouzabadi, N. Iranpoor and F. Nowrouzi, Chem. Comm., 2005, **6**, 789–791.

27 G. Bartoli, M. Bosco, A. Carlone, F. Pesciaioli, L. Sambri, P. Melchiorre, C. Organica and A. M. Studiorum, *Org. Lett.*, 2007, **9**, 8156–8157.

28 Z. P. Zhan, R. F. Yang and K. Lang, *Tetrahedron Lett.*, 2005, **46**, 3859–3862.

29 L. T. An, J. P. Zou, L. L. Zhang and Y. Zhang, *Tetrahedron Lett.*, 2007, **48**, 4297–4300.

30 H. M. Meshram, D. A. Kumar and B. C. Reddy, *Helv. Chim. Acta*, 2009, **92**, 1002–1006.

31 M. L. Kantam, S. Laha, J. Yadav and P. Srinivas, *Synth. Commun.*, 2009, **39**, 4100–4108.

32 L. T. An, L. L. Zhang, J. P. Zou and G. L. Zhang, *Synth. Commun.*, 2010, **40**, 1978–1984.

33 C. S. Schwalm, M. A. Ceschi and D. Russowsky, *J. Braz. Chem. Soc.*, 2011, **22**, 623–636.

34 R. S. Kumar and P. T. Perumal, *J. Heterocycl. Chem.*, 2006, **43**, 1383–1385.

35 X. Zhang, E. J. Mensah, J. Deobald and J. Magolan, *Adv. Synth. Catal.,*2019, **361,** 5548-5551.

36 G. D. Yadav and A. R. Yadav, *Micropor. Mesopor. Mat.*, 2014, **195**, 180–190.

37 R. N. Yadav, L. Garcia and B. K. Banik, *Curr. Organocatalysis*, 2018, **5**, 201–204.

38 R. Matsuzawa, S. Nishimura and K. Ebitani, *ChemistrySelect*, 2017, **2**, 10814–10817.

CHAPTER 7

CONCLUSION

&

FUTURE SCOPE

7.1 Introduction

This chapter concludes the work completed in Chapters 3-6. The work's future scope has also been explored.

7.2 Summary of the present thesis

Zeolites like HZSM-5, ultra-stable Y, beta, and mordenite were modified according to the need of the reaction and were used for esterification of glycerol with acetic acid, esterification of levulinic acid with ethanol, transesterification of glycerol with dimethyl carbonate, and alkylation of indole with methyl vinyl ketone respectively. The conclusion of each reaction is discussed separately below.

7.2.1 Esterification reaction

a. Esterification of glycerol

- The HZSM-5 zeolite was modified with 1, 3, 5, and 7% solutions of cerium ammonium nitrate and were designated as Ce_1ZSM-5, Ce_3ZSM-5, Ce_5ZSM-5, and Ce_7ZSM-5, respectively.
- The Ce_5ZSM-5 zeolite was shown to be the most effective catalyst for the esterification of glycerol with acetic acid, which results in the formation of monoacetin and diacetin.
- Maximum glycerol conversion of 98.32 % was obtained over 8 wt% catalyst, 9:1 molar ratio of acetic acid to glycerol at 120 ℃ which impart a mixture of products i.e. monoacetyl glycerol and diacetyl glycerol.
- Reusability was also tested up to four cycles and conversion was reduced to 88.25% which proves that the catalyst is quite stable.
- Kinetic analysis reveals that the reaction follows pseudo-first-order kinetics, with an activation energy of 63.72 $kJmol^{-1}$.

b. Esterification of levulinic acid

- The ultra-stable zeolite Y was modified using sulfuric acid and then used for the esterification of levulinic acid with ethanol.
- The maximum levulinic acid conversion obtained was 96% which was at catalyst 10 wt%, reaction temperature 80 °C, a mole ratio of levulinic acid: ethanol 1:11, and reaction time 5 h with 100% selectivity.

- The reusability of the catalyst was also examined for 4 cycles and conversion was reduced to 11.52%.
- The reaction follows a pseudo-first-order reaction with activation energy 19.570 $kJmol^{-1}$.

7.2.2 Transesterification reaction

- Zeolite beta was successfully modified with different alkali and alkaline earth metals using the wet-impregnation method for the transesterification of glycerol with dimethyl carbonate.
- Li-modified zeolite beta zeolite comes out to be the best catalyst and was used for all the reactions.
- A maximum glycerol carbonate yield of 81.48% was observed under optimal reaction conditions (glyecrol:dimethyl carbonate 1:5, catalyst dosage 10 wt% w.r.t. GLY, temperature 95 ℃, time 5 h).
- The stability and performance of Li-modified zeolite beta was experimented with by reusing it for five reaction cycles which shows 100% selectivity towards glycerol carbonate.
- The reaction showed second-order reaction kinetics having an activation energy of 34.60 kJ/mol.

7.2.3 Alkylation reaction

- Sulfuric acid-treated mordenite zeolite was used to perform the alkylation of indole with methyl vinyl ketone.
- A maximum of 92% isolated yield was obtained at optimal reaction conditions, indole:methyl vinyl ketone 1:2, 7.5 wt% of catalyst amount at room temperature, and reaction time of 20 min in the presence of ethanol as a solvent.
- The recyclability of the catalyst was also tested up to 3 cycles and yield was reduced to 42%.
- The reaction followed a pseudo-first-order reaction with a rate constant of 0.153 min^{-1}.

7.3 Future scope of the thesis work

Here are some ideas for the next project.

i. Various zeolite catalysts can be fabricated and altered for the particular chemical systems employed in this investigation.

ii. Zeolites can be modified with metal ions, LDH, MOF, or carbon dots to test their suitability for the particular reaction systems under study as well as to test them for various heterogeneous reactions.

iii. Zeolite-graphene composite can be made and used for these esterification, transesterification, alkylation, and transalkylation reaction systems.

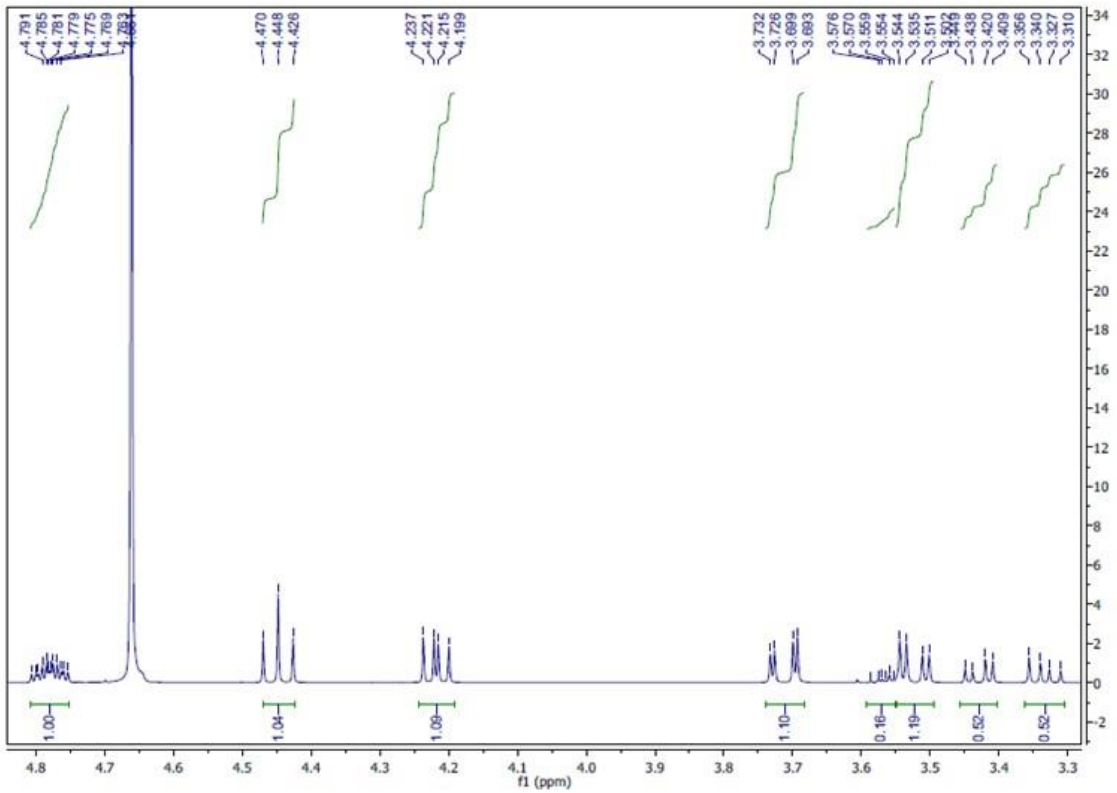

Figure A1. ^{1}H NMR spectrum of the reaction mixture.

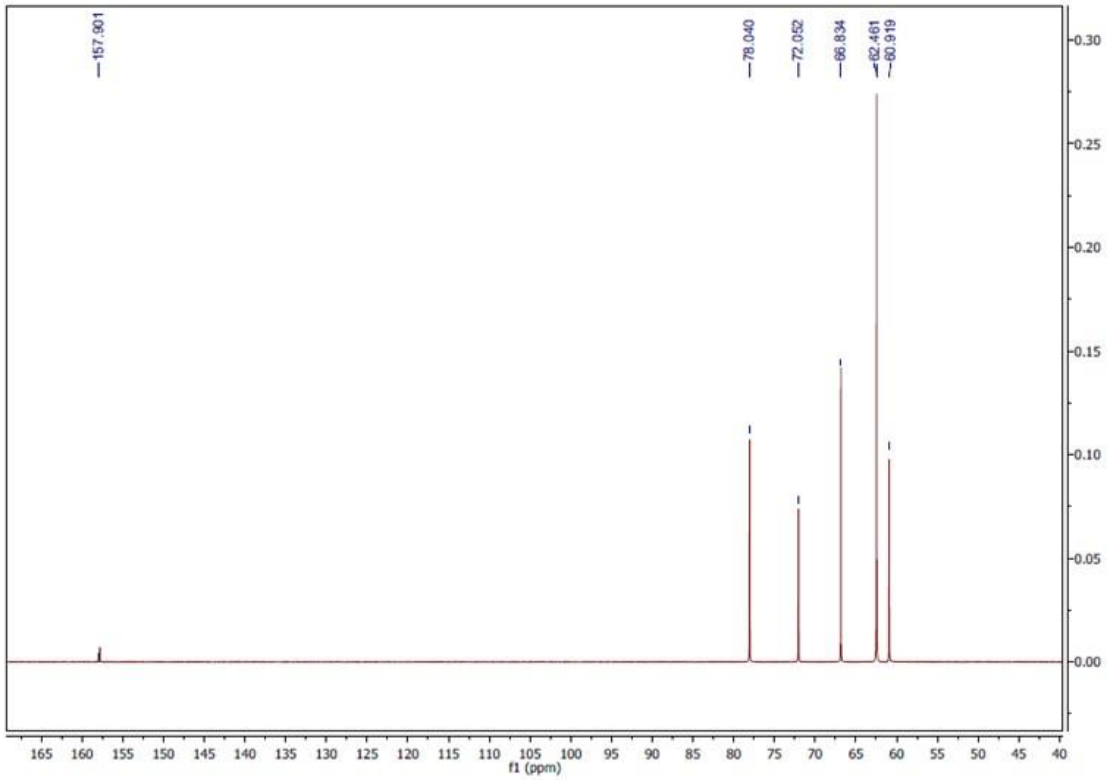

Figure A2. ^{13}C NMR spectrum of the reaction mixture.

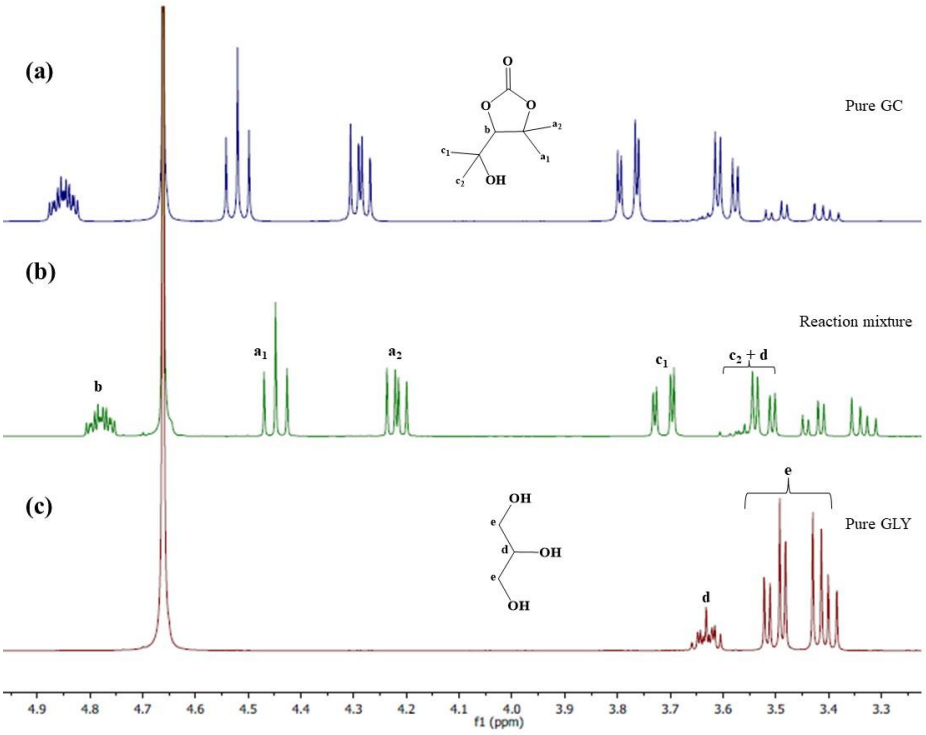

Figure A3. ^{1}H NMR spectra of (a) pure GC, (b) reaction mixture at optimized reaction conditions, and (c) pure GLY.

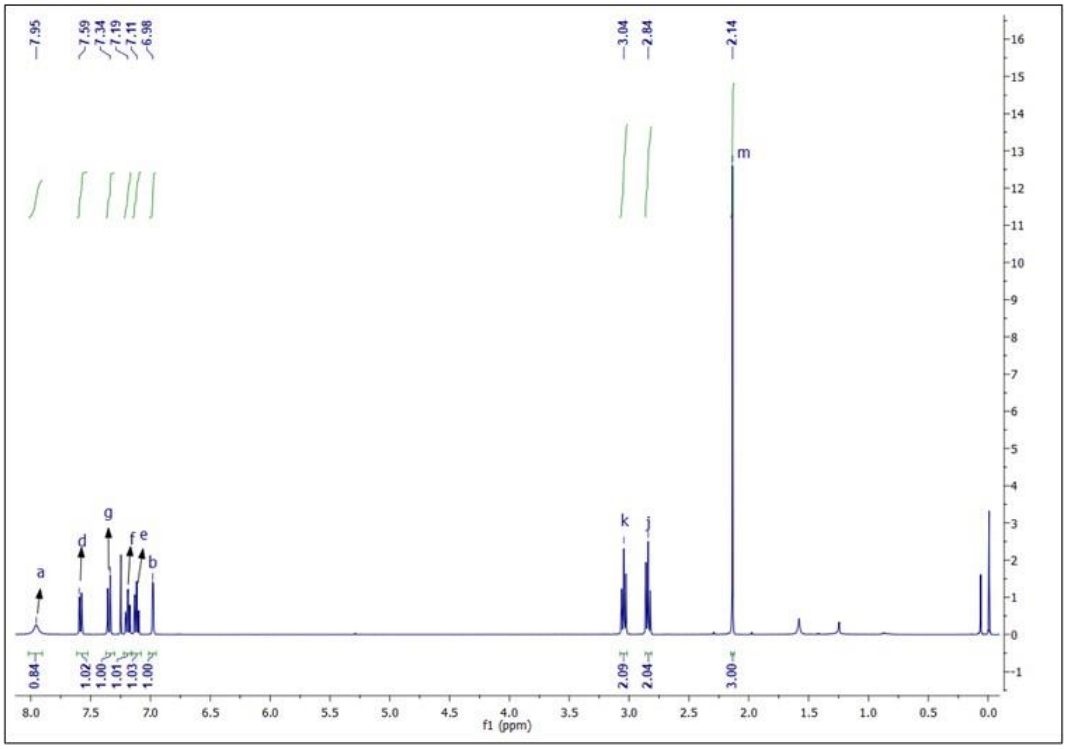

Figure B1. ^{1}H-NMR of 4-(1H-indol-3-yl) butan-2-one (β-indolyl ketone).

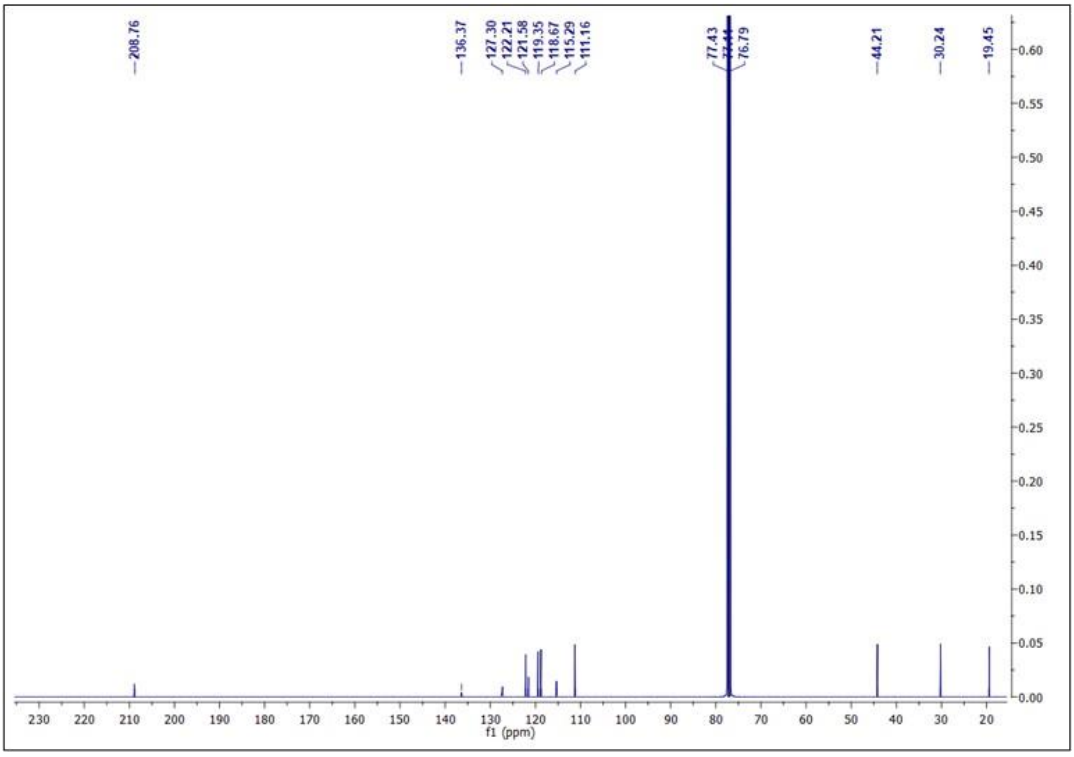

Figure B2. ^{13}C-NMR of 4-(1H-indol-3-yl) butan-2-one (β-indolyl ketone).

List of Publications

1. Priyanka Gautam, Sanghamitra Barman, and Amjad Ali, "Catalytic performance of cerium-modified ZSM-5 zeolite as a catalyst for the esterification of glycerol with acetic acid" *International Journal of Chemical Reactor Engineering,* 2020, 18(9), 20200081.
2. Priyanka Gautam, Sanghamitra Barman, and Amjad Ali, "A comparative study on the performance of acid catalysis in the synthesis of levulinate ester using biomass-derived levulinic acid: a review" *Biofuels, Bioproducts & Biorefining,* 2022, 16, 1095-1115.
3. Priyanka Gautam, Sanghamitra Barman, and Amjad Ali, "Catalytic Synthesis of Energy-rich Fuel Additive Levulinate Esters from Levulinic Acid using Modified Ultra-stable Zeolite Y" *ChemsitrySelect,* 2022, 7, e202203044.
4. Priyanka Gautam, Sanghamitra Barman, and Amjad Ali, "Synthesis of Glycerol Carbonate using Lithium-modified Zeolite Beta: A Kinetic Study" *New Journal of Chemistry,* (Communicated).
5. Priyanka Gautam, Sanghamitra Barman, and Amjad Ali, "Alkylation of indole with methyl vinyl ketone using sulfuric acid-treated mordenite zeolite as a heterogeneous catalyst" *International Journal of Chemical Reactor Engineering.* (Under review).

th

ORIGINALITY REPORT

14%	3%	13%	0%
SIMILARITY INDEX	INTERNET SOURCES	PUBLICATIONS	STUDENT PAPERS

PRIMARY SOURCES

1	Ganapati D. Yadav, Akhilesh R. Yadav. "Atom economical Michael addition of indole with methyl vinyl ketone over novel solid acid catalyst sulfated zirconia on silica tubes", Microporous and Mesoporous Materials, 2014 Publication	1%
2	www.researchgate.net Internet Source	1%
3	link.springer.com Internet Source	<1%
4	"Catalysis for Clean Energy and Environmental Sustainability", Springer Science and Business Media LLC, 2021 Publication	<1%
5	Sunil S. Ekbote, Anil G. Panda, Malhari D. Bhor, Bhalchandra M. Bhanage. "Polyvinylsulfonic acid as a novel Brønsted acid catalyst for Michael addition of indoles to α,β-unsaturated ketones", Catalysis Communications, 2009 Publication	<1%